THERMAL PERFORMANCE ENHANCEMENT OF MICRO-ENCAPSULATED PHASE CHANGE MATERIAL/GEOPOLYMER COMPOSITES THROUGH GRAPHITE PLATELETS AND NANO-ADDITIVES FOR BUILDING ENERGY STORAGE APPLICATIONS

A THESIS SUBMITTED TO
THE GRADUATE SCHOOL OF NATURAL AND APPLIED SCIENCES
OF
MIDDLE EAST TECHNICAL UNIVERSITY

BY

TOLGA TAMER

IN PARTIAL FULFILLMENT OF THE REQUIREMENTS
FOR
THE DEGREE OF MASTER OF SCIENCE
IN
MICRO AND NANOTECHNOLOGY

JANUARY 2023

Approval of the thesis:

THERMAL PERFORMANCE ENHANCEMENT OF MICRO-ENCAPSULATED PHASE CHANGE MATERIAL/GEOPOLYMER COMPOSITES THROUGH GRAPHITE PLATELETS AND NANO-ADDITIVES FOR BUILDING ENERGY STORAGE APPLICATIONS

submitted by **TOLGA TAMER** in partial fulfillment of the requirements for the degree of **Master of Science** i**n Micro and Nanotechnology, Middle East Technical University** by,

Prof. Dr. Halil Kalıpçılar
Dean, Graduate School of **Natural and Applied Sciences** _____

Prof. Dr. Deniz Üner
Head of the Department, **Micro and Nanotechnology** _____

Assoc. Prof. Dr. Çağla Akgül
Supervisor, **Micro and Nanotechnology, METU** _____

Prof. Dr. Derek K. Baker
Co-Supervisor, **Mechanical Engineering, METU** _____

Examining Committee Members:

Assoc. Prof. Dr. Hüsnü Dal
Mechanical Engineering, METU _____

Assoc. Prof. Dr. Çağla Akgül
Civil Engineering, METU _____

Prof. Dr. Derek K. Baker
Mechanical Engineering, METU _____

Assoc. Prof. Dr. İpek Gürsel Dino
Mechanical Engineering, METU _____

Assoc. Prof. Dr. Hatice Duran Durmuş
Material Science and Nanotechnology Eng., TOBB ETU _____

Date: 26.01.2023

I hereby declare that all information in this document has been obtained and presented in accordance with academic rules and ethical conduct. I also declare that, as required by these rules and conduct, I have fully cited and referenced all material and results that are not original to this work.

Name Last name : Tolga Tamer

Signature :

ABSTRACT

THERMAL PERFORMANCE ENHANCEMENT OF MICRO-ENCAPSULATED PHASE CHANGE MATERIAL/GEOPOLYMER COMPOSITES THROUGH GRAPHITE PLATELETS AND NANO-ADDITIVES FOR BUILDING ENERGY STORAGE APPLICATIONS

Tamer, Tolga
Master of Science, Micro and Nanotechnology
Supervisor : Assoc. Prof. Dr. Çağla Akgül
Co-Supervisor: Prof. Dr. Derek K. Baker

January 2023, 111 pages

The demand for sustainable, low-energy buildings with minimized operating costs is increasing. Meeting this ever increasing demand while providing sufficient occupant thermal comfort is a challenge. In the recent years, solutions that try to utilize the thermal energy storage potential of the building envelope are being developed at a rapid pace. Combining the high storage capacity of micro-encapsulated phase change materials (mPCM) with high thermal conductivity waste materials lead to sustainable, low-carbon and low-cost composites. This research is intended to measure and analyze the mechanical, microstructural, and thermophysical properties of different types of mPCM incorporated geopolymer composites for building envelope applications. Several types of locally available waste materials with varying chemical compositions will be prepared with PCMs with melting point of 24°C. Furthermore, nano-SiO_2, nano-TiO_2, and graphite platelets were added in order to enhance the mechanical and thermal properties of the mPCM/geopolymer composites. The experiment results showed that geopolymer composites with

enhanced thermal and sufficient mechanical properties were developed by incorporating nanoparticles and graphite platelets into the geopolymer matrix.

Keywords: Microencapsulated phase change materials, Geopolymers, Nanoseed activation, Graphite, Thermal conductivity

ÖZ

BİNA UYGULAMALARINDA ENERJİ DEPOLAMA AMACIYLA KULLANILAN MİKRO KAPSÜLLÜ FAZ DEĞİŞTİREN MADDE/JEOPOLİMER KOMPOZİTLERİNİN TERMAL PERFORMANSININ GRAFİT VE NANO PARÇACIKLAR ARACILIĞIYLA İYİLEŞTİRİLMESİ

Tamer, Tolga
Yüksek Lisans, Mikro ve Nanoteknoloji
Tez Yöneticisi: Doç. Dr. Çağla Akgül
Ortak Tez Yöneticisi: Prof. Dr. Derek K. Baker

Ocak 2023, 111 sayfa

Sürdürülebilir ve enerji harcamalarının minimum düzeye indirildiği düşük enerjili bina ihtiyacı artmaktadır. Giderek artan bu ihtiyacı kullanıcı termal konforunu gözeterek karşılamak ise başlıca zorluğu oluşturmaktadır. Son yıllarda, binaların dış cephesinin ısıl enerji depolama kapasitesinden yararlanmaya çalışan yöntemler hızlı bir şekilde geliştirilmektedir. Mikroenkapsüle faz değiştiren maddelerin (mFDM) yüksek depolama kapasitesini, yüksek ısı iletkenliği olan atık malzemelerle birleştirmek; ısıl depolama kapasitesi ile birlikte, üretilen malzemenin genel performansının da artmasını sağlayarak, sürdürülebilir, çevre dostu ve düşük maliyetli kompozitlerin üretilmesine olanak tanımaktadır. Bu çalışmanın amacı, farklı tipteki bağlayıcı/ mFDM kompozitlerinin termofiziksel, mekanik ve mikroyapı özelliklerini analiz etmek ve bu kompozitleri bina dış cephesi uygulamaları için incelemektir. Kompozitler, değişik kimyasal kompozisyonlarda ve yerel olarak temin edilebilen farklı tipteki atık malzemeler ve mFDM erime sıcaklıkları (24°C) göz önüne alınarak hazırlanacaktır. Ayrıca, nano-tanecik ve grafit ilavesi ile mFDM/jeopolimer kompozitlerinin ısıl ve mekanik özelliklerinin iyileştirilmesi

amaçlanmıştır. Deney sonuçları, gelişmiş termal ve yeterli mekanik özelliklere sahip jeopolimer kompozitlerin, jeopolimer matrisine nanopartiküller ve grafit levhacıklar dahil edilerek geliştirildiğini göstermiştir.

Anahtar Kelimeler: Mikroenkapsüle faz değiştiren malzeme, Jeopolimer, Nanoçekirdek aktivasyonu, Grafit, Termal iletkenlik

To my family…

ACKNOWLEDGMENTS

First and foremost, I would like to express my deepest gratitude to my thesis supervisor Assoc. Prof. Dr. Cagla Meral Akgül for her guidance and consistent support throughout this research. Dr. Akgül has been an important figure in my professional and personal growth since the first day of my graduate studies. I consider myself extremely lucky to have had the opportunity to work with her.

Besides, I would like to express special thanks to my co-supervisor Prof. Dr. Derek Baker for all guidance and support. Having the chance to work with Prof. Baker was a great privilege.

I am also very grateful to Assoc. Prof. Dr. İpek Gürsel Dino for her support and guidance during my graduate studies.

I would like to thank the examining committee members Assoc. Prof. Dr. Hatice Duran Durmuş and Assoc. Assoc. Prof. Dr. Hüsnü Dal for their invaluable feedback.

I am thankful to all my friends, especially Sepehr Seyedian, Hossein Mazaheri, Amirali Hashemzadeh and Erman Tunçer for their support on the lab work, and their valuable recommendations.

I am thankful to the Microtek Laboratories/CAVU group for providing microencapsulated phase change materials.

Finally, I would like to thank my family, for their emotional support, and patience during the stressful times. I would not be able to achieve without their support in every step of my life. I dedicate my thesis to them.

This research was supported by TUBITAK-Royal Academy of Engineering TSP Programme Grant No. 220N292

TABLE OF CONTENTS

LIST OF TABLES

TABLES

LIST OF FIGURES

FIGURES

CHAPTER 1

INTRODUCTION

The building sector significantly contributes to total energy consumption, accounting for approximately 30% of global final energy use and nearly 15% of direct CO_2 emissions. Energy-related CO_2 emissions from electricity generation and commercial heat used in buildings continued to rise with an average of 1% per year between 2010 and 2020 due to population growth, rapid urbanization, global warming, preference for larger floor spaces, and other driving factors [1]. International Energy Agency (IEA) indicates that all new buildings and 20% of the existing building stock should be zero-carbon to achieve the ambitious carbon neutrality target by 2050 as a part of the European Green Deal [1]. Furthermore, the current energy crisis created by the COVID-19 pandemic and the Russia – Ukraine war forces countries to seek new alternatives to replace conventional fossil fuels with renewable energy sources. In this regard, reducing heating and cooling-related energy use in buildings has become a top priority for many countries to achieve the carbon neutrality target and respond to the growing energy crisis.

Therefore, as one of the major contributors to energy consumption and direct CO_2 emissions, the building sector should immediately respond to the rising energy use and energy-related CO_2 emissions in terms of different building design alternatives and enhanced energy efficiency measures.

In buildings, heating, ventilation, and air-conditioning (HVAC) systems account for more than 50% of the total energy consumption [2], placing a considerable strain on energy supply systems with significant environmental and economic consequences. Thus, various policy measures have been implemented in many countries to enhance the energy efficiency of HVAC systems [3]. However, instead of solely relying on

improving the efficiency of the HVAC systems, passive energy-saving system approaches are also considered to curb the growing energy demand. Thermal energy storage in buildings can be accomplished by sensible heat (for instance, by increasing and reducing the temperature of the building envelopes) or latent heat (incorporating PCMs to increase thermal inertia). The primary benefit of latent heat storage is its high storage density at low temperatures. Latent storage can be utilized for building heating and cooling and can be included in a passive or active system [4].

Cabeza et al. [5] divide the possible use of PCMs in buildings into four categories: free cooling, peak load shifting, active building systems, and passive building systems. Table 1 gives each type a brief description of the respective application.

Table 1. Possible use of PCMs in buildings

PCM utilization	**Description**
Free cooling	The ability to store outside coolness and release it indoors during the day. The ambient temperature must be above the PCM's phase change temperature during the day and below it at night for these systems to function.
Peak load shifting	By transferring peak load away from peak hours of electricity demand using PCMs, peak load can be distributed throughout the day, minimizing the highest peaks.
Active systems	PCMs can be incorporated into applications such as solar heat pump systems, heat recovery systems.

Table 1 (Cont'd)

Passive systems	The use of PCMs in building envelopes increases the thermal mass. The materials containing PCMs will be liquid during the day and solid at night. This will prevent rooms from overheating throughout the day during warm months and may lower the demand for nighttime heating during the winter.

Passive cooling approaches, which utilize ambient cooling sinks to moderate the increasing air temperatures in buildings, have proven to be a robust alternative to resource-consuming HVAC systems. Passive cooling techniques include solar and heat protection systems, modulation, and dissipation [6]. The heat modulation techniques benefit from the thermal storage capacity of building materials to discharge the stored heat gradually, eliminating the sudden temperature fluctuations in building spaces and reducing the energy use of buildings [4] [5]. As such, extreme outside temperatures have a diminished impact on indoor spaces, ensuring comfortable thermal conditions.

In recent years, PCM application to buildings and investigation of energy performance and thermal comfort by simulation tools have been studied by several researchers to optimize the overall efficiency of PCM systems [8]. Due to the fact that embedding PCM into cementitious materials affects both the thermophysical and mechanical characteristics of concrete, only a limited amount (mass fraction) of PCM can be introduced to cementitious materials for specific applications. This is typically the case with load-bearing structures, for which concrete is frequently employed because of its high strength. In contrast, lightweight concretes used for partition walls permit the incorporation of a greater quantity of PCM. There is also

the option of utilizing multilayer structures. The load-bearing core of the concrete structure can be composed of high-strength concrete, while the thermal storage surface layers exposed to the environment can be composed of PCM [9].

Due to the complex behavior of the PCM-integrated buildings, the most important features that characterize the PCM effectiveness, such as material selection, location, and quantity of the PCM in the envelope, have been studied in detail. Saffari et al. [8] studied the optimization of PCM melting temperature to enhance the cooling, heating, and total energy performance of a residential building considering different climatic regions in the world. Their results showed that cooling dominant climates achieved the best performance choosing PCM melting temperature of 26°C, and heating dominant climates achieved higher energy savings with PCM melting at 20°C. In a similar study, de Gracia [10] proposed a dynamic PCM system that modifies the PCM layer position inside the building envelope by optimizing PCM peak melting temperature and daily activations of the system using the Particle Swarm Optimization (PSO) algorithm. Bhamare et al. [11] developed five machine learning and one deep learning-based methods to predict the energy performance of PCM integrated roofs, considering different thermo-physical properties of the PCM. Their results showed that Gradient boosting regression showed the best performance compared to other machine learning models in predicting the performance of the PCM integrated roof. Park et al. [12] conducted a comparative analysis to find the best-performing PCM considering different building types and PCM melting points.

Although there is a high number of studies that investigated the effect of PCM incorporation into building envelopes to enhance the overall energy performance of the buildings, it has not yet been used in practice due to the undesirable features after PCM integration, such as loss of strength and questionable long-term stability [13]. The challenges associated with the integration of PCM may also be addressed by using geopolymer composites, which have distinct advantages over conventional ordinary Portland cement (OPC).

The production of OPC consumes a vast amount of energy and raw materials and releases a substantial amount of CO_2 that contributes to global warming [14]. Global yearly cement production is estimated to be 6 billion tons, with CO2 emissions exceeding 5 billion tons yearly [15]. This will be an unsettling condition; thus, there is an immediate need to reduce CO_2 emissions from the cement industry. There are two options: To save energy and raw resources and minimize CO_2 emissions, OPC can be partially or fully substituted with supplemental cementitious ingredients, and clinker-free cement can be produced [14].

Geopolymer is emerging as an alternative material having cementitious properties. It is produced by alkali activation of alumino silicate-containing industrial or agro-waste materials such as fly ash, slag, clay, silica fume, rice husk ash, etc. Geopolymer mortars and concretes are anticipated to be energy-efficient and environmentally friendly binding materials. Geopolymer manufacturing reduces waste and protects the environment. Therefore, using geopolymer as the binder material to produce PCM-incorporated composites, both energy storage on a building scale can be achieved with decreasing heating/cooling energy consumption, and industrial and agro waste materials can be used in terms of circular economy practices.

Incorporating PCM into cement matrix increases the heat storage capacity of the cementitious composites; thus, it provides an opportunity for heat storage applications in building applications. The thermal conductivity of PCM-incorporated cement-based systems is a key transport property that directly reflects the heat transfer rate. In addition to melting temperature and energy density dictated by the specific heat of fusion, the power capacity of the melting or solidification process is determined by the thermal conductivity as the actual thermal performance of the PCM composite. However, the low thermal conductivity of the PCM can inhibit heat transfer through the matrix, and the latent heat activation of PCM could not be achieved.

In order to increase the lower thermal conductivity of the PCM-incorporated composites, conductive fillers such as metal nanoparticles, carbon nanotubes,

graphene, or other carbon-based materials can be implemented. The minimal additive dose required to generate continuous conductive channels within the composite is referred to as the percolation threshold, which depends on numerous aspects, including additive composition (size and shape), concentration, and aggregation degree [16].

One such conductive additive is natural graphite, which, due to its wide availability and moderate cost, has the potential to be utilized in cementitious composites for heat transfer enhancement. The layered planar structure of graphite powder, along with its anisotropy and mild inter-planar forces, ability to conduct electricity and heat well, resistance to chemical attack, and stability under ordinary conditions, makes the graphite an excellent candidate to be used as a conductive filler in cementitious systems [16].

Although graphite has been combined with cementitious materials to investigate the thermoelectrical properties of composites for smart building applications such as self-sensing concrete, graphite's heat transfer advancement properties are an understudied area. In literature, in their study, Xiong et al. [17] examined the effect of graphite nanoplatelets in PCM-incorporated cementitious composites for better heat transfer performance. They used OPC (CEM I 52.5 N) and styrene/n-eicosane-based PCM. They incorporated both mPCM and graphite nanoplatelets into cement paste. mPCM content changed between 5 to 15 wt% cement, and graphite nanoplatelets were added between 1 to 5 wt% cement. The thermal conductivity results showed that the thermal conductivity of the cement paste decreased by 40% (0.865 W/mK to 0.525 W/mK) when 15% PCM was incorporated. However, utilizing 5 wt% graphite nanoplatelets increased the thermal conductivity of the composite by 40% (0.865 W/mK to 1.218 W/mK) compared to the control mix.

In addition, the effect of adding 5 wt% GP on the heat transfer performance of the composite improved as the PCM concentration increased. Besides, they concluded that it was discovered that the addition of graphite nanoplatelets influences the hydration process of the cement samples, which may change the samples' mechanical

qualities. However, they did not further comment on the mechanical properties of the composites; thus, the suitability of the developed cement composites for building applications in terms of mechanical performance is not detailed in this study.

Moreover, the mechanical strength loss due to PCM incorporation is another concern for the widespread application of the PCM incorporated building materials. The addition of nanoparticles could potentially enhance mechanical properties while developing composites for energy-harvesting applications. In this regard, the effect of nano-SiO_2 and nano-TiO_2 on the mechanical as well as thermal properties of PCM-integrated geopolymer composites is an understudied area and will be investigated further in this work.

As a result, this study focuses on developing environmentally friendly PCM-incorporated geopolymer composites for energy harvesting in building applications. The well-known drawbacks of PCM incorporation into cementitious systems, namely thermal conductivity reduction and loss in mechanical strength, will be addressed by utilizing graphite powder as well as nanoparticles such as silica and titania.

CHAPTER 2

LITERATURE REVIEW

2.1 Phase Change Materials (PCMs)

PCMs can be classified depending on their phase change state and the chemical composition of the material used in the production. According to the phase change state, PCMs are classified as solid-solid PCMs, solid-liquid PCMs, liquid-gas, and gas-solid PCMs, as shown in Figure 1. It should be noted that liquid-gas and gas-solid PCMs are not applicable to construction materials due to large volume and pressure changes during the phase change processes [18].

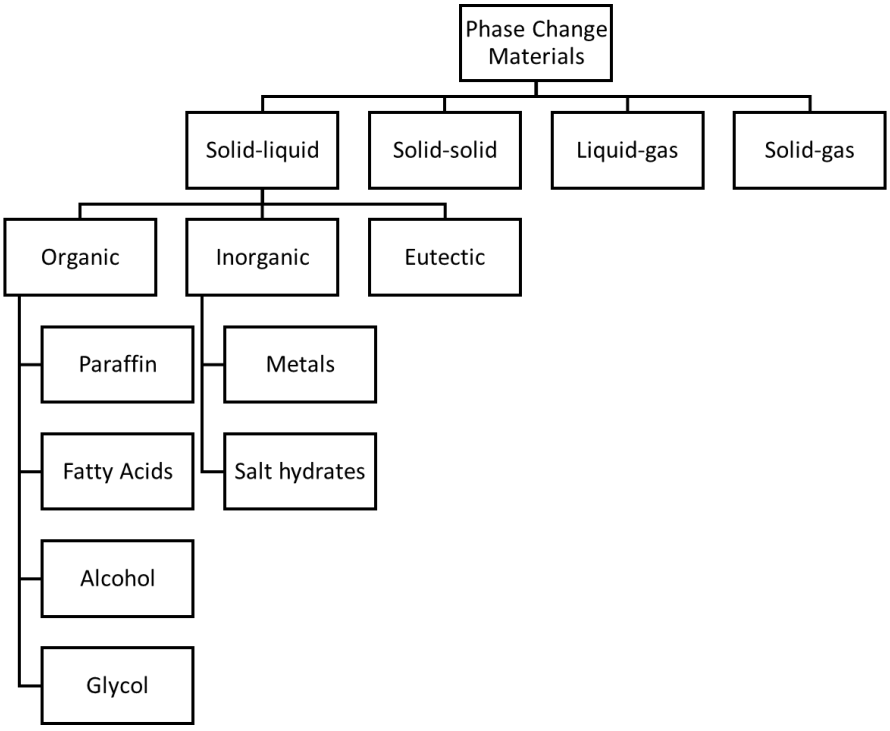

Figure 1. Classification of PCMs depending on their phase change states

Solid-solid PCMs absorb and release heat via reversible phase transitions. When the phase transition temperature is attained, solid-liquid PCMs change from the initial state of an ordered crystalline structure to a disordered amorphous structure by changing their internal molecular arrangement [19]. As a result, the crystalline structure of PCM transforms into a liquid state with randomly aligned atoms. On the other hand, when the temperature falls below the phase transition point, a nucleation process begins, and molecules rearrange themselves into an organized crystalline lattice. The rate of cooling, the kind of molecules present, and the presence of contaminants are only a few variables that affect the shape and quantity of crystals that form during crystallization [19].

Considering the wide variety of PCMs in terms of their chemical compositions and phase change states, the most desirable PCM for the latent heat storage system should be selected as a result of a detailed analysis considering PCMs' thermophysical, kinetic, chemical, economic, and environmental properties [19], which are summarized in Figure 2.

Since no PCM has all the desirable properties mentioned in Figure 2, a multi-criteria decision analysis can be performed to select the optimal PCM for a particular application [20]. Among all PCM types, solid-liquid PCMs ARE the most suitable for building applications, and they have been widely used for thermal energy harvesting in buildings [21].

Solid-liquid PCMs are divided into three categories based on the material they manufactured: organic PCMs, inorganic PCMs, and eutectics. Paraffin and non-paraffins, such as alcohols and glycols, comprise organic PCMs. Due to its extraordinary temperature range, which covers most applications, paraffin seems to have excellent characteristics and several advantages. Additionally, paraffins do not experience phase separation following numerous solid-liquid transitions since their latent heat is mass-based [23].

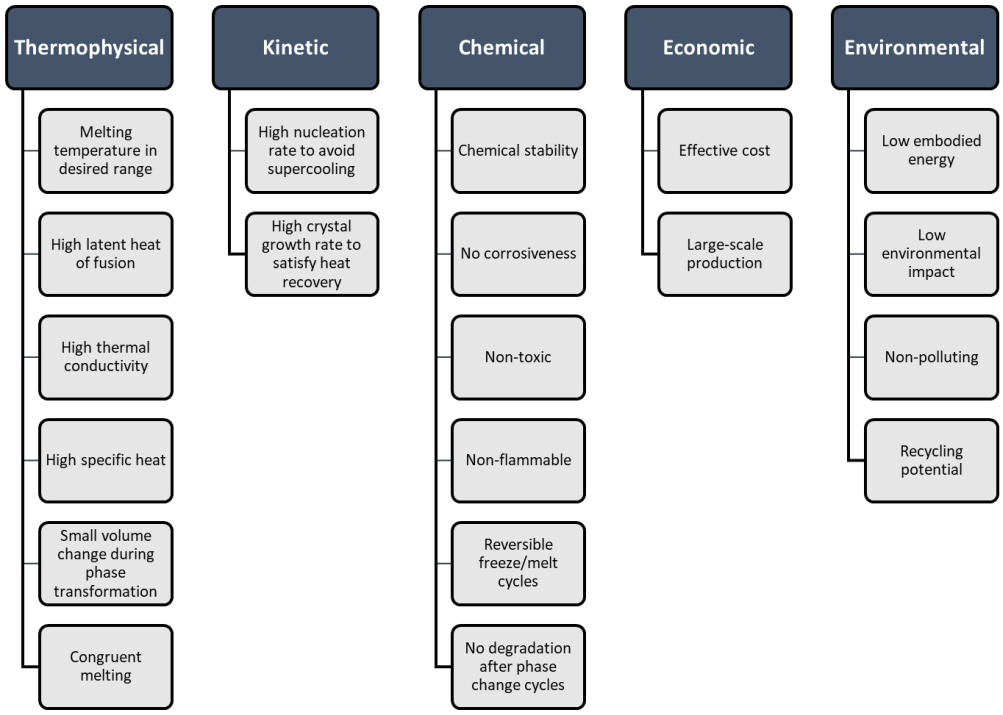

Figure 2. Selection criteria for PCM

However, the primary disadvantage of paraffin is its low heat conductivity, which ranges from 0.1 to 0.7 W/mK. Non-paraffins have desirable melting and crystallization properties but are three times more expensive than paraffins [23]. Additionally, inorganic PCMs are described as hydrated salts and metals. As the phase transition temperatures of metals exceed the thermal comfort limits of occupants, they are not suitable for passive building applications. Although hydrated salts have more thermal conductivity and latent heat than organic PCMs, phase-segregation, lack of thermal stability and corrosion limit their potential applications. A eutectic combines PCMs with two or more components with different melting points. During crystallization, each component simultaneously melts and freezes, resulting in a combination of component crystals. [20]. By mixing various component weight ratios, the melting points of eutectics have a substantial advantage over those of other solid-liquid PCM varieties.

Although different types of solid-liquid PCMs have been used in building applications, the advantages and disadvantages of the type of solid-liquid PCMs should be thoroughly investigated at the initial stage. Several researchers have examined the benefits and drawbacks of the various solid-liquid PCM types, as summarized in Table 2.

Table 2. Comparison of different types of solid-liquid PCMs considering benefits and drawbacks [4][22][23].

	Organic	**Inorganic**	**Eutectics**
Advantages	Larger phase change temperature range	Higher latent heat of fusion	No segregation
	High latent heat of fusion	Low-cost and readily available	Congruent phase-change
	Freeze with a little supercooling	Sharper phase-change	Sharp melting point
	Congruent phase-change	Higher thermal conductivity	
	No segregation	Non-flammable	
	Self-nucleation		
Disadvantages	Low thermal conductivity	Poor nucleating properties	No enough test data to determine thermal properties
	Lower melting enthalpy	Supercooling problems	
	Lower density	Phase segregation	
	Flammable	Decomposition	
	More expensive	Incompatible with some construction materials	

As solid-solid PCMs could be considered as an alternative for solid-liquid PCMs to overcome some of the drawbacks of using solid-liquid PCMs, such as the need for encapsulation and the occurrence of phase segregation after being subjected to thermal cycles, the slow charging/discharging rate, as well as ease of production and

cost, are the significant concerns preventing the broader application of solid-solid PCMs.

When used in passive energy storage applications in buildings, the melting temperature of the PCM becomes the most critical parameter, as satisfying thermal occupant comfort is crucial in buildings. It is recommended that the melting temperature of the PCM should be in the range of 15-30 ℃ or 20-32 ℃ for thermal comfort [24]. Table 2 presents the thermal properties of the solid-liquid PCMs that can be used for building applications.

Table 3. Thermophysical properties of PCMs for building applications [4] [25]

Compound	**Type**	**T_m (℃)**	**ΔH_m (kJ/kg)**	**λ_s (W/m K)**	**λ_l**	**ρ (kg/m^3)**
Acetic acid	Organic	17	192	0.30	0.27	1127
Caprylic acid	Organic	16	148.5	0.15		981
Glycerin	Organic	18	198.7	0.14		
Butyl stearate	Organic	18	123	0.21		760
Paraffin wax	Organic	0-90	150-250	0.20		880-950
n-Heptadecane	Organic	19	240	0.21		760
Polyglycol E600	Organic	22	127		0.19	1232
Coconut oil/xGNP	Organic	27	82	1.33		
n-Octadecane	Organic	28	200	0.34	0.15	814
Capric acid	Organic	32	153	0.15		1004
Calcium chloride hexahydrate	Salt hydrate	30	125	1.09	0.53	1710
Sodium sulfate decahydrate	Salt hydrate	32	180	0.56	0.45	1485
$Mn(NO_3)\cdot 6H_2O$	Salt hydrate	26	126			1738

Table 3 (cont'd)

$CaCl_2 \cdot 6H_2O$	Salt hydrate	29	191	1.09	0.54	1802
$Na_2SO_4 \cdot 10H_2O$	Salt hydrate	32	254	0.55		1485
$CaCl_2 \cdot (H_2O)_6$ $MgCl_2 \cdot (H_2O)_6$	Eutectic	25	127	0.93	0.55	1661
Urea $CH_3COONa \cdot (H_2O)_3$	Eutectic	30	200	0.63	0.48	1370

2.1.1 Incorporation methods of PCMs into construction materials

PCMs are incorporated into building elements using one of the following methods: direct incorporation and immersion, encapsulation (macro, micro, and nanoencapsulation), and shape-stabilized PCMs [26].

2.1.1.1 Direct incorporation and immersion

Direct incorporation is the most straightforward approach, as a liquid or powdered PCMs are applied directly to the gypsum, concrete, or plaster. Leakage and incompatibility with construction materials could be the most significant concerns with this method. In the immersion approach, gypsum, brick, or concrete are submerged in molten PCMs and then absorbed PCMs through their pores by capillary elevation. It should be noted that PCM incorporation using direct incorporation and immersion into construction materials is not widespread due to the fact that previous studies showed that PCMs could interact with the surrounding matrix and change its properties, and leakage problems frequently occur, which is not appropriate for long-term use [27]. However, in a recent study, Cunha et al. [28] developed innovative mortars with direct incorporation method in which non-encapsulated PCM is used with cement and fly ash-based mortars. Although they concluded that non-encapsulated PCM in mortars could be an effective and affordable way to increase building energy efficiency, they did not comment on the

developed composites' long-term performance considering that long-term thermal stability and leakage are the biggest obstacles to using non-encapsulated PCM in construction materials.

2.1.1.2 Encapsulation

Due to the melting-freezing process, PCMs can be encapsulated before application in order to increase their effectiveness. When PCMs are used in combination with other materials, leakage in the liquid state could cause chemical and physical alterations in the matrix. The PCM behaves as a core material, and the capsule is considered shell material. Furthermore, spreading liquid PCM in the matrix could inhibit the charging potential of PCM; hence, thermal stability and heat transfer characteristics would be damaged. Also, the PCM's encapsulation enhances thermal conductivity by increasing the surface area, which accelerates heat transfer [29]. Therefore, encapsulation strategies are crucial for improving PCMs' stability and heat transfer efficiency [30]. PCMs can be encapsulated using three processes: macroencapsulation, microencapsulation, and nanoencapsulation.

The encapsulation process is called "macro" if the PCM in the shell material has a size of more than 1 mm [16], and the shell can be made of any shape, such as tubes, channels, and thin plates. Common shell forms of macroencapsulated PCMs are presented in Figure 3.

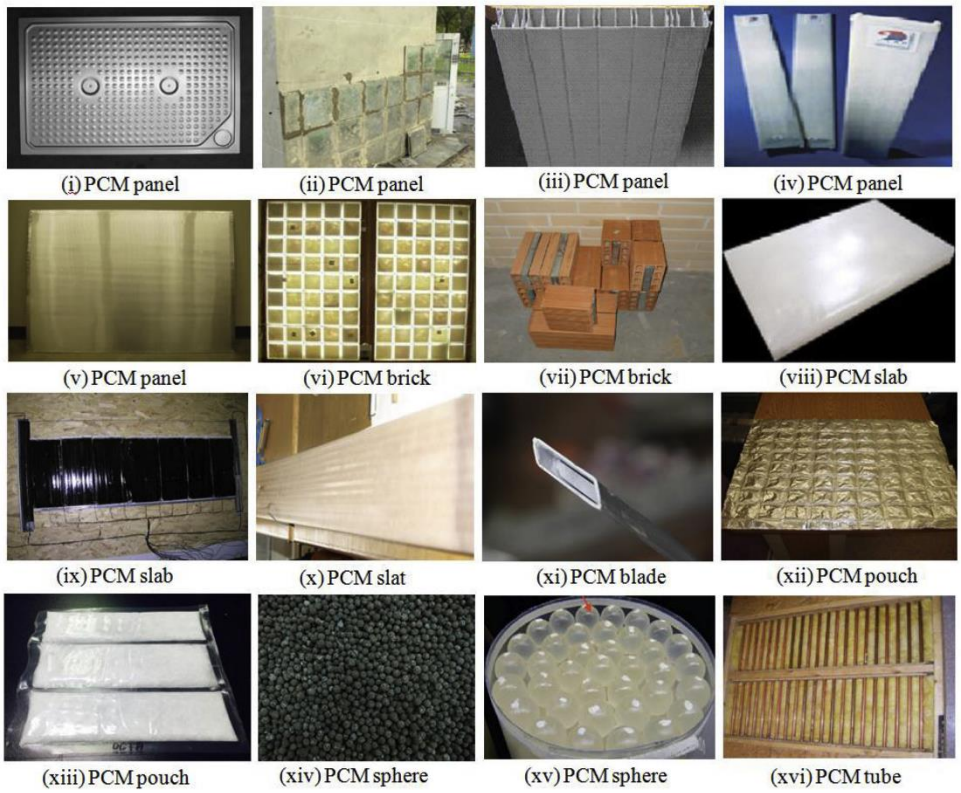

Figure 3. Common macro-encapsulated PCM shell types used in passive building applications [31]

[4] states that macro encapsulation enhances the material compatibility with the surrounding by building a barrier improves PCM handling during the production stage, and prevents external volume changes. However, the poor thermal conductivity, tendency of solidification at the edges, and difficulty of integrating them into building materials are the main problems of using macroencapsulated PCMs for passive energy-saving applications for buildings [32].

If the encapsulated PCM is between 1 μm and 1 mm in diameter, it is called "micro," It has the typical advantages of macroencapsulated PCMs. There are many ways to create the shell, including physical and chemical processes.

Besides, microencapsulated PCMs have better heat transfer to the surroundings due to their larger surface area, and they have enhanced thermal cycle stability because phase separation is restricted to microscopic distances [4]. Previous studies showed that after 3000 repeated dynamic cycles of fusion and solidification, the geometrical

shape and energy storage capability of microencapsulated PCM remained stable. However, the major disadvantage of microencapsulated PCMs is that the shell material has relatively low strength and stiffness. Also, similar to macroencapsulated PCMs, the low thermal conductivity of the shell material can hinder heat transfer performance. It should be noted that the already low thermal conductivity of the organic or inorganic PCM might further reduce the shell material's conductivity when encapsulation is done. Yu et al. [33] state that the overall thermal conductivity of microcapsules made of inorganic shell materials like calcium carbonate or silica is enhanced due to the fact that inorganic materials have higher thermal conductivity than organic materials. For instance, Zhang et al. [34] prepared silica encapsulation of n-octadecane using the sol-gel process. As n-octadecane has a thermal conductivity of 0.1505 W/m K as core material, using silica as shell material increased the thermal conductivity of the microencapsulated PCM to 0.6213 W/m K. However, organic shell materials like polymers have a thermal conductivity of around 0.20 W/m K and using organic shell materials with organic PCMs further decreases the thermal conductivity of encapsulated PCM.

The nanoencapsulation of PCMs has been offered as a novel technique in recent years. The method is expected to produce better energy storage efficiency due to the higher surface area to volume ratio of the nanoencapsulated PCM compared to the microencapsulated PCMs. In addition, the drawback of increasing the viscosity of the end fluid associated with the microencapsulation technique could be prevented using nanoencapsulation [30], and better leakage-proof properties can be obtained during the melting operation. However, Magendran et al. [35] state that higher production costs and the requirement for further purification treatment are the main problems with the nanoencapsulation techniques. Several researchers have recently studied the nanoencapsulation process for building applications. For instance, Hussain and Kalaiselvam [36] prepared nano-encapsulated PCM with oleic acid as core material and Ag_2O nanoparticles-based urea formaldehyde resin as shell material. In a similar study, Zhu et al. [37] investigated the properties of a nano-encapsulated PCM with a polymer-SiO_2 hybrid shell. Their results show that the

novel nanoencapsulation method enhanced the PCM's thermal reliability, thermal conductivity, and mechanical properties.

2.1.1.3 Shape stabilized PCMs

Organic PCM drawbacks include poor heat conductivity and phase transition leaks. To avoid these limitations, PCM is mixed with additional materials. Two supporting materials used for this purpose: a porous material that prevents PCM leakage and a nanomaterial that improves PCM's thermal characteristics. The combination of PCM, a porous material, and a nanomaterial is therefore referred to as shape-stabilized PCM.

The primary role of porous material is to provide a larger surface area, high thermal conductivity, and enhanced chemical compatibility. Due to the interaction between PCM and porous material, leakage of the PCM can be prevented as a result of capillary force and surface tension. Various porous supporting materials are combined with PCMs, such as porous carbon, graphite, polyurethane foam, silica, and clays. On the other hand, nanoparticles like Cu, Ag, Al_2O_3, ZnO, carbon nanotubes, and graphene oxide are preferred to increase the thermal conductivity of organic PCMs. For instance, Yang et al. [38] prepared a novel ceramsite-based shape-stabilized composite PCM for building applications. They used organic PCM (lauryl alcohol and stearic acid) as core material. Al_2O_3 nanoparticles used for thermal enhancement and ceramsite were provided as a porous material for better adherence properties, as seen in Figure 4.

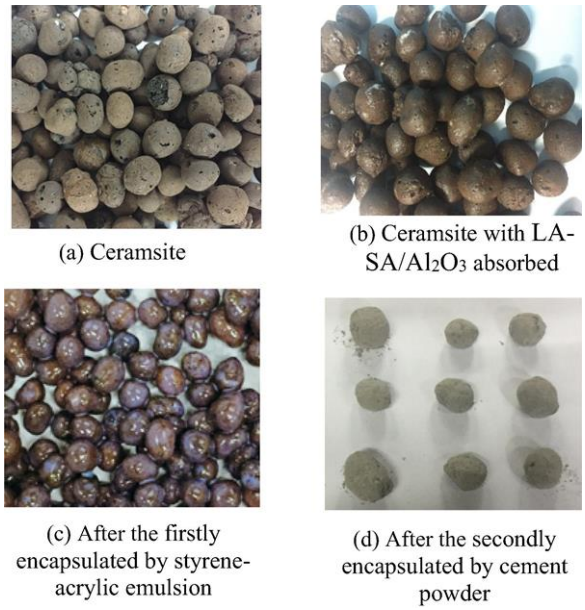

Figure 4. Preparation of ceramsite-based shape-stabilized PCM [38]

2.1.2 Thermal conductivity enhancement of PCMs

PCMs have been proposed to be utilized in latent heat thermal storage systems to improve the energy efficiency of building cooling and heating systems, and PCMs have been included in construction materials for this purpose. However, the limited thermal conductivity of these materials dramatically slows down the thermal charging and discharging processes of PCMs, reducing their efficiency.

Several approaches have been tried to overcome the low thermal conductivity of PCMs considering both shell and core to enhance the heat transfer characteristics, such as the addition of nanoparticles (carbon nanotubes (CNT), graphene nanoparticles, silver nanoparticles), expanded graphite (EG), metallic foams (nickel foam, copper foam, graphite foam), and encapsulation [39]. It should be noted that carbon-based nanoparticles outperform metal-based nanoparticles in terms of low density, improved stability, and dispersion in PCMs. Furthermore, because of its high thermal conductivity, reliable thermo-physical characteristics, and high

porosity, metallic foam is frequently utilized to improve PCM's thermal conductivity. Metallic foams are preferred over metallic nanoparticles due to their relatively low density, extensive aspect ratio, and stability [39].

In literature, several researchers studied the thermal conductivity improvement of PCMs considering building applications. Amin et al. [40] investigated the thermal properties of an organic beeswax PCM when graphene nanoparticles were added (Figure 5). Their results showed that adding graphene-enhanced both latent enthalpy and thermal conductivity of beeswax as thermal conductivity increased from 0.25 W/m K to 2.89 W/m K with 0.3 wt% addition of graphene. In a similar research, Rathore et al. [41] examined the properties of paraffin/expanded perlite shape stabilized PCMs with graphene nanoparticles as a thermal energy storage material in buildings, and they found that 5 wt% graphene incorporation resulted in thermal conductivity enhancement of 106%.

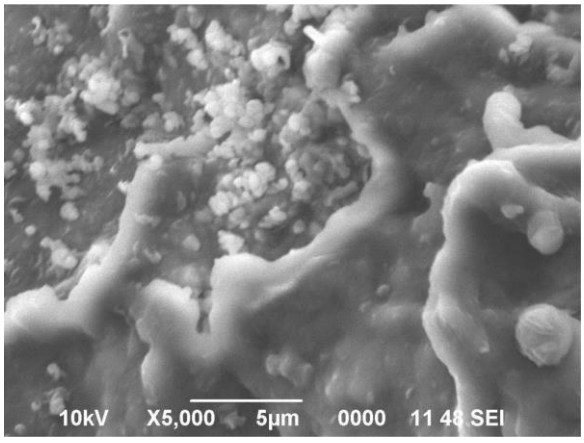

Figure 5. SEM image of organic beeswax PCM when graphene nanoparticles were added [40]

Kainafar and Niazmand [42] studied the thermophysical properties of PCM containing multi-wall carbon nanotubes (MWCNT) for free-cooling applications in buildings. Their results showed that the charging of PCM was increased by 24.1%

with 0.5 wt% MWCNT addition compared to the pure PCM. Cheng et al. [43] investigated the thermal performance of an encapsulated PCM to improve buildings' thermal comfort. In their work, they used CNT microcapsules to overcome the low thermal conductivity of organic shell material. The results confirmed that the CNT microcapsule increased the thermal stability of the PCM. In addition, improved energy saving and thermal comfort were obtained with CNT microcapsule. Rathore et al. [44] prepared shape-stabilized composite PCM using expanded graphite and vermiculite to investigate the thermophysical properties of building energy applications. They pointed out that the thermal conductivity of the PCM composite increased by 114.4% after seven thermal cycles due to the presence of EG.

Although several studies utilize composites with PCMs and nanoparticles to enhance thermophysical properties for passive building applications, there are limited studies that use metallic foams and PCM composites for building applications. In their research, Isa et al. [45] examined the properties of copper foam integrated PCM gypsum wallboard for improved thermal energy storage in a building façade.

When used in buildings, the interaction between PCM and the matrix in which PCM is incorporated should be considered in an integrated approach to understanding the overall heat transfer characteristics. For instance, having a highly thermally conductive PCM would not result in better overall charging/discharging properties if the thermal conductivity of the matrix is too low, and similarly, the thermophysical characteristics of the shell material should be evaluated for encapsulated PCMs.

2.2 PCM incorporated mortars

In general, mortar is a matrix formed by mixing fine aggregates with cement or other cementitious materials, such as lime or alkali-activated binders, in the presence of sufficient water [46]. When the hydration process is complete, and calcium silicate hydrate (C-S-H) gels are produced, the mortar will obtain adequate mechanical strength.. However, incorporating PCMs to obtain composites with high thermal

storage capacity can hinder the formation of C-S-H gels, consequently reducing the compressive strength of the mortar.

In this literature review section, PCM-incorporated mortars were examined in terms of the materials used and the T_m of PCM incorporated. A summary of the studies with PCM-incorporated mortars in the last decade is presented in Table 4.

Table 4. Summary of the PCM incorporated mortars considering binder type, PCM properties, the objective of the study, and remarks.

Binder(s)	**PCM properties**	**Objective**	**Remarks**	**Ref.**
OPC	Microencapsulated T_m: 10-28℃	Development of hybrid PCM mortars by combining more than one type of PCM	Incorporating many PCM types into plastering mortars has demonstrated a promising performance capability.	[47]
OPC Lime Gypsum	Microencapsulated T_m: 23℃	The microstructure of different mortars investigated considering heat storage efficiency	The macroporosity of lime-based mortars reduced drastically with the addition of PCMs; thus, mechanical strength increased. However, the mechanical strength of cement composites were reduced with increasing PCM amount. In addition, the heat storage capacity of mortars decreased due to internal porosity.	[48]
OPC	Microencapsulated T_m: 25℃	Cement/PCM mortars were prepared with textile to examine mechanical and physicochemical properties	In the presence of microencapsulated PCM, the ductile mechanical behavior of textile reinforcement composites is preserved; PCM rate.	[49]

Table 4 (Cont'd)

CEM I 52.5R	Microencapsulated T_m: 25℃	Novel cementitious mortars were prepared to be used as building envelope component	The potential for energy storage increases as PCM is added; however, the thermal inertia creates a limitation because of the corresponding decline in thermal conductivity and density.	[50]
Type I PC	Direct incorporation Immersion T_m: -0.5 to 4.5℃	The thermal behavior of cement mortar containing PCMs for building applications was investigated.	The lowest specimen temperature was increased with increasing PCM content as the latent heat capacity of the composite is directly proportional to the PCM content.	[51]
Cement Fly ash	Direct incorporation T_m: -0.5 to 4.5℃	Different mortar formulae were developed with direct incorporation of PCMs; physical, mechanical, and thermal properties were investigated	The inclusion of PCM at 5% and 10% had no noticeable effects. However, a higher PCM percentage results in a more significant drop in mechanical strengths as water content increases due to direct incorporation. Furthermore, adding 20% of PCM resulted in higher thermal performance.	[28]
OPC	Shape-stabilized T_m: 36.5℃	Aggregates for thermal energy storage were utilized to create mortar for wall plastering.	The compressive strength of the PCM-incorporated mortar was reduced by 71% compared to the control mortar.	[52]

Table 4 (Cont'd)

OPC	Shape-stabilized T_m: 23℃	To create a form-stable PCM composite, recycled expanded glass aggregate was creatively employed as a PCM carrier.	The mechanical strength of the mortar was reduced due to the porous structure and lower strength of PCM. The thermal performance test showed that the cement mortar incorporated composite had a significantly higher specific heat capacity and a lower heat transfer rate.	[53]
Clay GGBFS	Immersion T_m: 35.6℃	Investigated clay geopolymer mortars with PCM addition	Clay geopolymer mortar containing has a compressive strength of 8.0 MPa and a heat conductivity coefficient of 0.46 W/mK.	[54]
Class F FA	Microencapsulated T_m: 28℃	Experimental investigation of PCM-incorporated alkali-activated geopolymer	The compressive strength and thermal conductivity of the composites decreased with PCM incorporation.	[13]
OPC GGBFS	Microencapsulated T_m: 27.7℃	Micro-encapsulated PCM and carbon fiber were added to alkali-activated slag composites for energy storage.	The thermal conductivity of the composited with both cement and slag decreased with PCM addition. It was also observed that the presence of carbon fiber enhanced the thermal conductivity of the composites due to its high thermal conductivity.	[55]

Table 4 (Cont'd)

Red-mud	Microencapsulated T_m: 26°C	Expanded graphite/paraffin-based PCM was prepared to be used in red-mud geopolymer composite	The thermal analysis supports the mechanical and chemical stability of the PCM and expanded graphite within the geopolymer composite. The thermal conductivity of the composite was 2.46 W/mK.	[56]
FA OPC	Microencapsulated T_m: 26°C	Investigation of PCM-incorporated alkali-activated FA composites in terms of mechanical properties and cost analysis	FA-based alkali-activated mortars' compressive strength reduced drastically after adding PCMs due to the increased water porosity; however, mortars showed higher compressive strength after exposure to high temperatures.	[57]

As seen in Table 3, different cementitious materials such as ordinary Portland cement, lime, gypsum, and alkali-activated binders were tried to be used in combination with PCMs with varying encapsulation techniques and various melting temperatures considering the impact of climate conditions. The results mainly show that the mechanical strength of the binder reduces with increasing PCM content due to micropores and the low compressive strength of PCMs. In addition, thermal energy storage capacity increases with increased PCM content. However, the latent heat capacity does not constantly improve with PCM content as micropores formed after PCM addition can affect the heat transfer mechanism inside the composites. Similarly, the thermal conductivity of the mortar reduces with PCM incorporation for two reasons: lower thermal conductivity of PCM/shell and micropores that directly affect the heat transfer.

Although different binders show similar behavior in terms of mechanical strength development and thermal storage capacity when incorporated with PCM, the advantages and disadvantages of various mortars that utilize cement, lime, and geopolymers in combination with PCMs are summarized in Table 5.

Table 5. Advantages and disadvantages of Portland cement mortar, lime mortar, and geopolymer mortar in combination with PCMs [46]

	Advantages	**Disadvantages**
Portland cement mortar	* Availability of standard code for mortar mix design * High rate of carbonation * Enhanced thermal inertia with PCM incorporation	* Non-environmentally friendly * Reduction in compressive strength with PCM incorporation
Lime mortar	* Improved mechanical and thermal properties * Enhanced thermal inertia with PCM incorporation	* Less heat of fusion compared to Portland cement mortar * Slow carbonation * High porosity
Geopolymer mortar	* Stability at high temperatures * Cheaper raw material * Compatible with PCM * Adequate thermal and mechanical properties for building applications	* No standard code for mix design * Availability of raw materials * Suitability of raw materials

The studies investigating the Portland cement mortar with PCM incorporation showed that good mechanical and thermal properties could be achieved for energy-saving applications in buildings; however, geopolymer composites that utilize geopolymers in combination with PCMs have been gaining attention due to environmental concerns. In the next part of the review, studies on PCM-incorporated

geopolymers will be investigated in detail, considering the mechanical and thermal performance of the composites. Table 6 summarizes the properties of the geopolymer composites

Table 6. Properties of geopolymer composites

Materials	**Activator**	**PCM properties**	**PCM amount**	**Test methods**	**Ref.**
Class F FA	NaOH	T_m: 28°C C_p : 180-195 J/g Mean particle size: 17-20 μm	0, 5, 10, and 20% replacement by the same volume of sand	UCS test SEM DSC Thermal test	[13]
Red-mud Quartz sand	Na_2SiO_3 NaOH	T_m: 26°C C_p : 127-131 J/g	30% replacement by volume	UCS Thermal conductivity Thermal testing DSC	[56]
Clay BFS	Na_2SiO_3 NaOH	T_m: 32-36°C C_p : 158.1 J/g	30% replacement by volume	UCS SEM DSC Thermal conductivity	[54]
FA GGBS	Na_2SiO_3	T_m: 23°C C_p : 81.2 J/g	15% and 30% wt% replacement of the binder	FT-IR TGA DSC UCS SEM	[58]
Class F FA GGBFS	Na_2SiO_3 NaOH	T_m: 24 and 28°C C_p : 98.1 and 96.1 J/g	0, 10, and 20% replacement by the same volume of sand	UCS SEM X-ray microCT Energy saving Setting time Slump test	[59]
GGBFS FA Dune sand	Na_2SiO_3 NaOH	T_m: 28-33.8°C C_p : 124.1 J/g	25, 50, and 75% replacement by the same volume of sand	U-value test UCS	[60]

In their study, [13] created geopolymer composites with PCM incorporation. They utilized class F FA, fine aggregate, and a sodium hydroxide (NaOH) solution with a 9 M concentration as an alkaline activator. The mPCM utilized in the study has a melting point of 28 ° C. and a fusion heat of 180-195 J/g. Using a mixer, the fly ash and sand were combined for three minutes to achieve homogeneity; the NaOH solution was added, and the mixture was combined for five minutes; finally, the PCM was added, and the mixture was added was combined for two minutes. The PCM was added as the final component at the conclusion of the mixing procedure to reduce PCM degradation induced by mixing. Using three different ratios, they replaced PCM with the same volume percentage of sand: 5%, 10%, and 20%. In order to assess the effect of cold and hot curing settings on the performance of the composites, mortars were also cured in air and an oven at 60°C. Their findings reveal that cold and hot specimens containing the same amount of PCM differ somewhat in compressive strength and thermal characteristics. In line with the literature, the compressive strength of the specimens diminishes with increasing PCM content; for example, 20% PCM replacement resulted in a 35% loss in compressive strength at 28 days compared to the control mix. As illustrated in Figure 6, the number of broken particles on the failure plane became evident due to PCM's low shear strength and stiffness.

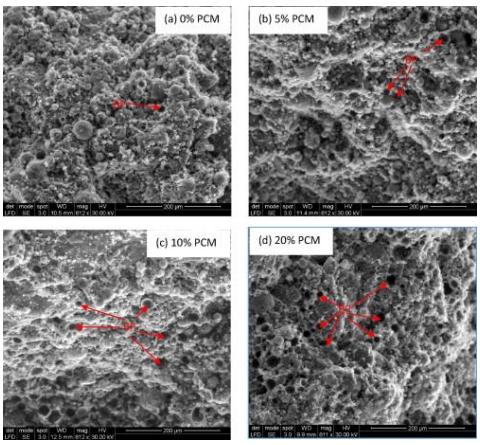

Figure 6. SEM images of the mixes containing a) 0%, b) 5%, c) 10%, and d) 20% PCM, respectively [13]

The DSC results showed that an endothermic peak for the composites was observed for 10 and 20% PCM incorporation; however, no peak was apparent for 5% PCM incorporation because the effect of PCM in the composite could be achieved for PCM amounts higher than 10%. As expected, the specific heat capacity of the composites increased from 0.6 J/g ℃ to 0.7 J/g ℃ for geopolymers containing 10% and 20% PCM, respectively.

Afolabi et al. [56] investigated the properties of PCM-incorporated red-mud geopolymer composites for building applications. They used quartz sand and red-mud with a ratio of 5:1 and 7.5 M NaOH with 1.5 M sodium trisilicate solution for the geopolymer activation. The PCM composite was prepared using paraffin/expanded graphite as the core and $CaCl_2$/sodium silicate as the shell, and they adopted hot and cold curing conditions to see the effect of phase transition on the final properties of the composite. Their results showed that the 25-day compressive strength of the composite increased with the PCM ratio as 20% PCM incorporation resulted in 8.1 MPa, whereas the compressive strength of the control specimen was only 6.3 MPa, and applying hot and cold curing conditions had no significant effect on the mechanical results. The thermophysical analysis showed that PCM geopolymer composite had a specific heat of 2.18 MJ/m^3K, whereas expanded graphite encapsulated PCM had a specific heat capacity of 1.01 MJ/m^3K. It should be pointed out that this result is not consistent with the literature because the heat capacity of the expanded graphite encapsulated PCM was expected to be higher than of geopolymer's heat capacity. The study's authors concluded that the 23% decline in the specific heat was due to the influence of other additives within the geopolymer composite, and no further explanation was included. In terms of thermal conductivity, they reported that using expanded graphite in combination with PCM increased the already low thermal conductivity of the paraffin by 90%, in line with the existing literature, and they stated that the enhanced regenerative ability of paraffin during the solid-to-liquid-to-solid phase transformation could contribute to the thermal improvement of the red clay geopolymer composite. Incorporating

polymer additives decreased the heat conductivity of the composite by 22% as compared to red mud.

In a similar study, Wang et al. prepared a PCM-incorporated geopolymer using clay, blast furnace slag, and a mixture of water glass and NaOH solution as alkaline activators by keeping the water-to-binder ratio at 0.12. Besides, they prepared paraffin/expanded perlite-based PCM composites to be used in the geopolymer composite. The PCM was added as a 30% volume replacement of sand. The thermal conductivity measurement showed that the heat conduction coefficient was decreased from 0.62 W/mK to 0.46 W/mK when paraffin/expanded perlite PCM was added to the geopolymer.

2.3 Thermal conductivity enhancement of cement

The incorporation of PCM into cement matrix increases the heat storage capacity of the cementitious composites, thus, providing an opportunity for heat storage applications in building applications. The thermal conductivity of PCM-incorporated cement-based systems is a crucial transport property that directly reflects the heat transfer rate [61]. In addition to melting temperature and energy density governed by the specific heat of fusion, the thermal conductivity of the PCM composite influences the overall efficiency of the melting or solidification process. However, the PCM's low thermal conductivity inhibits heat flow across the matrix, preventing the activation of PCM's latent heat. Inadequate solidification of PCMs throughout the night, for instance, limits their maximum heat storage capacity the following day, as they stay liquid and cannot absorb heat. In addition, the heat released during phase shift cannot be effectively utilized if the thermal conductivity of the matrix is insufficient for effective heat transfer.

Liu et al. [61] showed that the PCM-incorporated cementitious materials' thermal conductivity is directly dependent on the packing density of C-S-H particles at the nano-scale, increasing the packing density of C-S-H results in better thermal

conductivity. At the micro-scale, the thermal conductivity of the cement paste matrix is highly dependent on the water content. At w/c = 0.4, the thermal conductivity of the cement paste matrix is about 1.5 times the thermal conductivity when the matrix is dry. Likewise, the thermal conductivity of the PCM composite increases as PCM saturation increases. Furthermore, PCM incorporation decreases the total thermal conductivity of the composites at the mesoscale.

Past experimental studies on the PCM incorporated cement-based composites showed that adding PCM drastically reduced the thermal conductivity of the composites. Ricklefs et al. [62] stated that the thermal conductivity of both cement mortar and cement paste stayed constant between 10 and 50 °C and dropped as the volume fraction of mPCM increased. Due to the presence of quartz grains, it was greater for cement mortar composites (1.2–1.8 W/mK) than for OPC paste (0.8–1.2 W/mK) with the same PCM volume fraction. Xu and Li [63] found that the thermal conductivity of the composite decreases as the PCM replacement level increases. Compared to the control mix, the reduction of thermal conductivity for 10, 15, 20, and 30% replacement of PCM are 13.8%, 21.0%, 26.2%, and 33.6%, respectively. Shen et al. [38] concluded that adding 2 wt% and 4 wt% PCM reduced the thermal conductivity by 15.76% and 20% compared to pure concrete. Similarly, Hunger et al. studied the influence of phase change materials (PCM) on the thermal conductivity of concrete and discovered that the thermal conductivity of concrete was lowered by 14.7%, 32.4%, and 38.2%, respectively, when mixed with 1%, 3%, and 5% PCM.

In order to overcome the low thermal conductivity after PCM incorporation, the thermal conductivity of the matrix can be enhanced using thermally conductive fillers such as metal nanoparticles or different dimensional carbon materials like graphite, graphene, or carbon nanotubes. It should be noted that for low quantities of conductive additives, the space between conductive additive particles remains large if the percolation threshold is not reached. Due to this, the additives do not form a conductive network throughout the matrix, and the cement matrix's conductivity dominates the composite's thermal conductivity. In contrast, when the conductive

additive level is higher than the percolation threshold, the particles come into contact, and a well-developed conducting network forms within the cement matrix. In this circumstance, the conductivity of composites is mainly determined by the conductivity of conductive fillers.

In literature, several studies investigated the effect of conductive fillers on the conductivity enhancement of different cementitious materials. In their research, Jing et al. [64] used reduced graphene oxide (rGO) to improve the thermal properties of cement paste composites to control the generation of thermal cracks. rGO is produced by reducing graphene oxide, which has a multilayer structure with nanometer-scale thickness and micrometer-scale diameter. Although rGO's qualities cannot be compared to those of graphene due to residual functional groups, rGO possesses desirable features such as low cost and excellent heat conductivity, which could reach 1390 W/mK. Their results showed that the addition of 1.2% rGO increased thermal conductivity and thermal diffusivity coefficient by 7.8% and 29% compared to the control cement paste (Figure 7), respectively. Furthermore, using rGO increased the compressive strength at early age and did not effect the strength at 28 days.

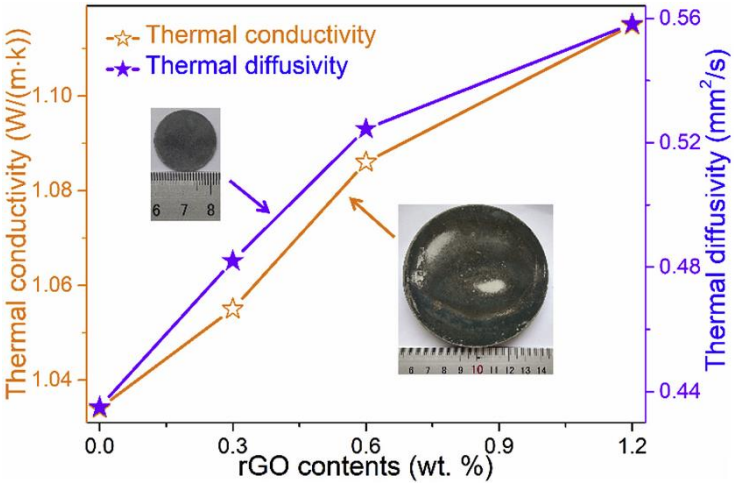

Figure 7. The thermal conductivity and thermal diffusivity of cured cement paste modified with rGO [64]

Phrompet et al. [65] investigated the thermal properties of rGO-nano C3AH6 incorporated cement composites for smart building applications. They changed the rGO content between 1 and 4 wt% of the cement. The results showed that the thermal conductivity of the composites increased significantly with 1 wt% addition of rGO by 350% compared to C3AH6; however, increased rGO content reduced the thermal conductivity, although 100% enhancement still obtained with 4 wt% rGO addition. In a similar research, Zhai et al. [66] prepared rGO-added OPC mortar. Their results showed that the sample's thermal conductivity increased significantly initially and then tended to stabilize as the rGO level increased. In addition, when the rGO level reached 1.00 wt%, the sample's thermal conductivity rose by 23% to 0.77 W/mK compared to the standard sample. However, the thermal conductivity did not increase when the rGO concentration reached 2% and 4%, as seen in Figure 8.

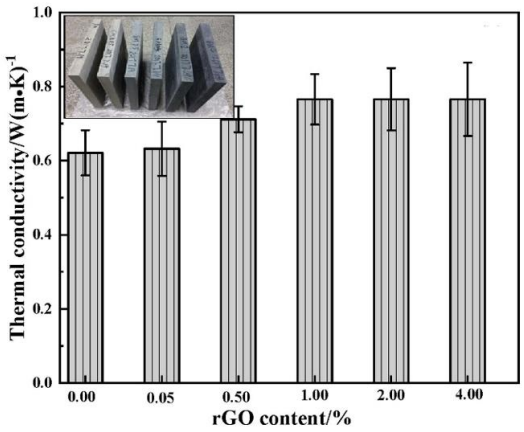

Figure 8. The thermal conductivity of samples of cement mortar with varying amounts of rGO [65]

Ghosh et al. [67] developed thermoelectrically enhanced cement composites with graphene and ZnO nano inclusions for energy storage in smart building applications. They utilized graphene nanoplatelets and ZnO nanoparticles by 5, 10, and 15 wt% of cement to increase the thermoelectrical characteristics of the composites. Thermal diffusivity measurements revealed that the composite with the highest wt% of graphene and ZnO has the highest thermal diffusivity, while the composite with no

graphene and ZnO has the lowest thermal diffusivity. They stated that thermal diffusivity result was expected because the inclusion of a high quantity of graphene in the composite facilitates the formation of a conductive network, allowing heat to permeate the composite with ease, increasing its thermal diffusivity. In addition, the average value for thermal conductivity was obtained as 0.69, 0.62, 0.99, and 0.92 W/mK for cement, 5, 10, and 15 wt% rGO-ZnO additions, respectively. They concluded that the thermal conductivity was decreased with increased rGO content due to the fact that phonons are primarily responsible for heat conduction in graphene, and high phonon scattering in cement matrix with increasing thermal resistance might reduce the thermal conductivity.

Wei et al. [68] investigated the thermoelectric properties of expanded graphite/cement-based composites for large-scale energy applications in buildings. They employed expanded graphite considering 5, 10, and 15 wt% of cement in the composites. Thermal conductivity results showed that the increased content of expanded graphite increased the thermal conductivity of the samples up to 130% compared to the control sample due to the fact that the thermal conductivity of cement-based composites is proportional to C-C sp3 concentration, density, or phonon scattering. It should also be noted that the compressive strength of the samples decreased with increasing expanded graphite content, as shown in Figure 9.b. The decrease in compressive strenth can be attributed to the higher apparent porosity and low compressive strength of expanded graphite.

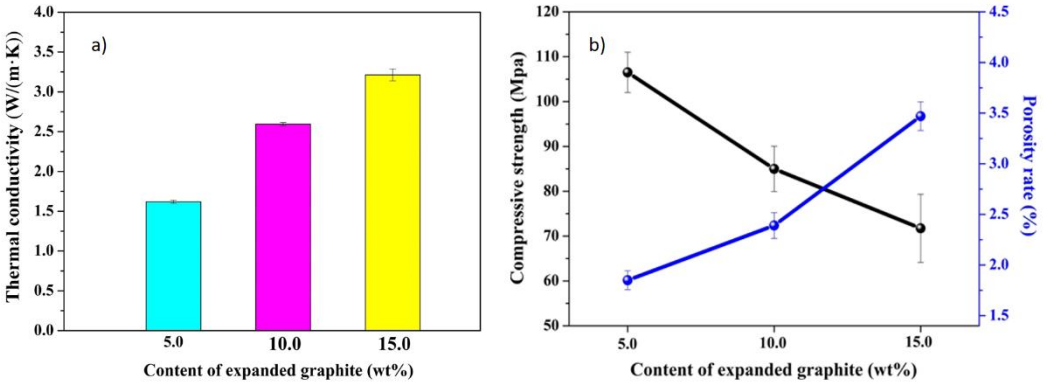

Figure 9. a) Thermal conductivity and b) compressive strength results of expanded graphite/cement-based composites containing 5,10, and 15 wt% expanded graphite [68]

In a similar study, Wei et al. developed carbon nanotube (CNT) reinforced cement composites with weight percentages of 5,10, and 15% of cement. The thermal conductivity of the samples was increased with increasing CNT content similar to other carbon materials such as rGO, graphene, and expanded graphite. However, they concluded that the high porosity of composites containing 5% CNTs increased phonon scattering and slowed the rise of thermal conductivity. Song et al. investigated the thermal conductivity enhancement of cement for geothermal well applications. They utilized powdered graphite, ferrum, and copper as thermally conductive materials. The results showed that adding 5% graphite, 20% ferrum, and 20% copper particles to cement paste increased its thermal conductivity by 20%, 19%, and 29%, respectively.

So far, investigations on thermal conductivity enhancement of cement matrix by conductive fillers are mainly conducted in order to improve thermoelectrical characteristics of cementitious composites considering smart building applications. However, limited studies examine the matrix's thermal conductivity enhancement when PCM is incorporated.

In their study, Xiong et al. [17] examined the effect of graphite nanoplatelets in PCM-incorporated cementitious composites for better heat transfer performance. They used OPC (CEM I 52.5 N) and styrene/n-eicosane-based PCM. They incorporated both mPCM and graphite nanoplatelets into cement paste. mPCM

content changed between 5 to 15 wt% cement, and graphite nanoplatelets were added between 1 to 5 wt% cement. The thermal conductivity results showed that the thermal conductivity of the cement paste decreased by 40% (0.865 W/mK to 0.525 W/mK) when 15% PCM was incorporated. However, utilizing 5 wt% graphite nanoplatelets increased the thermal conductivity of the composite by 40% (0.865 W/mK to 1.218 W/mK) compared to the control mix.

The results demonstrated that composites' storage and release rates were increased by up to 25.3% and 23.3%, respectively. In addition, as the PCM concentration rose, the effect of adding 5% GP on the composite's heat transfer performance improved. In addition, they observed that the inclusion of graphite nanoplatelets alters the hydration process of cement samples, which may influence the mechanical properties of the samples. However, they did not further comment on the mechanical properties of the composites; thus, the suitability of the developed cement composites for building applications in terms of mechanical performance is not detailed in this study. In another study, Gu et al. investigated the thermal properties of a shape-stable PCM cement panel when graphene is added to the matrix as a conductive filler. Their results showed that the heat conductivity rose significantly with increasing graphene content. Pure PCM has a thermal conductivity of only 0.32 W/mk. The thermal conductivity increased to 1.13 W/mK after incorporation into pure cement. The thermal conductivity continued to improve as graphene was added, with values of 1.50, 1.67, 1.85, 1.96, and 2.05 W/mK for 0.5, 1, 1.5, 2, and 2.5 wt% graphene addition, respectively.

In addition, a lab experiment was conducted to determine the impact of thermal conductivity improvement on the energy-saving efficiency of the PCM panel. Because of the low thermal conductivity, the cement panel with PCM alone could not absorb the comparatively significant heat flow from the exterior. The increase in thermal conductivity caused by the addition of graphene to the cement matrix improves its capacity to store heat.

Consequently, the cement panel, including graphene and PCM, can absorb more heat flux than the panel without graphene, further reducing interior temperature. Notably, as graphene continued to be added, the test chamber's interior temperature began to climb. This is because the extra graphene increased the thermal conductivity of the composite, which increased the total heat flow into the test chamber and consequently increased its overall temperature.

2.4 Nanoseed activation of geopolymers

Alkali activation or geopolymerization refers to the reaction of a solid aluminosilicate under alkaline environments to generate a hardened binder composed of hydrous alkali-aluminosilicate and/or alkali-alkali earth-aluminosilicate phases [69]. As a result of the alkali activation process, poorly crystallized aluminosilicate gel is formed as the major hydration product. Alkaline activators in alkali-activated cements and concretes can be classified as caustic alkalis (MOH), non-silicate weak acid salts (M_2CO_3, M_2SO_3, M_3PO_4, etc.), silicates ($M_2O.nSiO_3$), aluminates ($M_2O.nAl_2O_3$), aluminosilicates ($M_2O.Al_2O_3.(2\text{-}6)SiO_2$), and non-silicate strong acid salts (M_2SO_4). Among all, NaOH, Na_2CO_3, NaO. $nSiO_2$ and Na_2SO_4 are the most accessible and cost-effective activators [70].

Various aluminosilicate source materials such as fly ash (FA), slag, kaolin, metakaolin, rice husk ash and have been utilized with an alkaline activator to produce geopolymers. Among all aluminosilicate source materials, FA and GGBFS are the most studied materials utilized as geopolymers [69]. FA is a by-product of thermal power facilities that burn coal with particles ranging in size from 0.2 to 200 μm. The particle size range of any specific FA is mostly determined by the fineness of the pulverized coal and the type of collection equipment utilized at the thermal power plant. The types and relative proportions of mineral matter found in the coal used influence the chemical composition of FA [71]. More than 85 percent of the majority of FA is composed of silica (SiO_2), alumina (Al_2O_3), iron oxide (Fe_2O_3), lime (CaO), and magnesia (MgO). On the other hand, slags are by-products of pyrometallurgical

processes in the metal and alloy industries. The compositions of the slags depend on the manufacturing procedure and the materials utilized; the chemical composition of steel slag differs from batch to batch, even within the same facility, depending on the type of raw materials used, the type of steel produced, and the furnace conditions. CaO (35–40%), SiO_2 (25–35%), MgO (5–10%), and Al_2O_3 (5–15%) are the predominant components of slag, while S, Fe_2O3, MnO, and K_2O (less than 1%) are its minor constituents. Slag contains both network-forming anions $(SiO_4)^{4-}$, $(AlO_4)^{5-}$, and $(MgO_4)^{6-}$ as well as network-modifying cations Ca^{2+}, Al^{3+}, and Mg^{2+} [71].

Numerous alkali-activated cements have been utilized in recent decades. On the basis of the composition of respective cementitious components (the $CaO\text{-}SiO_2\text{-}Al_2O_3$ system), alkaline cement can be categorized into two broad groups: high calcium and low calcium cementCalcium and silicon-rich materials, such as blast furnace slag ($SiO_2 + CaO > 70\%$), are activated in high calcium systems. In this context, the main reaction product is a C-A-S-H (calcium silicate hydrate) gel with Al incorporated into its structure, comparable to the gel created during the hydration of Portland cement. [72]. In low-calcium cement, aluminum and silicon-rich materials like type F FA or metakaolin are used. In this instance, the primary reaction outcome is a three-dimensional inorganic alkaline polymer, an N-A-S-H gel (or alkaline aluminosilicate hydrate). It should be noted that high calcium and low calcium cement can be used in combination with or without OPC to produce different blends. As a result, a mixture of cementitious gels, including C-A-S-H and (N,C)-A-S-H can be obtained. The reaction mechanism of geopolymerizaton that forms (N,C)-A-S-H gel is given by the following [72]:

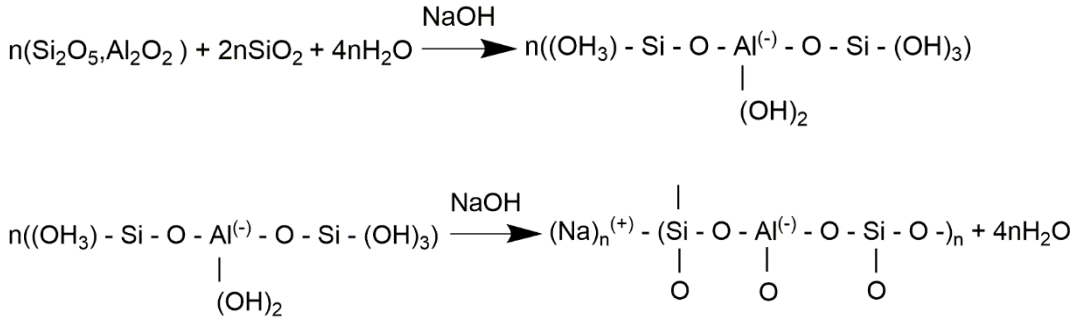

Usually, the geopolymerization procedure is approximated by the following oversimplified conceptual reactions: (1) The raw ingredients are dissolved in alkaline solutions, such as NaOH, to liberate the reactive aluminate and silicate monomers; (2) the aluminosilicate oligomers polymerize in the alkaline environment to create geopolymer gels. Due to the charge shortage of Al, which has a charge of 3+ compared to Si charge of 4+, Na or K cations are required to balance the presence of Al. During the dissolution of raw materials, water is consumed and released during the polymerization processes [73]. The 3D molecular representation of the N-A-S-H gel is given in Figure 10.

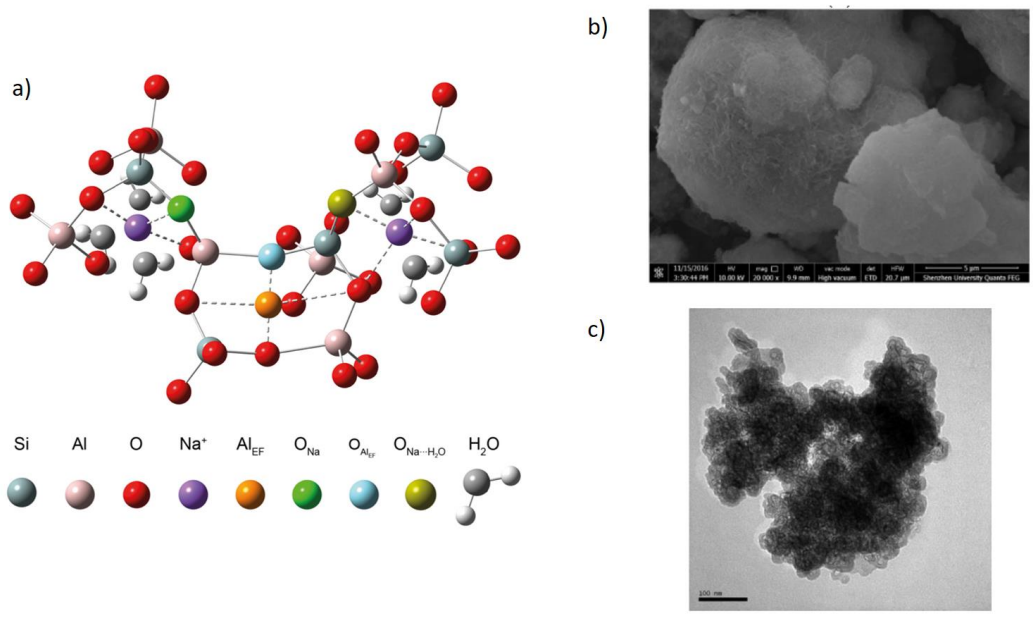

Figure 10. 3D representation of a polymerized portion of N-A-S-H gel with each species, Al_{EF} represents $Al(OH)_2$ or $Al(OH)^{2+}$ [74], b) SEM and c) TEM images of N-A-S-H system products [75]

Although geopolymers possess significant advantages such as reducing carbon footprint by reusing industrial by-products and having adequate durability and mechanical strength to be used as an alternative construction material, it is also known that geopolymers have a slightly high price, which is primarily attributable to the utilization of alkali or alkali-silicate. In addition, alkali concentration is an extremely critical component for geopolymerization, which is directly related to the development of strength and is even more relevant than curing temperature [76]. As a result, high alkali content may be required to produce geopolymers with desirable mechanical properties.

To reduce the amount of alkali activator used for the activation process, researchers have tried combining nanoparticles with geopolymers to enhance the durability and mechanical properties. The employment of nanoparticles in cementitious systems aims to improve the plastic and hardened material's properties. Filling the spaces between the cement grains and micro and nano-sized particles provide a filler effect. Due to the decreased capillary porosity, a higher packing density with the proper composition results in lower water demand of the mixture and also increases strength.

Several nanoparticle types are utilized in the cement industry, such as nano-SiO_2, nano-$Al2O_3$, nano-TiO_2, nano-clays, carbon-based materials like graphene nanoplatelets, and so on [77]. It should also be noted that the overall amount of nanoparticles in cementitious systems is too small that the total cost of geopolymers could be lowered by achieving equal strength and better performance by reducing the alkali activator dosage.

Table 7 summarizes the studies on the effect of nanoparticle addition on geopolymer mortars.

Table 7. Studies on different nanoparticles in geopolymer mortars

Binder	**Activator**	**Nanoparticle**	**Nanoparticle amount**	**Major Findings**	**Ref.**
Class F FA	Na_2SiO_3 NaOH	Nano-SiO_2	4%, 6%, 8% and 10% wt% of FA	*Due to the increased rate of alkali activation, the compressive strength of geopolymer mortars with or without nano-SiO_2 is enhanced at higher molar concentrations. *Beyond 6% nano-SiO_2 addition, a decrease in compressive strength is observed at all ages.	[78]
FA	Na_2SiO_3 NaOH	Nano-SiO_2	6% wt% of FA	*Nano-silica does not affect flexural performance compared to its effect on compressive performance. *At all ages, the compressive strength of specimens containing nano-SiO_2 was greater than that of specimens without nano-SiO_2	[79]

Table 7 (Cont'd)

Low calcium FA GGBFS OPC	Na_2SiO_3 NaOH	Nano-SiO_2	2 wt% of FA	*Due to nanosilica's high specific surface, the flow of freshly-mixed mortars rapidly dropped as its concentration increased. *The sorptivity of samples containing 2% nano- SiO_2 was lower than the control sample.	[80]
FA GGBS	Na_2SiO_3 NaOH	Nano-SiO_2	4%, 6%, 8% and 10% wt% replacement of GBFS	*The mixture containing 5% nano-silica instead of GBFS had the greatest elasticity modulus and compressive strength. *It was determined that the production of microstructures and dense gels (N,C-(A)-S-H) in mortars with less than 10% nano-silica was enhanced.	[81]
GGBS	Na_2SiO_3 NaOH	Nano-SiO_2	1 and 2 wt% of binder	*The impact of nano- SiO_2 on the strength of composite was minimal. *Nanoparticles have a negligible effect on flexural tensile strength.	[82]

Table 7 (Cont'd)

Class F FA GGBFS	Na_2SiO_3 NaOH	Nano-SiO_2	1, 2, 3, and 4 wt% of binder	*Compared to geopolymer mortars without nano-silica, geopolymer mortars containing nano-silica exhibit poor workability. Flow reduction is around 4.1%, 8.4%, 14.4%, and 21.3% for mixtures containing *Adding 1% nano-silica increases compressive strength by 30% and flexural strength by 33%. 1%, 2%, 3%, and 4% nano silica, respectively.	[83]
GGBFS Silica Fume	Na_2SiO_3 NaOH	Nano-SiO_2	2 and 4 wt% of GGBFS	*Due to nano-silica's high reactivity, nano-SiO_2 improved the flowability, compressive strength *More than 2% nano-silica addition to mortars did not result in additional strength increases.	[84]
Class F FA	Na_2SiO_3 NaOH	Nano-SiO_2 Nano-TiO_2	2 wt% replacement of FA	*Nao particles increases the geopolymers' strength by 17.38%-10.49%	[85]

Table 7 (Cont'd)

GFS	Na_2SiO_3 NaOH	nano-MgO nano-TiO_2	1, 3, and 5 wt% of GFS	*The ratio of flexural strength to compressive strength for mixes including nano-MgO/nano-TiO_2 is approximately 13 to 15 percent, which is greater than the ratio for control samples (12.4%).	[86]
FA	Na_2SiO_3 NaOH	nano-TiO2	5 wt% of FA	*After 28 days of curing, geopolymer mediated by 30 nm TiO_2 nanoparticles exhibited the highest compressive strength (53 MPa) and split-tensile strength (6.8 MPa).	[87]
Perlite	Na_2SiO_3 NaOH	nano-Al_2O_3 nano-CaO	1, 2, and 3% replacement of perlite	*Nano-CaO lowered compressive strength, whereas nano-Al_2O_3 improved strength.	[88]
Class F FA	Na_2SiO_3 NaOH	nano-$CaCO_3$	1,2, and 3 wt% of binder	*Compressive strength of the geopolymer, including nano-$CaCO_3$, were higher.	[89]

As seen from the Table 7, the most studied nanoparticle to enhance the performance of geopolymer mortar composites is nano-SiO_2, which has shown that nano-silica

accelerates hydration/polymerization events and improves microstructural and mechanical qualities. Its direct impacts on alkali-activated binders were accelerated hydration, refined microstructures, and improved mechanical characteristics [90]. Besides nano-SiO_2, nano-TiO_2 has received a growing interest in cementitious materials due to its unique features. Under ultraviolet light and humidity, titanium dioxide (TiO_2) decomposes various organic and inorganic air contaminants, resulting in cleaner air and improved human health [90]. Moreover, adding nano-titanium to concrete mixtures accelerates cement hydration and increases concrete durability by decreasing water permeability [87].

Since incorporating PCMs into cementitious composites results in lower strength values, the addition of nanoparticles, especially nano-SiO_2, and nano-TiO_2, could be considered potential candidates to enhance mechanical properties while developing geopolymer composites for energy harvesting applications. In this regard, the effect of nano-SiO_2 and nano-TiO_2 on the mechanical as well as thermal properties of PCM-integrated geopolymer composites is an understudied area and will be investigated further in this work.

2.5 Numerical modeling of PCM-integrated building materials

PCMs for building applications are defined by their phase change characteristics; therefore, the formation or melting processes of PCMs inside the matrix should be considered when the phase change occurs. In this specific case, the so-called Stefan problem for heat conduction explains the progression of the boundary between the two phases of a material experiencing a phase change, such as the melting of ice into the water can be utilized.

The following describes the governing equations for the PCM heat conduction problem for both solid–liquid (melting) andl iquid–solid (solidification) transitions. In the classical approach to the Stefan problem, the physical problem is supposed to be a conduction-based problem with a constant latent heat capacity (L), a constant

PCM melting temperature (T_m), a zero-thickness interface of the sharp surface front (i.e., no mushy transition zone is considered), and the nucleation and supercooling phenomena of the PCM are ignored. The mathematical model can be expressed by Eqns. (1), (2), and (3), given certain assumptions [91].

$$\rho C_S \frac{\partial T_S}{\partial t} = \nabla.(\lambda_S \nabla T_S) + \dot{q}_{v,S} \quad \forall x \in A_S \tag{1}$$

$$\rho C_L \frac{\partial T_L}{\partial t} = \nabla.(\lambda_L \nabla T_L) + \dot{q}_{v,L} \quad \forall x \in A_L \tag{2}$$

$$(\lambda_S \nabla T_S).\boldsymbol{n} - (\lambda_L \nabla T_L).\boldsymbol{n} = \rho L \frac{d\boldsymbol{x}}{d\boldsymbol{t}}.\boldsymbol{n} \quad \forall x \in A_I \tag{3}$$

Heat transfer problem in solid (S), liquid (L), and interfacial zone (I) is described by Equations (1), (2), and (3), respectively. In these equations, ρ represents density , λ is the thermal conductivity, C is the specific heat capacity, T is the temperature, and $\dot{q}$ is the heat source term. Furthermore, **n** represents the unit normal vector, $\frac{d\bar{x}}{dt}$ is the velocity of the interfacial zone where t represents the time [91].

Noting that the natural convection term might be incorporated while solving the heat conduction problem, the so-called Navier-Stokes equation should be used to solve the governing equations for the convective heat in a transient analysis of a PCM melting process. However, since cementitious composites contain a mere fraction of PCMs compared to the whole thermal system, only the conduction mode can be evaluated, which avoids the difficulty of simulating the natural convection flow in the mushy and liquid phases [91]. On the other hand, convection term and buoyancy force on the PCM can be considered to understand the heat transfer mechanism in PCM-integrated cementitious composites on a micro-scale. Therefore, the basic

equation of the heat conduction problem (Eqn 4) can be applied to PCM-integrated construction materials for macro-scale analysis.

$$\frac{\partial H}{\partial t} = \nabla.(\lambda \nabla T) + \dot{q}_v \quad \forall x \in A \tag{4}$$

In Eqn. (4), H represents the enthalpy of the system, λ(x,t) is the thermal conductivity of the material depending on both the temperature T and the position x, and $\dot{q}$ is the heat source term.

In order to solve the Eqn. (4), where T is temperature, q is the heat flux, h is the natural heat convection coefficient, and T_∞ is the temperature of the environment., Eqns. (5) and (6) can be applied as initial and boundary conditions:

$$T(x, t = 0) = T_0(x) \tag{5}$$

$$T(x, t) = T \tag{6}$$

$$(\lambda \nabla T).\boldsymbol{n} = q \tag{7}$$

$$(\lambda \nabla T).\boldsymbol{n} = h(T_\infty - T) \tag{8}$$

If the system is composed of two or more phases, such as solid, liquid, and mushy regions, Stefan conditions should be applied to solve the phase change problem.

For a thermal system containing a phase-changing region, three approaches could be applied for the solution of Eqn. (4): enthalpy-based, apparent heat capacity, and heat source methods.

2.5.1 Enthalpy-based method

In this method, the enthalpy of the system (H) is defined by Eqn. (9) and inserted into Eqn (4).

$$H(T) = \int_{T_{ref}}^{T} \rho C(T) dT \tag{9}$$

where ρC(T) is the volumetric heat capacity and T_{ref} is the reference temperature.

If the isothermal phase change is assumed, in other words, only solid and liquid phases are considered, and the mushy region, in which solid and liquid phases occur simultaneously, is ignored, Eqn. (8) can be expressed by Eqn (10):

$$H(T) = \begin{cases} \int_{T_{ref}}^{T} \rho C_{sol}(T) dT & when\ T \leq T_m \\ \int_{T_{ref}}^{T_m} \rho C_{sol}(T) dT + \rho L + \int_{T_m}^{T} \rho C_{liq}(T) dT & when\ T > T_m \end{cases} \tag{10}$$

However, if the mushy region is included, Eqn. (10) should be taken into account in the solution as in Eqn. (11).

$$H(T) = \begin{cases} \int_{T_{ref}}^{T_{sol}} \rho C_{sol}(T) dT & when\ T \leq T_{sol} \\ \int_{T_{sol}}^{T_{liq}} \rho C_{sol}(T) dT + \rho L f(T) & when\ T_{sol} < T < T_{liq} \\ \int_{T_{ref}}^{T_{sol}} \rho C_{sol}(T) dT + \rho L + \int_{T_m}^{T} \rho C_{liq}(T) dT & when\ T > T_{liq} \end{cases} \tag{11}$$

In Eqn. (11), the function f(T) is defined as the liquid fraction of PCM and represented as follows:

$$f(T) = \begin{cases} 0 & if\ T < T_{sol} \\ \dfrac{T - T_{sol}}{T_{liq} - T_{sol}} & if\ T_{sol} < T < T_{liq} \\ 1 & if\ T > T_{liq} \end{cases} \quad (12)$$

If ρC(T) term is taken as constant, Eqn. (11) can be written as follows:

$$H(T) = \begin{cases} \rho C_{sol} T & when\ T \leq T_{sol} \\ \rho\left(C_{sol}T_{sol} + L\dfrac{T - T_{sol}}{T_{liq} - T_{sol}}\right) & when\ T_{sol} < T < T_{liq} \\ \rho\left(C_{sol}T_{sol} + L + C_{liq}\left(T - T_{liq}\right)\right) & when\ T > T_{liq} \end{cases} \quad (13)$$

2.5.2 Apparent heat capacity method

During thermal phase changes, the apparent heat capacity approach considers an effective heat capacity [92] to account for the effect of enthalpy and its temporal evolution. The apparent heat capacity approach has only one unknown variable (temperature), making its solution easier and more computationally straightforward than the enthalpy method. For the effective heat capacity technique, the following form of the heat conduction equation is given:

$$\frac{\partial H}{\partial t} = \frac{\partial H}{\partial T}\frac{\partial T}{\partial t} \quad (14)$$

In Eqn. (14), $\frac{\partial H}{\partial t}$ is equal to $\rho C_{eff}(T)$, and if this term is inserted into Eqn. (4), the following representation is obtained:

$$\rho C_{eff}(T)\frac{dT}{dt} = \nabla.(\lambda \nabla T) + \dot{q}_v \quad (15)$$

In order to solve Eqn. (15), the effective heat capacity should be approximated, and several formulations have been applied to represent C_{eff}. For instance, Kodjo et al. [92] define the C_{eff} with Eqn. (16):

$$C_{eff} = \begin{cases} C_{sol} & if\ T < T_{sol} \\ \frac{1}{2}\left(C_{sol} + C_{liq}\right) + \frac{L}{T_{liq} - T_{sol}} & if\ \ T_{sol} < T < T_{liq} \\ C_{liq} & if\ T > T_{liq} \end{cases} \quad (16)$$

2.5.3 Heat source method

The heat source approach divides the enthalpy into sensible and latent components. In the classical heat equation, the latent term is employed as a source term as follows:

$$\frac{\partial H}{\partial t} = \frac{\partial H}{\partial T}\frac{\partial T}{\partial t} = \left[\rho C(T) + \rho L\frac{\partial f(T)}{\partial T}\right]\frac{\partial T}{\partial t} \quad (17)$$

Combining Eqn. (4) and Eqn. (17) gives:

$$\rho C(T)\frac{dT}{dt} = \nabla.(\lambda \nabla T) + \dot{q}_v - \rho L\frac{df(T)}{dt} \quad (18)$$

In Eqn. (18), $\rho L\frac{df(T)}{dt}$ indicates the source component because of the latent portion of the enthalpy.

Applying one of the aforementioned approaches, the whole building or only PCM-integrated parts can be modeled and simulated using computer simulation software or finite element method (FEM) solvers to understand the overall effect of the PCM on building energy performance. Energy simulation software is an essential instrument for researchers to examine energy needs, and the majority of researchers utilized simulation software to validate their experimental data [93]. In literature, several software packages such as EnergyPlus, ANSYS, TRNSYS, and COMSOL Multiphysics have been used to validate the results obtained from field testing. In addition, programming languages like MATLAB and python can solve the heat conduction problem by applying FEM or other numerical methods. Table 8 summarizes the research articles that use computer simulation to evaluate the performance of the PCM-integrated building components.

Table 8. The summary of research articles that use computer simulation to evaluate the performance of PCM-integrated building components

Simulation software	**Model description**	**PCM properties**	**Results**	**Ref**
TRNSYS	Office building in Algeria	T_m = 24℃	The modeling findings revealed that the utilization of PCMs in the concrete ceiling and hollow brick walls had caused a 3 to 4 ℃ increase in the office temperature during the winter months.	[94]
EnergyPlus	Lightweight building located in Spain	T_m = 23-27℃	PCM has enhanced cooling and heating performance	[95]

Table 8 (Cont'd)

TRNSYS	Test cubicle in Mediterranian climate	T_m = 29°C ΔH = 165-200 J/g	Utilizing PCM resulted in energy reductions between 21.7% and 28.6%.	[96]
TRNSYS	PCM layer in floor	Type 56 to type 1270 components in the TRNSYS interface	The simulation findings demonstrated that the successful deployment of PCM in buildings is highly dependent on the material's melting point and latent heat.	[97]
ANSYS	PCM-based plasterboard	T_m = 26°C ΔH = 110 J/g	It was concluded that the effective heat capacity technique is preferred for both charging and discharging simulations because it can be derived with minimal knowledge regarding PCM	[98]
ANSYS Fluent	Three-layer wall	T_m = 24-35°C ΔH = 170 J/g	PCM in the exterior layer of an external wall could lower the summer peak inner wall surface temperature, minimizing heat gain.	[99]
ANSYS Fluent	Living room in Baltic	T_m = 22°C ΔH = 160 J/g	The active TES system lowers interior air temperature by 9.5°C during analysis.	[100]

Table 8 (Cont'd)

COMSOL	50.8x50.8 mm mortar sample	T_m = 6 and 28℃ ΔH = 150-160 J/g	Using a PCM with a melting point close to the occupant's comfort zone makes the inside temperature profile more uniform and enhances the duration spent in the comfort zone.	[101]
COMSOL	Wall	T_m = 40℃ ΔH = 160 J/g	The results show that in summer, the wall with a phase change temperature of 29–31 °C and a thickness of 20 mm has a higher heat storage capacity, a lower average internal surface temperature (28.63 °C), and a higher average phase change usage (61.5%),	[102]

Thus, it can be inferred that simulation software can also be employed to study and optimize the energy demands of a building envelope. These software tools are particularly efficient for verifying the findings of field testing. In addition, these instruments provide the assessment of typical building structures under varied climates.

CHAPTER 3

MATERIALS AND METHODOLOGY

3.1 Materials and preparation

3.1.1 Raw Materials

This study used Class F fly ash (FA), ground-granulated blast furnace slag (GGBFS), fine aggregate, SiO_2, and TiO_2 nanopowders, graphite powder, and sodium hydroxide (NaOH) solution was utilized to prepare the mPCM-incorporated geopolymer mortar.

3.1.1.1 GGBFS

GGBFS was obtained from the ISDEMIR steel production plant located in Iskenderun, Hatay. The chemical composition of the GGBFS is provided in Table 9. The particle size distribution of the GGBFS was determined with Malvern Mastersizer 2000 conducting dry analysis. The average particle size of the GGBFS is 3.19 μm with a specific surface area of 1.88 m^2/g. d10, d50, and d90 were obtained as 1.03 μm, 5.84 μm, and 7.70 μm, respectively. The particle size distribution of GGBFS is given in Figure 11. Particle size distribution of FA and GGBFS.

3.1.1.2 Fly ash

The FA was supplied by ISKEN Sugözü thermic power plant located in Yumurtalık, Adana. The chemical composition of the FA is provided in Table 9. The particle size distribution of the GGBFS was determined with Malvern Mastersizer 2000 conducting dry analysis. The average particle size of the GGBFS is 5.20 μm with a

specific surface area of 1.88 m^2/g. d10, d50, and d90 were obtained as 2.93 µm, 20.30 µm, and 80.50 µm, respectively The average particle size of the FA is 20.3 µm with a specific surface area of 0.64 m^2/g. The particle size distribution of FA is given in Figure 11. The SEM images of GGBFS and FA are provided in Figure 12.

Table 9. Chemical compositions of GGBFS and FA

Oxide composition	**GGBFS (wt%)**	**FA (wt%)**
CaO	37.8	3.74
SiO_2	36.3	55.6
Al_2O_3	12.5	23.1
MgO	6.07	1.38
SO_3	1.38	0.52
Fe_2O_3	0.91	9.12
TiO_2	1.67	1.38
K_2O	0.93	2.95
Na_2O	0.24	0.87

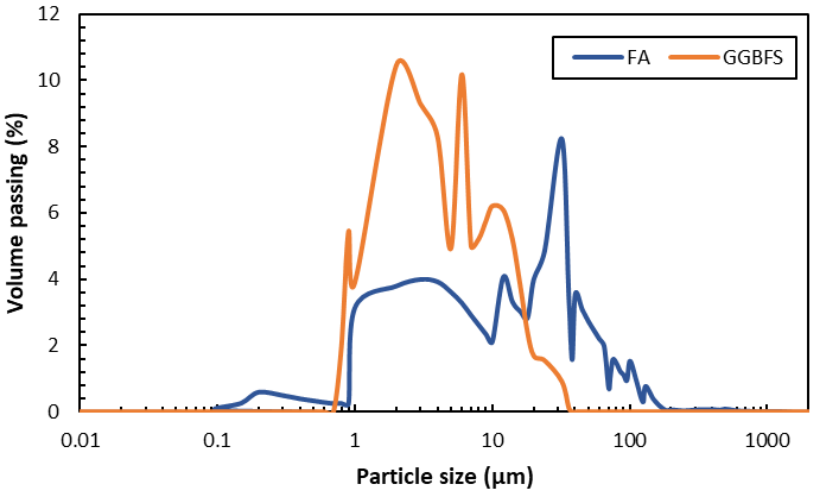

Figure 11. Particle size distribution of FA and GGBFS

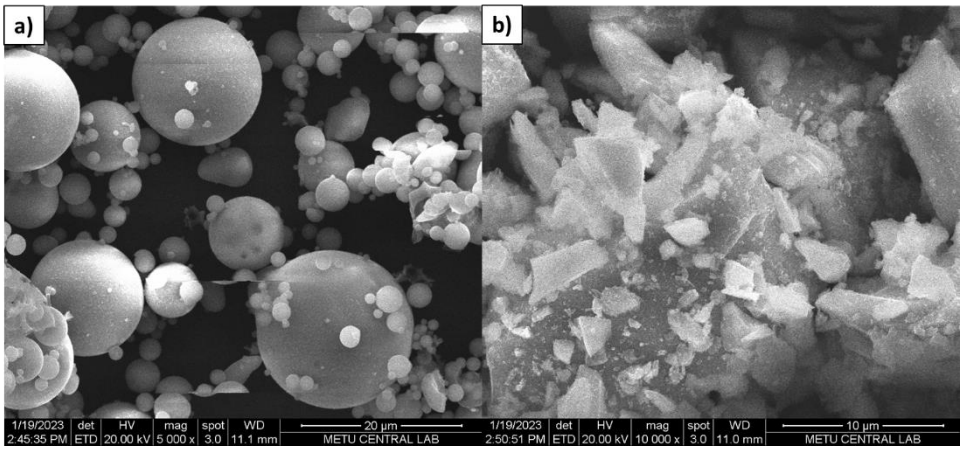

Figure 12. The SEM images of a) FA b) GGBFS

3.1.1.3 Aggregate

Quartz sand with a particle size between 0.1 mm and 3 mm was used as aggregate. The gradation of the sand used in this study is given in Figure 13. The gradation of the standard sand was done considering maximum and minimum passing limits according to the ASTM C33 standard. The specific gravity of the sand was 2.75.

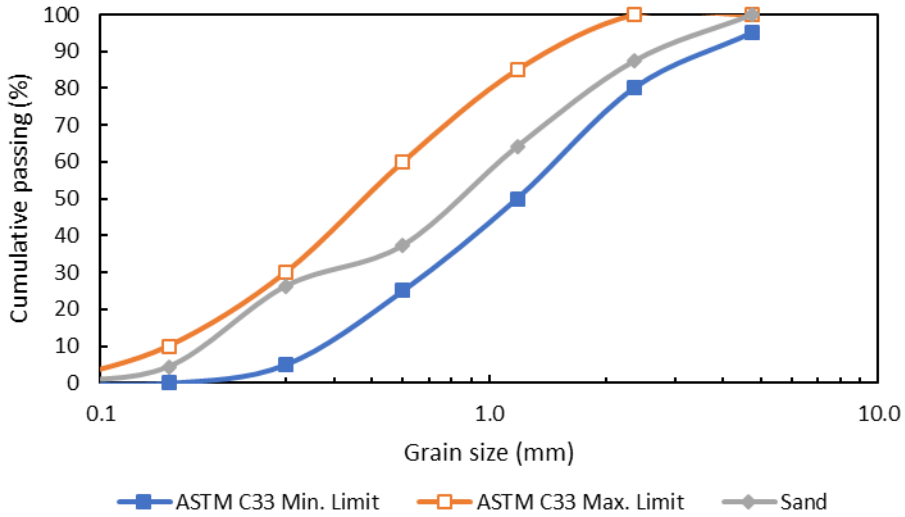

Figure 13. The grain size of the sand used in the study.

3.1.1.4 Alkali activator

Sodium hydroxide (NaOH) pellets with 98% purity were purchased from Sigma-Aldrich, USA, to prepare the alkaline solution.

3.1.1.5 SiO_2 and TiO_2 nanoparticles

Commercially available SiO_2 and TiO_2 nanopowders were purchased from Nanokar Nanotechnology, Turkey. As received nano-SiO_2 has a high purity (99.5%) with an average particle size of 15-35 nm. Similarly, as received nano-TiO_2 has a high purity (99.5%) with an average particle size of 18 nm. The physical properties of nanopowders are summarized in Table 10. The SEM images and EDS spectrum of SiO_2 and TiO_2 nanoparticles are shown in Figure 14. The EDS analysis confirmed that the main elements were Si and Ti for nano-SiO_2 and nano-SiO_2, respectively.

Table 10. Properties of nano-SiO_2 and nano-TiO_2

Property	**nano-SiO_2**	**nano-TiO_2**
Purity (%)	+99.5	99
Average particle size (nm)	15-35	18
Specific surface area (m^2/g)	440	200-240
True density (g/cm^3)	2.65	3.9
Color	White powder	White powder

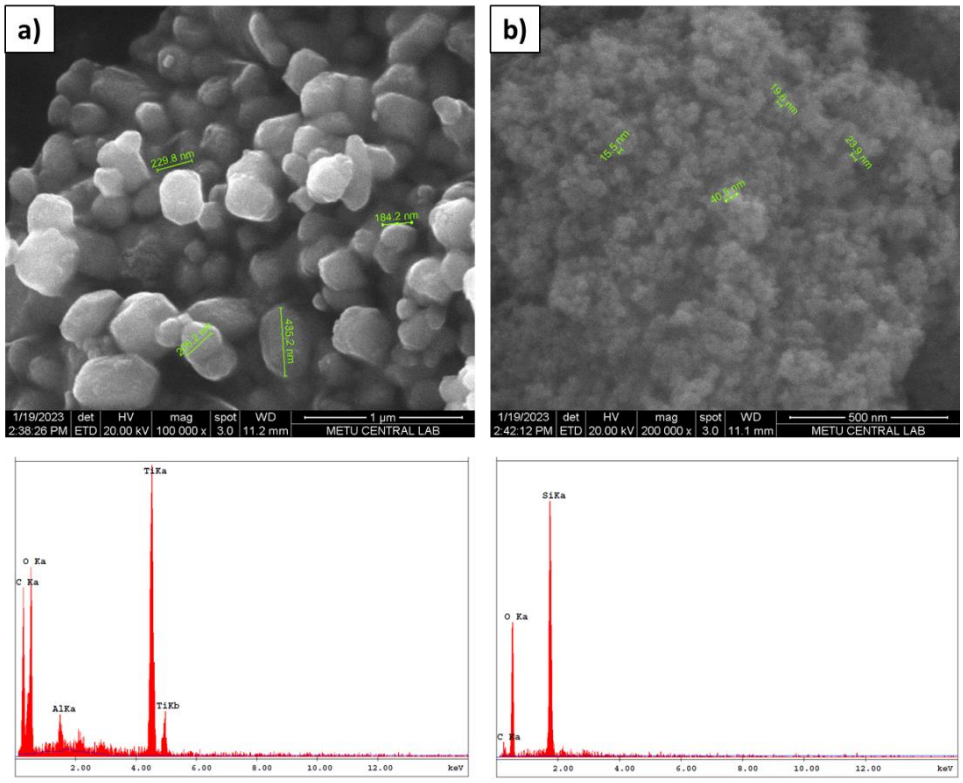

Figure 14. The SEM images and EDS analysis of a) nano-TiO_2 and b) nano-SiO_2 particles

3.1.1.6 Graphite

A commercial product of natural graphite powder was supplied from ChemPure (Aklar Kimya, Turkey). The supplier only provided the mesh size of the product; thus, only the mesh size was used to describe the mean size of the material instead of giving particle size distribution. The graphite powder has a mean size of 74 µm with a specific density of 2.09-2.25 g/cm^3. The fixed carbon content of the graphite powder is specified as 87.38% on the product data-sheet. SEM images were provided in Figure 15 to understand the morphology of the graphite used in this study. The granular shape and relatively coarse particle size of the particles around 50 µm of the graphite are seen in Figure 15.

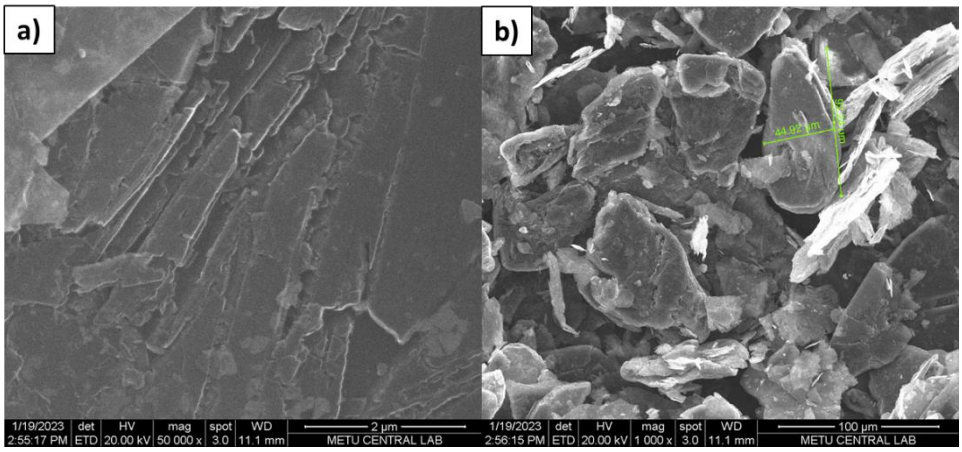

Figure 15. The SEM images of graphite powder used in the study a) Graphite layers are observable at 2µm resolution, and b) granular shape of the particles around 50 µm in size are seen

3.1.1.7 PCMs

The present study used commercially available microencapsulated PCMs with two different melting temperatures. Considering Turkey's climate and occupant thermal comfort limitations, nextek 24D® was selected and purchased from Microtek Laboratories in Dayton, Ohio, USA. The general properties of the PCMs are given in Table 11. The microencapsulated PCM particles consist of a core substance (PCM) and a shell or capsule wall. The capsule wall is a polymer or plastic that is inert and stable. The PCM in the capsule melts at 24 ℃. However, the polymer shell is engineered not to melt under standard processing and usage conditions. The SEM images and EDS analysis of the PCMs are given in Figure 16. As can be seen, the particle size of the nextek 24D was around 15 µm and 30 µm, and agglomeration of the mPCM particles was observable in b. In addition, the EDS analysis result showed a high-intensity peak of C due to the polymeric shell material used to encapsulate the PCM.

Table 11. General properties of the commercial PCMs used in the study

Properties	**nextek 24D®**
Melting point (℃)	24
Latent heat of fusion (J/g)	170
Mean particle size (μm)	15-30
Form	Dry powder
Color	White to slightly off-white
Specific gravity	0.9

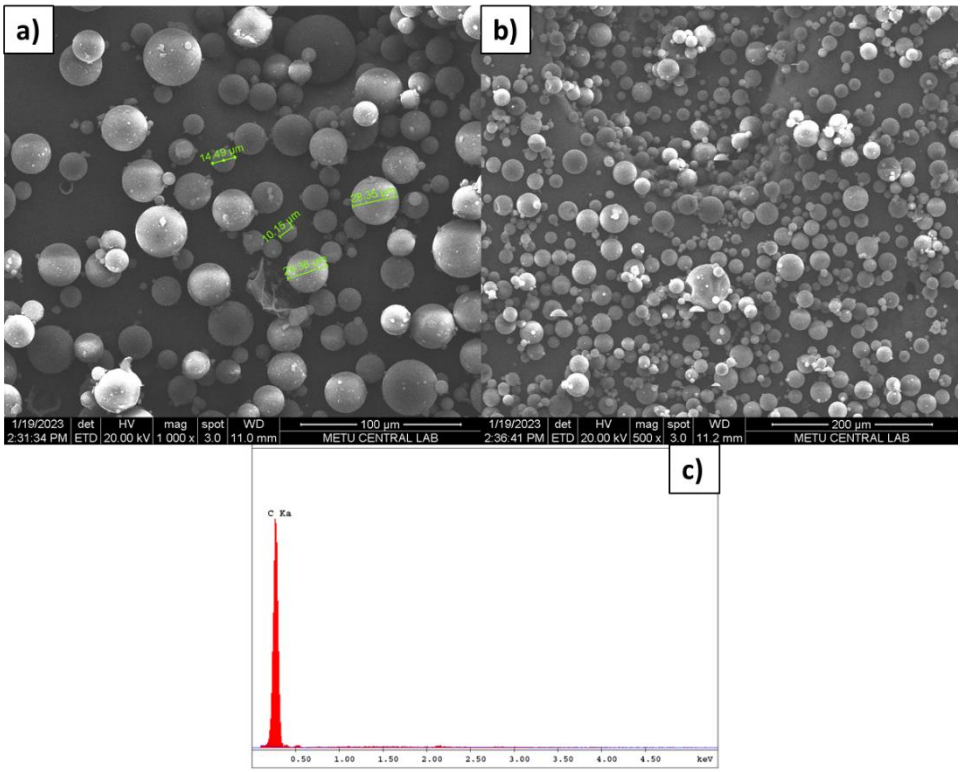

Figure 16. SEM images of nextek 24D were used in this study a) 100 μm resolution and b) 200 μm resolution. c) EDS analysis result of the mPCM

3.1.2 Mix designs

In this study, a total of 30 different mixes were prepared to understand the effect of PCM, nanoparticles, and graphite incorporation into the geopolymer matrix. A five-step mixing procedure was followed to produce geopolymer mortar because nano-SiO2, nano-TiO2, and graphite addition into the geopolymer matrix need special attention to prevent a possible agglomeration problem. Although nano-SiO_2 and nano-TiO_2 can be well distributed in water, they tend to agglomerate in alkaline solutions. The cementitious environment, whether paste or mortar, is filled with various ions, including sodium, potassium, calcium, sulfur, and hydroxyl ions, which are the principal constituents, along with aluminum and silicon ions at lower amounts [103]. In addition to Van der Waals forces, the ions' bridging effect due to the cement's ionic character is responsible for the agglomeration of nanoparticles inside ionic systems. Due to the bridging action of Ca^{2+}, it appears from a detailed examination of nano-SiO_2 dispersion behavior in a cementitious environment that the ionic composition of cementitious systems is a significant limiting factor to the appropriate and uniform distribution of nano-SiO_2 particles [103]. Therefore, nano-SiO_2 and nano-TiO_2 particles were dispersed in water using a sonicator to overcome the agglomeration of nanoparticles. In literature, different amounts of nano-SiO_2 and nano-TiO_2 particles changing between 0.5 and 10 wt% of the binder have been tried to examine their effectiveness of them in terms of mechanical strength gain [104], and it was seen that nano-SiO_2 and nano-TiO_2 addition contributes the mechanical strength improvement because they serve as nuclei, react with cement hydration products, and fill voids. However, excessive nano-SiO2 and nano-TiO2 addition might have undesirable effects such as agglomeration, increased water demand, and lowered cement-based product setting. In this study, nano-SiO_2 and nano-TiO_2 particles were replaced for 0.8 wt% of the binders.

The water-to-binder ratio in the preparation of the mixes was tuned to generate a workable mortar and to guarantee that the GGBFS, FA, and graphite powders were well combined. Through preliminary testing, the water-to-binder ratio (w/b) and the water-to-graphite ratio (w/g) were fixed at 0.35 and 1, respectively, for all mixes. A GGBFS to FA ratio was chosen as 3:1, and the sand to binder (GGBFS + FA) ratio was kept constant as 1:1 for the mPCM-incorporated geopolymer mortars. PCM can be added as an additive or used to replace sand in the concrete mixture. This study used the required volume % of PCM to replace the same volume % of sand. Sand-to-PCM unit weight ratio was used to compute PCM weight. [13].

The NaOH solution was prepared one day before the mixing procedure to ensure that it reached room temperature before adding it. The sodium hydroxide pellets were added to all mixtures by 10 wt% of the total binder. Similarly, graphite powder content was kept constant at 10 wt% of the binder and added as additions instead of binder replacement. It should be noted that the graphite powder content was determined as a result of a preliminary test to reach the percolation threshold. Hence increasing the content of graphite powder is detrimental to the strength gain of the mortar; as a result of growing porosity and slowing down of geopolymerization reactions, it was important to keep the graphite powder content as minimum as possible. According to the result of the preliminary analysis, it was observed that the 2 wt% and 5 wt% addition of graphite powder did not result in adequate thermal conductivity increase, and the addition amount was determined as 10 wt%.

In the lab, the fresh mortar mix was prepared according to five steps: (1) Weighing each group's raw materials and dispersing nano-SiO_2 and nano-TiO_2 in water using a sonicator dispersion equipment for 10 minutes, (2) Adding FA, GGBFS, and sand to the mixer and mixing them for 3 min at low-speed to ensure the homogeneity of the mixture, (3) The already-prepared sodium hydroxide solution was included in the mixture with nano-SiO_2 or nano-TiO_2 aqueous solution gradually, which was then mixed for five minutes, the sodium hydroxide solution and nano-SiO_2 or nano-TiO_2 aqueous solution mixed at low speed for 1 min, and then high-speed mixing was applied for the remaining 4 min (4) graphite and water were mixed separately for 3

min until the graphite paste became homogenous, then graphite paste was added to the mortar mix and mechanically mixed for 2 min, (5) the PCM was incorporated into the mixture, which was then mixed for a further 3 minutes. The PCM was included as the final component at the end of the mechanical stirring to minimize PCM damage caused by disturbances during mixing [13].

The different components used to produce the different PCM-incorporated geopolymer mortar samples are given in Table 12.

Table 12. Details of mix design

Code	**PCM (%)**	**GGBFS (g)**	**FA (g)**	**NS (g)**	**NT (g)**	**G (g)**	**NaOH (g)**	**W_B (g)**	**W_G (g)**	**Sand (g)**	**PCM (g)**
G0-PCM0	0	375	125	0	0	0	50	175	0	500	0
G0-Si-PCM0	0	372	124	4	0	0	50	175	0	500	0
G0-Ti-PCM0	0	372	124	0	4	0	50	175	0	500	0
G0-PCM20	20	375	125	0	0	0	50	175	0	400	33.2
G0-Si-PCM20	20	372	124	4	0	0	50	175	0	400	33.2
G0-Ti-PCM20	20	372	124	0	4	0	50	175	0	400	33.2
G0-PCM40	40	375	125	0	0	0	50	175	0	300	66.4
G0-Si-PCM40	40	372	124	4	0	0	50	175	0	300	66.4
G0-Ti-PCM40	40	372	124	0	4	0	50	175	0	300	66.4
G10-PCM0	0	375	125	0	0	50	50	175	50	500	0
G10-Si-PCM0	0	372	124	4	0	50	50	175	50	500	0
G10-Ti-PCM0	0	372	124	0	4	50	50	175	50	500	0
G10-PCM20	20	375	125	0	0	50	50	175	50	400	33.2
G10-Si-PCM20	20	372	124	4	0	50	50	175	50	400	33.2
G10-Ti-PCM20	20	372	124	0	4	50	50	175	50	400	33.2
G10-PCM40	40	375	125	0	0	50	50	175	50	300	66.4
G10-Si-PCM40	40	372	124	4	0	50	50	175	50	300	66.4
G10-Ti-PCM40	40	372	124	0	4	50	50	175	50	300	66.4

* NS: nano-SiO_2, NT: nano-TiO_2, G: graphite, W_B: water required for binder, W_G: water required for graphite

Procedures 1 to 6 were followed to prepare geopolymers containing nextek 24D and nextek 28D. Immediately after mixing, 4×4×16 cm prism (for mechanical tests) and Φ7×4 cm cylindrical (for thermal constant measurement) were cast, consolidated, and leveled by a trowel (Figure 17. a) 4×4×16 cm prism and b) Φ7×4 cm cylindrical

specimens were prepared for mechanical and thermal measurement testings, respectively.). After 24 hr day, the specimens were removed from their molds and cured under ambient conditions (20 ± 3 ℃ and ≈ 20% relative humidity) for 28 days.

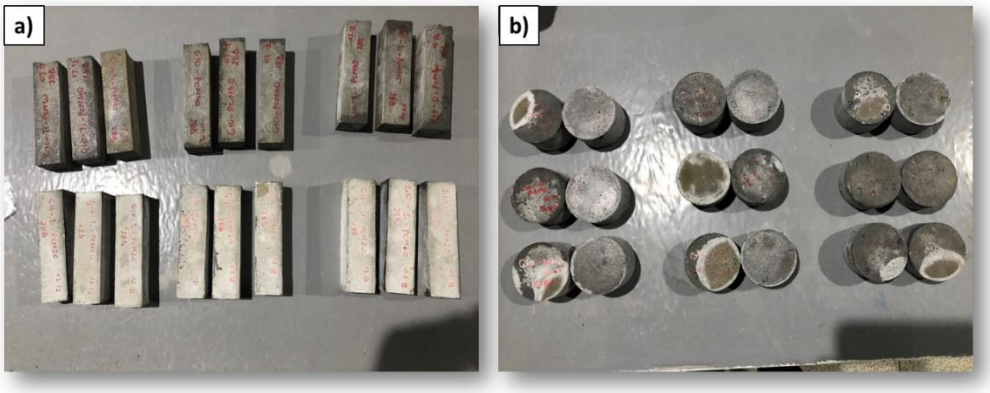

Figure 17. a) 4×4×16 cm prism and b) Φ7×4 cm cylindrical specimens were prepared for mechanical and thermal measurement testings, respectively.

3.2 Test methods

3.2.1 Fresh properties

The consistency of fresh mortar was determined immediately after mixing by using the flow table test according to ASTM C1437 standard [105]. The mold was filled with 25 mm mortar and tamped 20 times. As with the first layer, the second mortar layer was poured and tamped. The tabletop was cleaned and dried before removing the mold, giving special attention to the flow mold's edge. Then, the mold was taken from the mortar for 1 minute to finish mixing. (Figure 18.a). The table was dropped 25 times in 15 seconds. The diameter of the mortar was measured along the two lines as can be seen in Figure 18.b, recording each diameter to the nearest millimeter, and the average of the two measurements minus the inside base diameter of the mold, which is 10 mm, was recorded as the flow value.

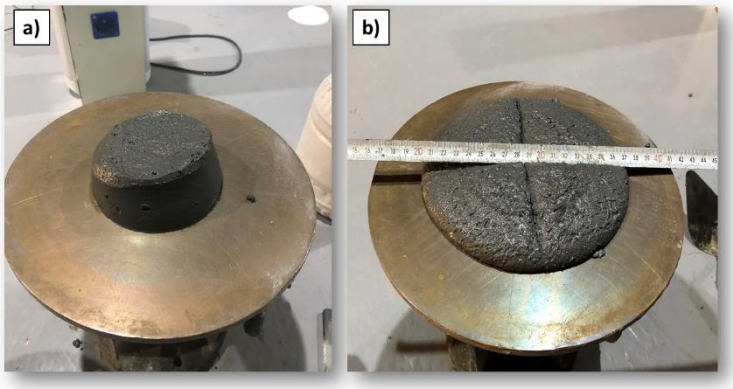

Figure 18. The consistency of fresh mortar was determined by using the flow table test

3.2.2 Physical properties

The bulk density and porosity of the geopolymer mortars were measured according to Archimedes' methods [106][107][108] with water as an immersion medium to determine the physical properties of the samples. The specimens' apparent density (ρA) was determined using Eqn. (19), where m_d is the dry mass, m_i is immersed mass, and m_w is the wet mass of the samples. The ρ_L is the liquid density, which is 1.0 g/cm^3 for water. The specimens were kept in an oven at 40℃ for 24 hours to avoid damaging geopolymerization products before measuring their dry mass. To find the m_i and m_w, the specimens were submerged in water at room temperature for 24 hr. However, it is important to note that saturation with water was regarded improper for geopolymers due to the possibility of ions such as Na^+ seeping into the water. Therefore, measured densities and apparent porosities are not regarded as absolute but as relative values [109]. The specimens were weighted while hanging by a thin wire and totally submerged in water after 24 h. The mass was recorded as m_i. After that, the specimens were taken from the water, and the mass recorded. as m_w.

$$\rho_A = \frac{m_d}{m_w - m_i} \times \rho_L \tag{19}$$

3.2.3 Mechanical properties

The flexural strength of the mortar samples was measured in triplicates at 28 days according to ASTM C348 standard [110]. The center point loading method was used in making flexure tests on the prism specimens at a loading rate of 0.04 kN/s. The uniaxial compressive strength of the samples was determined according to ASTM C349 standard [111], in which broken portions of the prism during the flexure test were used. In determining the compressive strength, specimens that were obviously flawed after flexure testing or provided values that deviated by more than 10 percent from the average value of all test specimens made from the same sample and tested at the same time were not included to the final result. Before performing the test, the specimens' end surfaces were polished to ensure that they are precisely flat and parallel, and a loading rate of 1.5 kN/s was applied for compression test. The mechanical tests were conducted using a universal test machine for flexural and compression tests as seen in Figure 19.

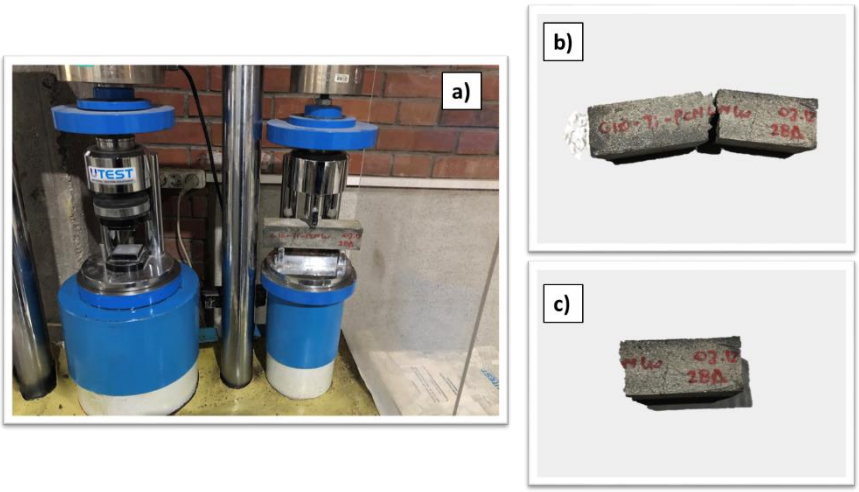

Figure 19. a) Universal test machine used for measuring flexural and compressive strenght b) The broken prism after flexural test c) The broken prism used for compresson test

3.2.4 Microstructure

SEM was used to reveal the morphology of the raw materials as well as the microstructure of the composites. Before SEM analysis, specimens were broken into tiny pieces and oven-dried at 40℃ for several days to ensure that all moisture had been extracted for better vacuuming. Small pieces from each mixture were then placed on metal stubs using a carbon band and sputter-coated with gold before to being placed under the microscope. In addition to SEM, energy-dispersive spectroscopy (SEM-EDS) was conducted on the samples to understand the chemical compositions of the samples.

3.2.5 Thermophysical properties

3.2.5.1 Thermal conductivity measurement

The thermal conductivity of the composites was measured using Hot Disk TPS 2500 S thermal constants analyzer (Thermtest Europe AB, Sweden) in accordance with ISO 22007-2, as seen in Figure 20. The transient plane source (TPS) thermal characterization method is a valuable instrument for assessing the thermal properties of various materials because to its robust design, short characterization time, and capacity to detect the thermal conductivity and thermal diffusivity of complicated materials.

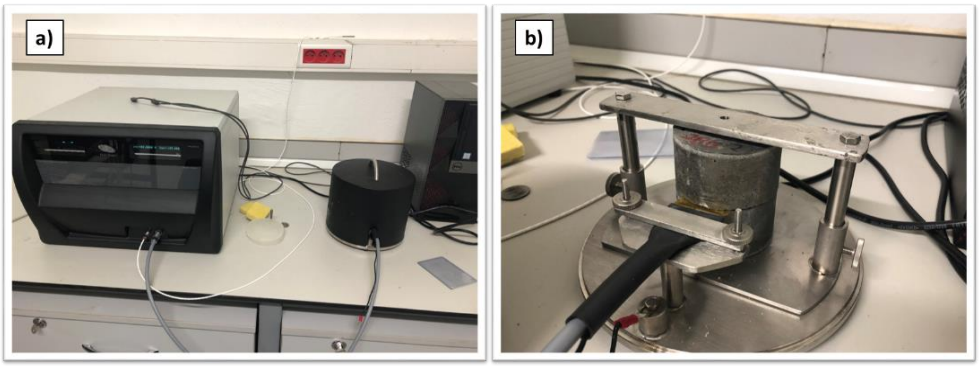

Figure 20. a) Hot Disk equipment used during thermal conductivity measurement, b) The sensor was sandwiched between two cylindrical specimens prepared for the thermal constant measurement test

A sensor element in the form of a double helix acts as both a heat source for heating the sample and a resistance thermometer for monitoring the time-dependent increase in temperature of the heat source itself. In the analysis, 200 resistance measurements are performed over a predetermined period to establish the relationship between temperature and time. To theoretically define how the hot disk operates, the heat conduction equation is solved under the assumption that the hot disk consists of an infinite number of concentric ring heat sources. If the hot disk is electrically heated, the resistance increase over time can be expressed as Eqn. (20), where R_0 is the resistance of the disk before heating, Ω is the resistivity temperature coefficient, ΔT_i is the constant temperature difference between two sides of the sensor, and $\Delta T_{ave}(\tau)$ is the average temperature rise of the sample surface.

$$R(t) = R_0[1 + \Omega\{\Delta T_i + \Delta T_{ave}(\tau)\}] \quad (20)$$

From the TPS theory, the time-dependent temperature increase can be expressed by Eqn. (21), where P_0 is the heat power given by the sensor, r is the radius of the disk, and k is the thermal conductivity of the sample that is being tested. $D(\tau)$ is the dimensionless time-dependent function.

$$\Delta T_{ave}(\tau) = \left[\frac{P_0}{\left(\pi^{\frac{3}{2}} rk\right)}\right] D(\tau) \tag{21}$$

In Eqn. (21), τ is defined with Eqn. (22), where t is the amount of time measured from the beginning of the transient recording, and θ is the characteristic time.

$$\tau = \left(\frac{t}{\theta}\right)^{1/2} \tag{22}$$

The characteristic time, θ is defined by Eqn. (23), where α is the thermal diffisuvity of the tested sample.

$$\theta = \frac{r^2}{\alpha} \tag{23}$$

Since α; thus, θ are unknown before to the experiment, the final straight line from which thermal conductivity is determined is derived by iteration. In this manner, thermal conductivity and diffusivity can be determined from a single transient observation.

For measurements, two cylindrical samples representing each mix design with a diameter and height of 70 mm and 40 mm were casted and cured under respective environments for 28 days. One of the samples was placed inside the measurement chamber and the Hot Disk Kapton sensor with a diameter of 6.403 mm (Sensor code: 5501) was centered, and the second sample was placed on top of the sensor so that it was totally covered. The probing depth was set to 40 mm. The measurement time changed between 20 and 40 seconds. The heating power was set between 100 - 150 mW to satisfy the recommended total temperature increase of 2 to 5 K. It was ensured that the residual curve showed a random scatter pattern around a horizontal line, and the transient curve displayed a continuous temperature increase without sudden jumps, discontinuities, and negative temperature development. Since the composites

are heterogeneous, the sensor was moved between a few measurement points to avoid random artifacts in the residual graph due to density changes, boundaries, and voids; hence, an average thermal conductivity was obtained by measuring three different points on the same sample. Following the aforementioned protocols, the thermal conductivities of each composite were recorded at 22℃; therefore, PCMs were in the solid state during measurement.

3.2.5.2 Differential scanning calorimetry (DSC)

Using differential scanning calorimetry, the latent heat capacity of mortar specimens containing varying quantities of microencapsulated PCM and the melting and solidification temperatures of nextek 24D and nextek 28D was determined. Unless otherwise specified, the enthalpies mentioned throughout this study are for latent heat. A PerkinElmer 8000 DSC with a thermal cycle from 10 °C to 50 °C was utilized. Mortar specimens were crushed to powder form after 28 days, and a small mass of about 10 mg was measured. The heating/cooling rate was selected as 5 ℃/min to have minimum hysteresis in DSC response considering different mixes [112]. During the DSC scans, one entire endothermic/exothermic cycle was followed by a second endothermic/exothermic cycle. After subtracting the basis line for an empty aluminum pan, the results of the second endothermic cycle were used for the analysis.

CHAPTER 4

RESULTS AND DISCUSSIONS

4.1 Flowability

Figure 21 shows the flow values of the mixes without graphite addition, in which the spread changes between 11 cm and 5 cm for the mixtures.

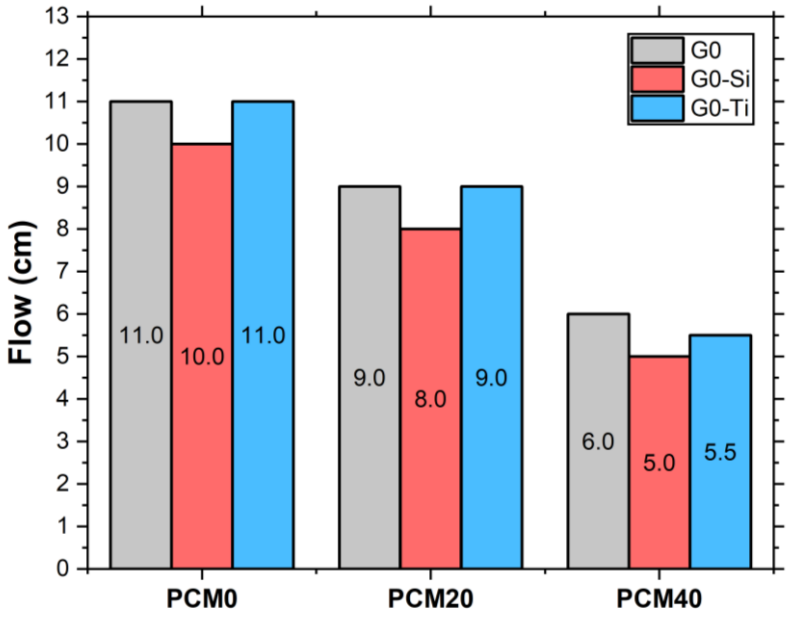

Figure 21. Flow results of PCM-incorporated geopolymer mixes without graphite addition

As can be seen from Figure 21, replacing binders with nano-SiO_2 led to reduced flowability for all geopolymer mortar mixes. The embedding of water by the formed nano-SiO_2 network and the formation of coagulates in the pore fluid environment may be significant factors in lowering the flowability of the composites containing nano-SiO_2 [113]. Furthermore, additional surface area due to nanoparticle addition adsorbs some of the available water in the matrix and reduces the spread. On the

other hand, replacing nano-TiO_2 with binders did not considerably reduce the mixtures' flowability considerably. This behavior may be linked to nanoparticle agglomeration, which reduces the accessible surface area for interaction and water absorption. Casagrande et al. [114] state that the flow decreases with nano-TiO_2 addition was observed if nano-TiO_2 addition was higher than 10 wt% of the binder, and lower values of nano-TiO_2 addition did not affect the flowability of the mixes.

On the other hand, increasing mPCM incorporation content reduced the samples' flowability significantly. The spread value of the control mix G0-PCM0 was reduced by -2 cm (-18.2%) and -3 cm (-45.5%) with the replacement of 20% and 40% of the sand with mPCM, respectively. A similar trend was observed for G0-Si-PCM0 and G0-Ti-PCM0 mixes. The lowest spread was measured for the G0-Si-PCM40 mix, in which flow was reduced by 54% compared to the control sample from 11 cm to 5 cm. The reduced flowability of the mPCM incorporated mixtures is explained by increasing in solid content and high water absorption capacity of mPCM. Furthermore, the volume replaced by mPCM has a much finer particle size distribution than the sand; thus, increasing surface area of the mPCM inevaitably results in higher water demand than the same volume of the sand replaced.

Figure 23 shows the flow values of the mixes with 10% graphite addition. It should be noted that graphite paste was prepared before adding it to the mortar mix with a 1:1 water ratio due to the fact that it has a high pore content [115]; thus, it is expected to increase the water demand. In addition, the graphite particles' angular shape and coarse texture were further considerations [116]. It was noted before that particle with a rough surface prevented particles from sliding, decreasing the mixtures' workability. For instance, the viscosity of the graphite-added cement mixes increased to 80% with 10% addition compared to the control mix [16]. As can be seen in Figure 23, using extra water for the graphite powder increased the flowability compared to the mixtures without graphite addition. This can be attributed to the fact that the water absorption capacity of the graphite particles was reached with the extra water added, and the remaining water on the graphite particles was released to the geopolymer mortar mix while combining graphite paste into the mixture. For

instance, the spread of G10-PCM0 was increased by 9% (11 cm to 12 cm) compared to G0-PCM0. The same behavior was observed when nano-SiO_2 and nano-TiO_2 were added. However, the most significant increase in flow with graphite addition was observed for the mixes with 40% mPCM incorporation. The flow values increased by 50% (+3 cm), 60% (+3 cm), and 54.5% (+3 cm) for G10-PCM40, G10-Si-PCM40, and G10-Ti-PCM40 compared to G0-PCM40, G0-Si-PCM40, and G0-Ti-PCM40.

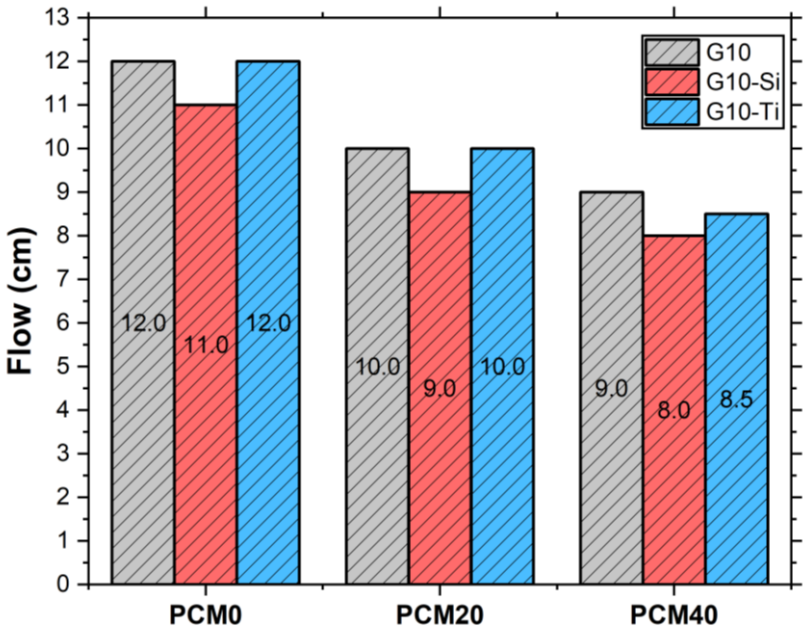

Figure 22. Flow results of PCM incorporated geopolymer mix with graphite addition

4.2 Apparent density

The apparent density results for all mixes are shown in Figure 23. As seen in Figure 23, nano-SiO_2 added mixes have a higher density than the other composites. Similarly, nano-TiO_2 addition resulted in higher apparent density than the control sample, G0-PCM0. The increase in apparent density is 3.8% and 2.21% for G0-Si-PCM0 and G0-Ti-PCM0 compared to the control mix. Filling the spaces between

the grains, nano-sized silica and titania particles provide a filler effect. Due to the decreased capillary porosity, a higher packing density is observed. In addition to this physical action, nano-SiO_2 exhibits pozzolanic reactivity, accelerating the formation of (C, N)-A-S-H gels and contributing to a denser matrix. Therefore, an increase in apparent density with nano-TiO_2 can be attributed to the filler effect, while higher apparent density with nano-SiO_2 addition results from both the filler effect and increased geopolymerization products.

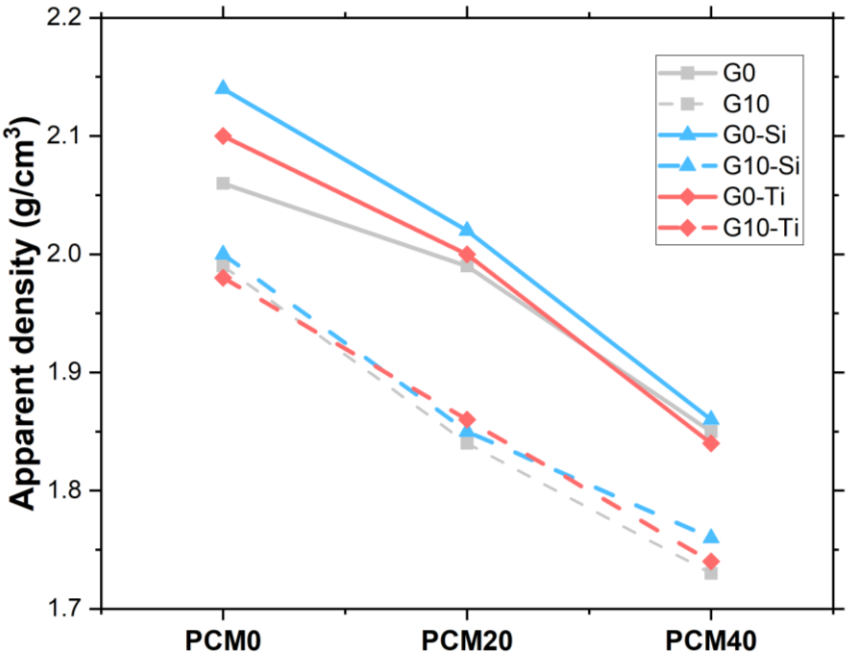

Figure 23. Apparent density results for different PCM replacement amounts. Dashed lines represent the mixes with graphite powder addition.

Furthermore, it is observed that the apparent density reduces almost linearly as the fraction of mPCM in the composites increase. It should be noted that the mPCM is replaced with sand, and mPCM has a much lower specific gravity than the sand used in this study (0.9 vs. 2.7). The obtained results are in line with this observation. For instance, the apparent density was reduced by -3.9% (-0.10 g/cm^3) and -9.9% (-0.21

g/cm^3) for G0-PCM20 and G0-PCM40 compared to the control mix. A similar trend is observed for both nano-SiO_2, and nano-TiO_2 added composites.

When graphite is added to the mixture, the apparent density for all composites is reduced significantly. Without aggregates or fillers, the density of a cementitious substance is around 1.9 to 2.0 g/cm^3, whereas pure graphite has a density of 0.9 g/cm^3 [117]. Furthermore, graphite's porous structure increases the composites' total pore volume, reducing the apparent density. Compared to G0-PCM0, the apparent density decreased from 2.06 g/cm^3 to 1.99 g/cm^3 for G10-PCM0. It should be noted that adding nanoparticles into composites containing graphite did not make a difference in terms of apparent density gain as geopolymerization reactions might be affected, and it could be related to the weak bond between the hydrophobic graphite particles and the binding matrix [118].

4.3 Flexural and compressive strength

The flexural and compressive strength results after 28 days are given in Figure 24, a and b, respectively. As shown in Figure 24, the mechanical properties of the mPCM incorporated mixtures decreased with increasing PCM content. Because of its low shear strength and stiffness, mPCM is easily damaged under loading, and the resulting voids likely functioned as weak spots after breaking, contributing to the overall degradation of the mechanical strength cementitious composites [119]. The reduction in compressive strength was -18.41% (-9 MPa) and 46.40% (-22.75 MPa) for the mixes G0-PCM20 and G0-PCM40 compared to G0-PCM0, respectively. The compressive and flexural strength of specimens containing nano-SiO_2 was greater than that of specimens without nano-SiO_2.

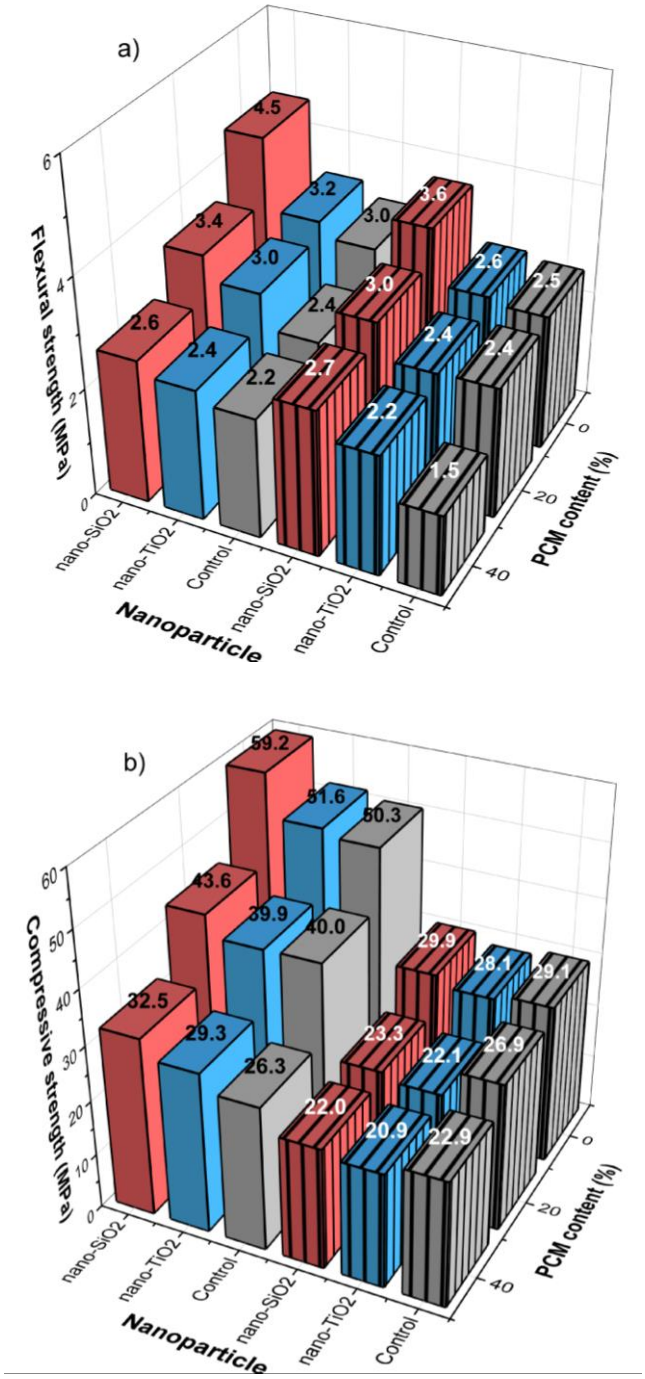

Figure 24. a) Flexural and b) compressive strength results of the composites at 28 days. The dashed prisms represent composites with 10 wt% graphite addition.

The increase in mechanical properties with nano-SiO_2 addition is attributed to the inclusion of soluble silicates, enhanced the rate of the reaction, facilitated the formation of long-chain silicate oligomers in the geopolymer matrix, and ultimately improved the mechanical strength since soluble silicon concentration is the most critical parameter that has to be considered for the geopolymerization process [120]. For instance, the flexural and compressive strength of G0-Si-PCM0 enhanced by 53% (+1.57 MPa) and 19% (+9.22 MPa) compared to G0-PCM0, respectively. A similar trend was observed when mPCM was added to the mixture, and the effect of nano-SiO_2 on strength gain was considerable even though mPCM particles prevented further geopolymerization in the matrix. Adding nano-SiO_2 particles enhanced the tensile and compressive strength of 40 vol% and replaced composite by 13% (+0.33 MPa) and 24% (+6.24 MPa) compared to G0-PCM40. The mechanical strength gain provided with nano-SiO2 is important for mPCM incorporated mortars because mPCM negatively affects the strength and may prevent the mPCM composites from building applications, as a minimum strength should be satisfied for safety reasons. Therefore, nano-SiO_2 addition to mPCM incorporated composites may allow the inclusion of higher content of mPCM with minimum strength lost, which may enable producing composites with better latent heat storage capacity.

Similar to nano-SiO_2 addition, nano-TiO_2 also increased the mechanical strength of the mixes due to the filler effect of the nanoparticles in which densification of the matrix and reduction of pore structure is achieved. However, the strength gain was limited for the composites that contain nano-TiO_2. The flexural and compressive strength of G0-Si-PCM0 enhanced by 9% (+0.27 MPa) and 5% (+2.52 MPa) compared to G0-PCM0. When mPCM is added to the matrix, the filler effect of the nano-TiO_2 particles is further reduced. Adding nano-TiO_2 particles enhanced the tensile and compressive strength of 40 vol%, replaced composite by 6% (+0.07 MPa) and 3% (+1.54 MPa) compared to G0-PCM40. In addition, the relatively lower strength gain of nano-TiO_2 added composites can be attributed to the agglomeration of finer nano-TiO_2 particles.

As can be seen in Figure 24, composites with graphite addition resulted in lower mechanical performance regardless of the nanoparticle or mPCM incorporation than the composites without graphite powder. The summary of the strength gain or loss in strength compared to the control sample, G0-PCM0, is given in Table 13.

Table 13. Gain or loss in mechanical performance for all mixes with respect to the control mix, G0-PCM0

Mix	**Flexural strength change (%)**	**Compressive strength change (%)**
G0-Si-PCM0	+52.81	+18.8
G0-Ti-PCM0	+8.99	+5.14
G0-PCM20	-20.79	-18.42
G0-Si-PCM20	-14.61	-14.13
G0-Ti-PCM20	-5.82	-18.49
G0-PCM40	-21.34	-46.40
G0-Si-PCM40	-11.24	-33.67
G0-Ti-PCM40	-19.11	-43.26
G10-PCM0	-26.96	-46.42
G10-Si-PCM0	+1.12	-42.79
G10-Ti-PCM0	-22.47	-39.12
G10-PCM20	-19.10	-45.07
G10-Si-PCM20	-12.36	-52.62
G10-Ti-PCM20	-20.22	-52.41
G10-PCM40	-50.56	-53.33
G10-Si-PCM40	-10.11	-57.48
G10-Ti-PCM40	-25.84	-55.13

The graphite addition lowered the mechanical strength of the composites due to the fact that the layers of graphite only interact via weak van der Waals forces, and excessive graphite particles in the matrix promote the agglomeration of graphite, which increases the matrix damage under load. Furthermore, this study used relatively coarser graphite particles with an average particle size of 74 μm.

Considering the particle size distribution of FA and GGBFS given in Figure 11, coarser graphite particles might lead to a decrease in geopolymerization reactions as the bond between binders is broken due to the presence of graphite particles; thus, the filler effect of nanoparticles added to the matrix or enhanced geopolymerization rate due to nano-SiO_2 addition was diminished as a result of the graphite incorporation. However, it should be noted that the compressive strength was affected more than the flexural strength of the composites. The flexural and compressive strength of G10-PCM0 was reduced by 27% (-0.80 MPa) and 46% (-22.76 MPa) compared to G0-PCM0. When mPCM is added to the matrix, the mechanical performance of the composites is further reduced, as expected.

4.4 Scanning electron microscopy (SEM)

Figure 25 shows the SEM images of the geopolymer specimens without nanoparticle addition from the failure surface of the compressive strength test at 28 days. As the amount of PCM rises, the number of broken particles on the failure surface becomes readily apparent. This is due to the PCM's poor shear strength and stiffness and the failure of some PCM particles during shearing [13]. As seen in Figure 25.c, the broken particles with 40% PCM addition are much more evident in the matrix than in the specimens with 20% PCM addition. This is in line with apparent density and mechanical strength results, as the inclusion of 40% mPCMs caused a decrease in compressive strength by 20% compared to the specimen containing 20% PCM addition. Furthermore, graphite powder addition increased the microcracks observed in the surface because coarse graphite particles behaved like an obstacle for geopolymerization reactions, as seen in Figure 25. By looking at the interface between the graphite particles and the geopolymerization products, we can see that the coarse graphite has an interfacial transition zone similar to aggregates [16], which could lead to weak planes and a decrease in mechanical performance as graphite addition decreased the compressive strength performance of the specimens up to 60% compared to G0-PCM0.

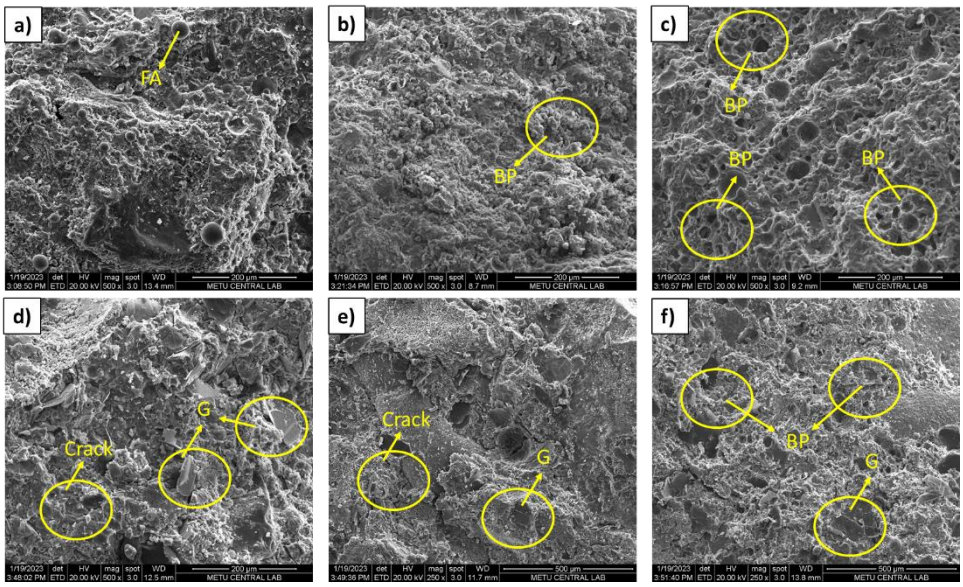

Figure 25. The SEM images of a) G0-PCM0, b) G0-PCM20, c) G0-PCM40, d) G10-PCM0, e) G10-PCM20, and f) G10-PCM40. BP: Broken mPCM particles and G is graphite.

The mechanical strength results showed that adding nanoparticles to the composites enhanced the mechanical performance due to the denser matrix due to the filler effect and increased pozzolanic activity. Figure 26 shows the SEM images of nano-SiO2 incorporated specimens. As can be seen in Figure 26.a, it can be seen that the microstructure of the G0-Si-PCM0 is dense and uniform without pores. The dense microstructure of the sample may be generated by the high activity of nano-silica particles, which enhances the geopolymerization reactions to form more C,N-A-S-H gel for a higher mechanical strength than the sample without nanosilica. In addition, no agglomerated nano-SiO_2 particles were observed in the images, indicating that nanoparticle dispersion was sufficient. Similar to the control mixes, broken particles of mPCMs were observed for 20 and 40% of mPCM incorporated samples. Besides, the inclusion of graphite into the matrix increased the visible cracks.

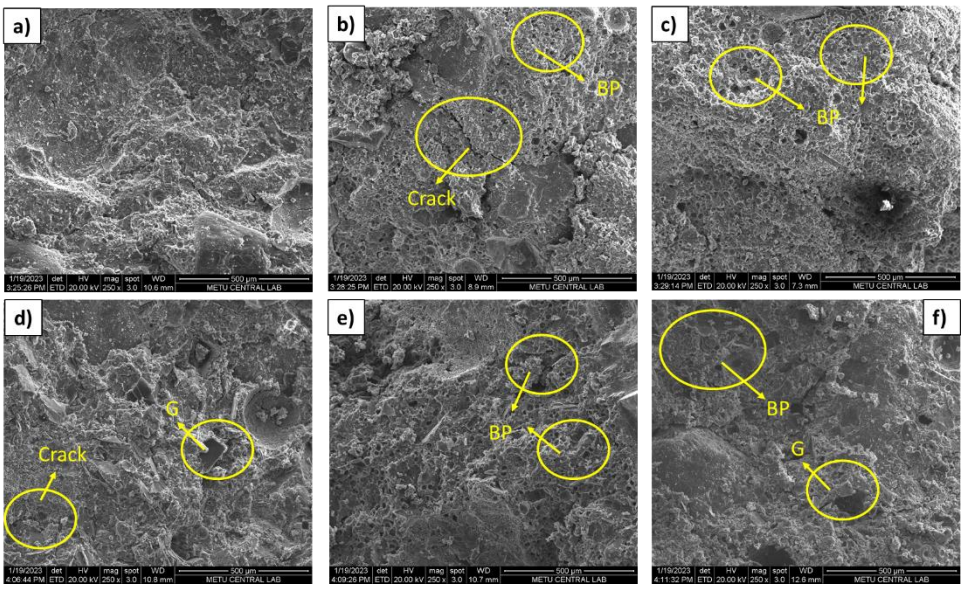

Figure 26. The SEM images of a) G0-Si-PCM0, b) G0-Si-PCM20, c) G0-Si-PCM40, d) G10-Si-PCM0, e) G10-Si-PCM20, and f) G10-Si-PCM40. BP: Broken mPCM particles and G is graphite.

Similar to nano-SiO_2 addition, nano-TiO_2 resulted in a denser matrix due to the filler effect. However, as can be seen in Figure 27.a, agglomerated nano-TiO_2 particles were observed in SEM images, in which agglomerates are well-bonded to the matrix. nano-TiO_2 was confirmed with Ti-rich EDS spectra. Previous research is done on nano-TiO_2 incorporated cementitious systems also revealed a high agglomeration tendency of nano-TiO_2 particles [121][122]. For instance, Shafaei et al. [122] used a high-shear mixer to de-agglomerate the nano-TiO_2 particles as they tend to agglomerate when mixing with water. However, their results also showed agglomerated particles in the hardened composites after reaching a certain addition amount. Similar to the control mixes, broken particles of mPCMs were observed for 20 and 40% of mPCM incorporated samples. Besides, the inclusion of graphite into the matrix increased the visible cracks.

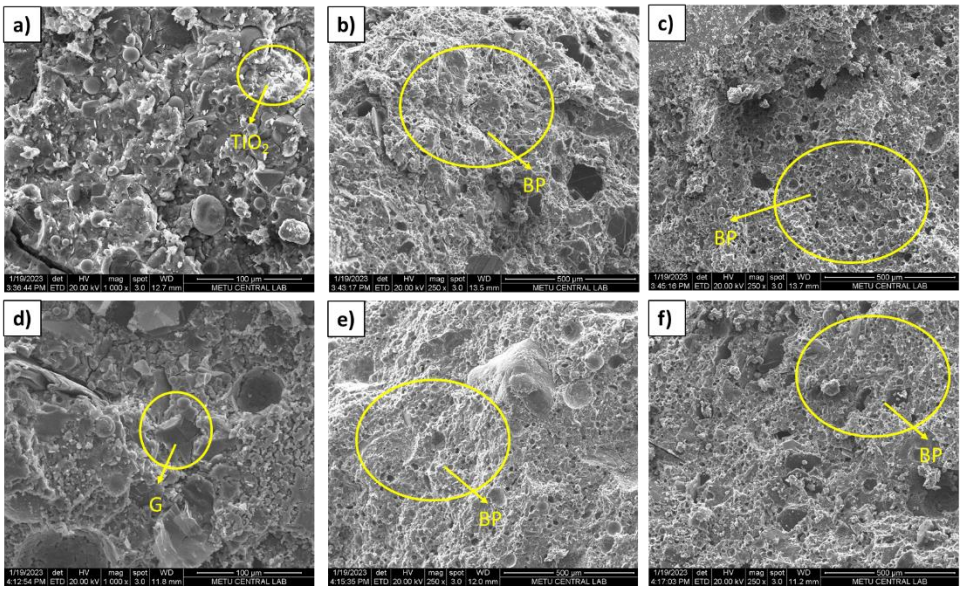

Figure 27. The SEM images of a) G0-Ti-PCM0, b) G0-Ti-PCM20, c) G0-Ti-PCM40, d) G10-Ti-PCM0, e) G10-Ti-PCM20, and f) G10-Ti-PCM40. BP: Broken mPCM particles, G is graphite, and TiO_2 is agglomerated nano-TiO_2.

4.5 Differential scanning calorimetry (DSC)

The DSC results of the composites are given in Figure 32. In addition, the melting and freezing processes' phase change temperatures and latent heat values are described in Figure 28 to Figure 33. The latent heat capacities are derived by numerically integrating the entire area beneath the peaks of the solid–liquid transition curves of the PCMs in the composite [63]. As seen, the curves of PCM-incorporated mortars exhibit peaks at almost the same temperature, around 20-25 °C within the phase change range of PCM, whereas the curve of the reference samples is smooth. As expected, the latent heat capacity of the samples was increased with the increasing amount of mPCM incorporation, and the thermal inertia of the specimens doubled for 20 vol% and 40 vol% samples, respectively. As can be seen in the figures, the presence of the endothermic peaks for PCM20 and PCM40 samples confirms that the phase transition occured. For instance, the latent heat capacity of G0-PCM20 was 4.29 J/g, and it increased to 8.07 J/g for G0-PCM40 mixture. The similar trend was observed for all samples due to the fact that mPCMs

are the only latent heat storage medium in the composites; thus, inclusion of nanoparticles or graphite powder would not affect the heat storage capacity of the samples.

The differences in latent storage capacities between samples are related to the heterogenous nature of the composites. Therefore, with the addition of 20 vol% mPCM, melting enthalpy of the samples was changed between 3.10 and 4.29 J/g, on the other hand, 40 vol% addition, melting enthalpy of the samples was changed between 6.20 and 10.51 J/g, which are consistent with the literature [47][123][124][112].

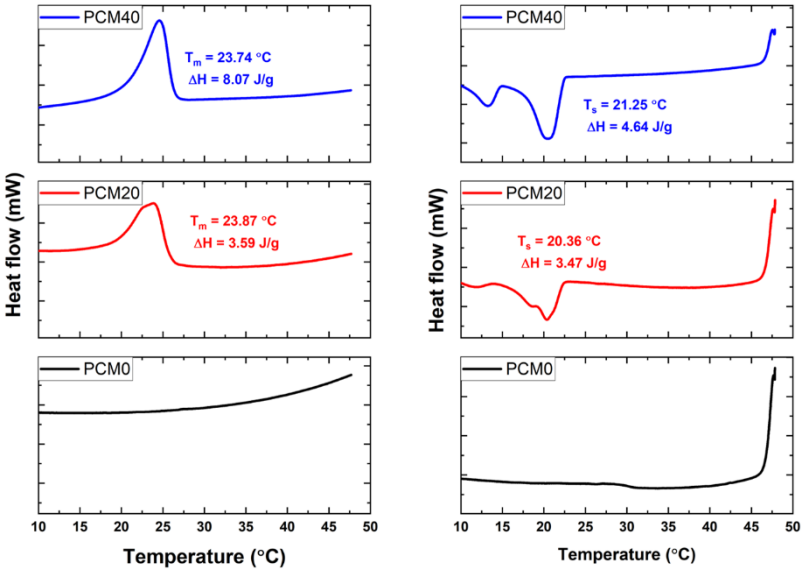

Figure 28. The endothermic and exothermic curves from the obtained DSC results for G0-PCM0, G0-PCM20, and G0-PCM40

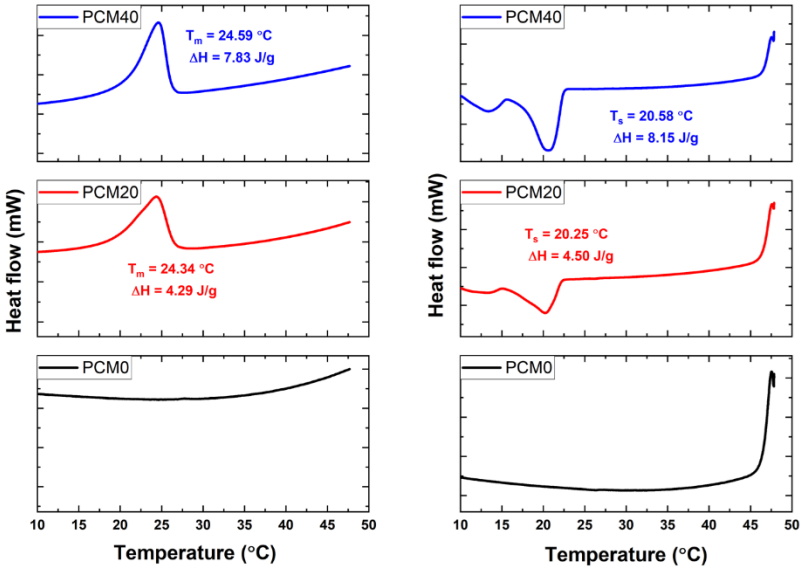

Figure 29. The endothermic and exothermic curves from the obtained DSC results for G0-Si-PCM0, G0-Si-PCM20, and G0-Si-PCM40

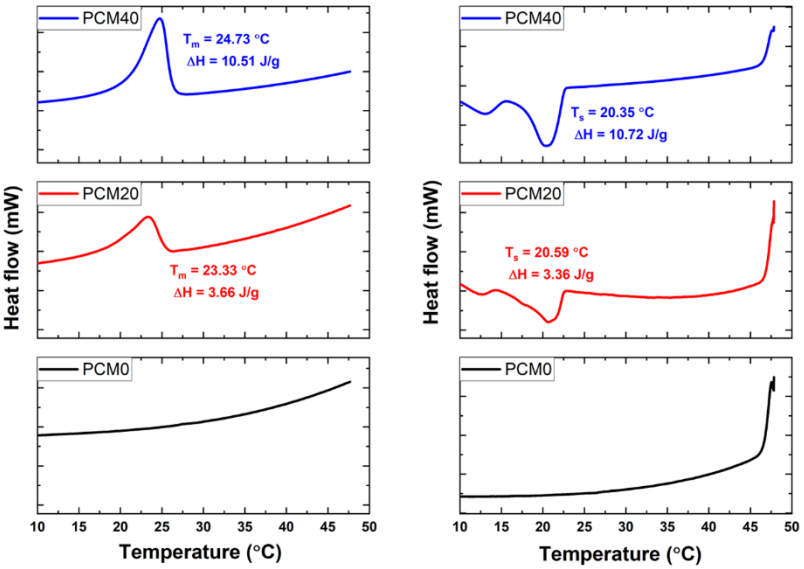

Figure 30. The endothermic and exothermic curves from the obtained DSC results for G0-Ti-PCM0, G0-Si-PCM20, and G0-Ti-PCM40

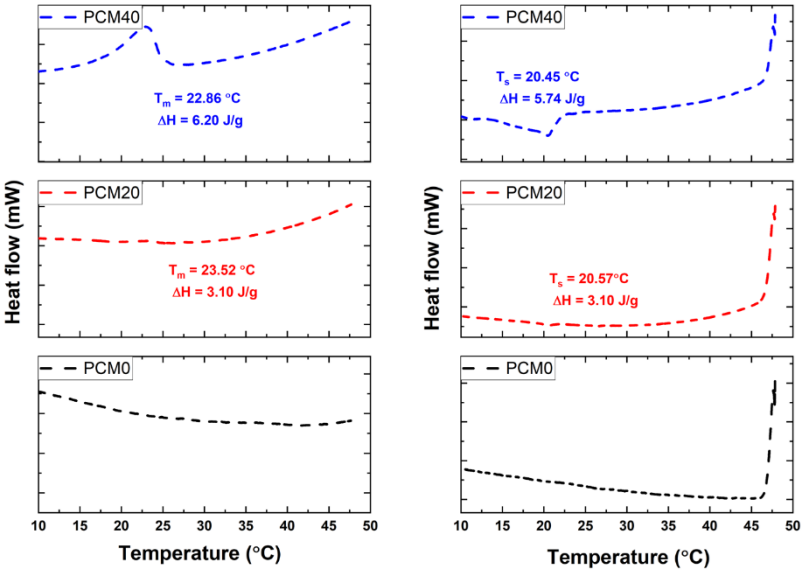

Figure 31. The endothermic and exothermic curves from the obtained DSC results for G10-PCM0, G10-PCM20, and G10-PCM40

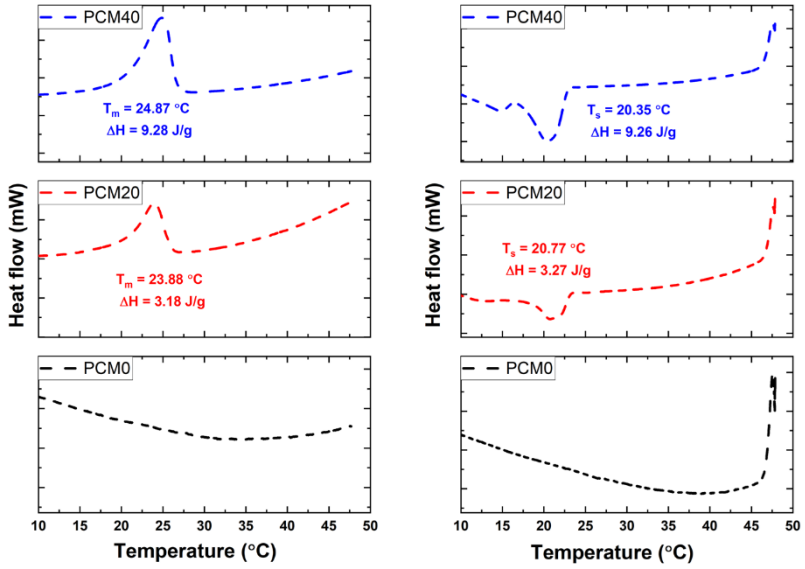

Figure 32. The endothermic and exothermic curves from the obtained DSC results for G10-Si-PCM0, G10-Si-PCM20, and G10-Si-PCM40

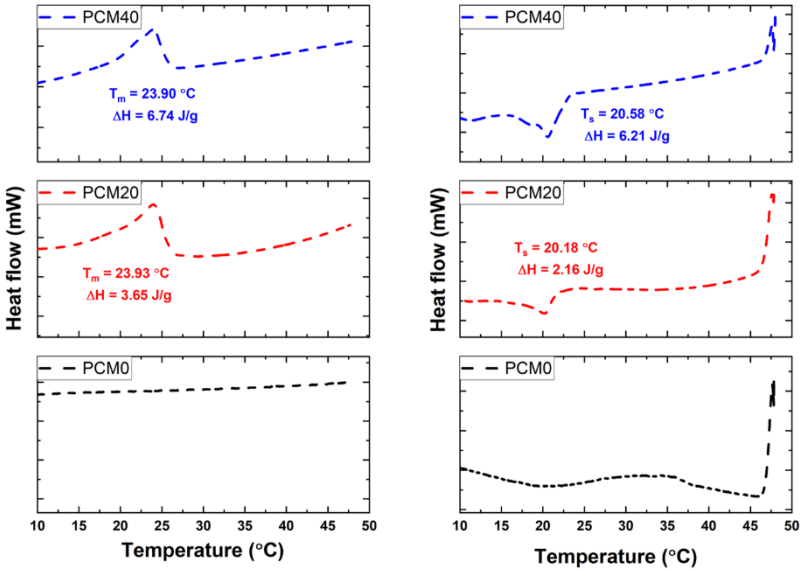

Figure 33. The endothermic and exothermic curves from the obtained DSC results for G10-Ti-PCM0, G10-Ti-PCM20, and G10-Ti-PCM40

Pomianowski et al. [125] propose 4 different methods to evaluate the specific heat capacity of PCM integrated inhomogenous composite: the theoretical method, the simple method, the numerical simple method, and the inverse method. In this study, the simple method was applied to find the specific heat capacity of the composites as METU Central Laboratory was unable to perform the experimental ASTM method named "Sapphire method" to find the specific heat capacity of the samples.

The simple method makes it possible to find an average specific heat capacity from DSC curves in a defined temperature range using the Eqns. (24) and (25), where ΔQ is the internal energy increase of the sample, m is the mass sample, C_p is the specific heat capacity, and dT is the temperature difference between the beginning and the end of the sample heating process.

$$C_p = \frac{\Delta Q}{m \times dT} \tag{24}$$

and

$$\Delta Q = \int_{T_{start}}^{T_{end}} q(T)dT \tag{25}$$

To determine ΔQ, the integrated part of the heat flow vs. temperature graph was used.

Table 14. Thermophysical properties of mPCM and PCM incorporated composites.

Mix	**Melting process**		**Crystallization process**		
	T_p (°C)	**ΔH_m (J/g)**	**T_p (°C)**	**ΔH_c (J/g)**	**C_P (J/g °C)**
nextek 24D	24.59	155.69	19.78	160.22	32
G0-PCM20	23.87	3.59	20.36	3.47	1.41
G0-Si-PCM20	24.34	4.29	20.25	4.50	1.76
G0-Ti-PCM20	23.33	3.66	20.59	3.36	1.40
G0-PCM40	23.74	8.07	21.25	4.64	1.40
G0-Si-PCM40	24.59	7.83	20.58	8.15	2.54
G0-Ti-PCM40	24.73	10.51	20.35	10.72	4.25
G10-PCM20	23.52	3.10	20.57	3.10	1.24
G10-Si-PCM20	23.88	3.18	20.77	3.27	1.29
G10-Ti-PCM20	23.93	3.65	20.18	2.16	1.16
G10-PCM40	22.86	6.20	20.45	5.74	2.34
G10-Si-PCM40	24.87	9.28	20.35	9.26	3.71
G10-Ti-PCM40	23.90	6.74	20.58	6.21	2.59

4.6 Thermal conductivity

Figure 34 shows the thermal conductivity results of the composites by the Hot Disk measurement. As seen in Figure 34, the thermal conductivity of all samples decreases with mPCM addition. In this study, mPCM was incorporated into the

mixtures to replace the same volume percentage of the sand. The thermal conductivity of the quartz sand used was around 0.4 W/mK, whereas the mPCM has a much lower thermal conductivity of about 0.08 W/mK. Therefore, a reduction in thermal conductivity was inevitable, and incorporating mPCM resulted in 7.19% (-0.09 W/m K) and 24.19% (-0.31 W/m K) reduction in thermal conductivity for G0-PCM20 and G0-PCM40 samples, compared to G0-PCM0, respectively. A similar trend was also observed for the samples containing nano-SiO_2 and nano-TiO_2.

Although previous studies showed that the higher amount of nano-SiO_2 addition to the cement matrix could decrease the composites' thermal conductivity [126], the current study's results showed that adding nano-SiO_2 particles enhanced the overall thermal conductivity of the system. This can be attributed to the fact that 0.8 wt% addition of nano-SiO_2 was not enough to reach the percolation threshold; thus, their physical effect was minimal on the total thermal conductivity of the composites. Moreover, combining the filler effect and increasing geopolymerization reactions results in a denser matrix, as seen in both mechanical strength and apparent density results. Therefore, a denser matrix with better heat transfer properties was Compared to the G0-PCM0 sample, and the thermal conductivity of G0-Si-PCM0 was enhanced by 18% by nano-SiO_2 addition. The same effect was also observed for G0-Si-PCM20, in which thermal conductivity was improved by 7% compared to G0-PCM20. On the other hand, adding nano-SiO_2 was ineffective in increasing the thermal conductivity of G0-Si-PCM40, in which thermal conductivity was reduced by 15% compared to G0-PCM40. The decrease in thermal conductivity was due to the higher amounts of mPCMs incorporated into the matrix, which caused a lowering in geopolymerization reactions, increasing the overall porosity.

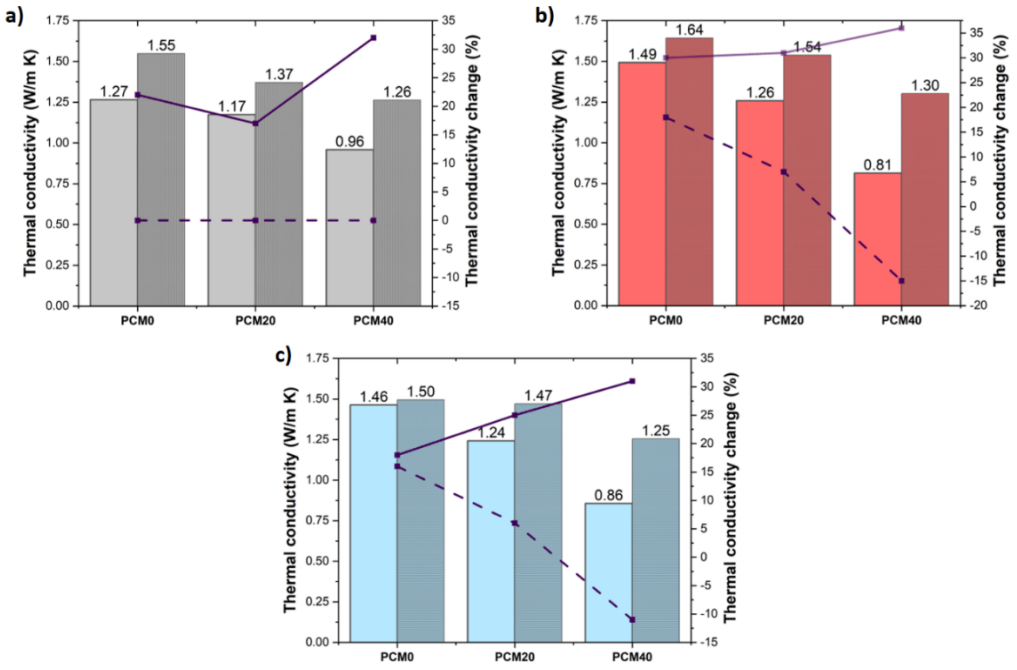

Figure 34. The thermal conductivity results from Hot Disk measurement. a) Control, b) nano-SiO2 added, and c) nano-TiO2 added composites. The light-colored column bars represent the samples without graphite, and the dark ones represent those with graphite. The lines represent the thermal conductivity change, straight lines represent the change with respect to control samples without graphite, and the dashed line represents graphite addition.

Similar to nano-SiO_2, nano-TiO_2 addition also increased the samples' thermal conductivity. For instance, compared to the G0-PCM0 sample, the thermal conductivity of G0-Si-PCM0 was enhanced by 16% by nano-SiO_2 addition. However, with 40% mPCM addition, the thermal conductivity was decreased by -11% (-0.102 W/m K) because the total porosity was increased further with increasing mPCM as can be understood from flexural and compressive strength results.

When graphite was added to the composite, the thermal conductivity of all samples was increased, and the loss due to mPCM incorporation was recovered. As low heat conduction in the matrix might effect the charging/discharging properties, the recovery of thermal conduction by adding graphite is an important step to increase the overall energy storage performance of the composites. Compared to the G0-PCM0 sample, the thermal conductivity was improved by +22% (0.28 W/m K), +30% (0.38 W/m K), and 18% (0.23 W/m K) for G10-PCM0, G10-Si-PCM0, and

G10-Ti-PCM0, respectively. The same trend in thermal conduction increase was also observed for the samples containing mPCMs.

CHAPTER 5

CONCLUSIONS

Reducing heating and cooling-related energy use in buildings has become a top priority for many countries to achieve the carbon neutrality target and respond to the growing energy crisis. Furthermore, utilizing alternative binders to decrease the dependency on ordinary Portland cement is important to reduce global greenhouse gas emissions, as manufacturing of ordinary Portland cement is responsible for nearly 10% of the total global CO_2 emission.

In this study, a novel mPCM incorporated geopolymer composite was developed to be used in passive building applications to reduce buildings' heating and cooling energy demand. Furthermore, different locally available industrial wastes, FA and GGBFS, were activated to produce low-carbon and affordable composites.

Although mPCM-incorporated cementitious systems have been tried in buildings for various applications, the mechanical strength loss due to mPCM incorporation into the matrix is one of the biggest obstacles to the widespread application of the mPCM incorporated building elements. In addition, the low thermal conductivity of the matrix due to mPCM incorporation affects the charging and discharging properties of the cementitious composites as an effective melting/solidification process is vital for efficiently utilizing the latent heat capacity of the mPCMs.

Therefore, nanoparticles and graphite platelets were utilized to address the abovementioned problems. First, nano-SiO_2 and nano-TiO_2 particles were added to increase the geopolymer nanocomposites' mechanical properties. Secondly, graphite platelets were incorporated into the system to enhance the heat transfer properties of the geopolymer matrix. The overall effect of using nanoparticles and graphite platelets on the geopolymer composites' thermal and mechanical properties was

investigated systematically. Based on the experimental results, the following conclusion can be drawn:

- Nano-SiO2 and mPCM addition reduced the flowability of the mixtures. The reduced flowability of the mPCM incorporated mixes is explained by increasing in solid content and high water absorption capacity of mPCM. Furthermore, the volume replaced by mPCM has a much finer particle size distribution than the sand; thus, increasing surface area of the mPCM inevaitably results in higher water demand than the same volume of the sand replaced. On the other hand, replacing nano-TiO_2 with binders did not considerably reduce the mixtures' flowability considerably. This behavior may be linked to nanoparticle agglomeration, which reduces the accessible surface area for interaction and water absorption.
- The apparent density of the mixtures was increased with nanoparticle addition due to the filler effect of the nanoparticles. Due to the decreased capillary porosity, a higher packing density was observed. In addition, nano-SiO_2 exhibits pozzolanic reactivity, accelerating the geopolymerization and contributing to a denser matrix.
- The mechanical properties of the mPCM incorporated mixtures decreased with increasing PCM content. The reduction in compressive strength was – up to 50% compared to the control specimen. The compressive and flexural strength of specimens containing nano-SiO_2 was greater than those without nano-SiO_2 due to the denser matrix achieved. The mechanical strength was reduced with graphite addition due to the fact that the layers of graphite only interact via weak van der Waals forces, and excessive graphite particles in the matrix promote the agglomeration of graphite, which increases the matrix damage under load.
- The effectiveness of nanoparticles in increasing the mechanical performance of the geopolymer composites was decreased with graphite addition due to the progression of interfacial transition zone comparable to that of aggregates for the coarse graphite.

- All developed composites had 28-day compressive strength higher than 20 MPa, making them suitable for building applications.
- The SEM images revealed that composites with nanoparticle addition have a denser matrix than the control specimen and the composites with graphite addition. The increasing quantity of micropores due to mPCM addition was observed with broken particles as a result of the compression test.
- The DSC results showed that mPCM incorporated composites have latent heat storage capacity changing between 3-10 J/g depending on the geopolymer composition, and latent heat storage capacity increased with the increasing amount of PCM added.
- Graphite inclusion greatly improved the composites' thermal conductivity. Due to the high thermal conductivity and high surface area of the graphite platelets present, thermally conductive networks were formed in the cement matrix, enhancing the latent heat storage and release rates of the mPCMs.

The experiment results showed that geopolymer composites with enhanced thermal and sufficient mechanical properties were developed by incorporating nanoparticles and graphite platelets into the geopolymer matrix. However, there are some limitations regarding the scope of this study. First, the numerical and experimental validation should be done to observe the overall effect of the mPCM integrated composites on reducing the buildings' cooling/heating energy demand. In particular, the impact of increasing the thermal conductivity of the matrix should be investigated thoroughly by investigating different wall configurations. Secondly, despite adding more mPCM into the matrix resulting in better thermal energy storage capacity, the workability and mechanical properties of the composites were seriously affected. Besides, the addition of nano-SiO_2 further reduced the workability of the composites. Therefore, the water-to-cement ratio in the mix design could be increased if more mPCM is added. However, due to the reduction in workability and mechanical properties, as well as the economic concerns regarding the relatively high price of the mPCM, 40% volume addition was seen as adequate. However, the effectiveness of the developed composites can be measured after conducting further experimental

and numerical investigations considering the real-life applications. For instance, an increase in thermal conductivity could lead to more charging/discharging and more energy stored in the composite; however, how occupant comfort and energy demand will be affected should be extensively investigated considering various parameters such as climatic conditions, wall configuration and the thickness of the PCM integrated layer. In future studies, the performance of the developed composites will be investigated.

REFERENCES

[1] "Tracking Buildings 2021 – Analysis - IEA." [Online]. Available: https://www.iea.org/reports/tracking-buildings-2021. [Accessed: 05-Feb-2022].

[2] D. B. Kim, D. D. Kim, and T. Kim, "Energy performance assessment of HVAC commissioning using long-term monitoring data: A case study of the newly built office building in South Korea," *Energy Build.*, vol. 204, p. 109465, Dec. 2019.

[3] B. Kim, Y. Yamaguchi, S. Kimura, Y. Ko, K. Ikeda, and Y. Shimoda, "Urban building energy modeling considering the heterogeneity of HVAC system stock: A case study on Japanese office building stock," *Energy Build.*, vol. 207, p. 109590, Jan. 2020.

[4] L. F. Cabeza, A. Castell, C. Barreneche, A. De Gracia, and A. I. Fernández, "Materials used as PCM in thermal energy storage in buildings: A review," *Renew. Sustain. Energy Rev.*, vol. 15, no. 3, pp. 1675–1695, 2011.

[5] S. Álvarez, L. F. Cabeza, A. Ruiz-Pardo, A. Castell, and J. A. Tenorio, "Building integration of PCM for natural cooling of buildings," *Appl. Energy*, vol. 109, pp. 514–522, 2013.

[6] D. K. Bhamare, M. K. Rathod, and J. Banerjee, "Passive cooling techniques for building and their applicability in different climatic zones—The state of art," *Energy Build.*, vol. 198, pp. 467–490, 2019.

[7] E. Solgi, Z. Hamedani, R. Fernando, H. Skates, and N. E. Orji, "A literature review of night ventilation strategies in buildings," *Energy and Buildings*, vol. 173. Elsevier Ltd, pp. 337–352, 15-Aug-2018.

[8] M. Saffari, A. de Gracia, C. Fernández, and L. F. Cabeza, "Simulation-based optimization of PCM melting temperature to improve the energy performance in buildings," *Appl. Energy*, vol. 202, pp. 420–434, 2017.

[9] Y. Konuklu, M. Ostry, H. O. Paksoy, and P. Charvat, "Review on using

microencapsulated phase change materials (PCM) in building applications," *Energy Build.*, vol. 106, pp. 134–155, 2015.

[10] A. de Gracia, "Dynamic building envelope with PCM for cooling purposes – Proof of concept," *Appl. Energy*, vol. 235, pp. 1245–1253, Feb. 2019.

[11] D. K. Bhamare, P. Saikia, M. K. Rathod, D. Rakshit, and J. Banerjee, "A machine learning and deep learning based approach to predict the thermal performance of phase change material integrated building envelope," *Build. Environ.*, vol. 199, p. 107927, Jul. 2021.

[12] J. H. Park, J. Jeon, J. Lee, S. Wi, B. Y. Yun, and S. Kim, "Comparative analysis of the PCM application according to the building type as retrofit system," *Build. Environ.*, vol. 151, pp. 291–302, Mar. 2019.

[13] R. Shadnia, L. Zhang, and P. Li, "Experimental study of geopolymer mortar with incorporated PCM," *Constr. Build. Mater.*, vol. 84, pp. 95–102, Jun. 2015.

[14] N. B. Singh and B. Middendorf, "Geopolymers as an alternative to Portland cement : An overview," *Constr. Build. Mater.*, vol. 237, p. 117455, 2020.

[15] N. Mohamad, K. Muthusamy, R. Embong, A. Kusbiantoro, and M. Hanafi, "Materials Today : Proceedings Environmental impact of cement production and Solutions : A review," *Mater. Today Proc.*, vol. 48, pp. 741–746, 2022.

[16] I. Papanikolaou, C. Litina, A. Zomorodian, and A. Al-Tabbaa, "Effect of natural graphite fineness on the performance and electrical conductivity of cement paste mixes for self-sensing structures," *Materials (Basel).*, vol. 13, no. 24, pp. 1–19, 2020.

[17] T. Xiong, K. W. Shah, and H. W. Kua, "Application of graphite platelets for heat transfer enhancement of cementitious composites containing microencapsulated phase change materials," *Constr. Build. Mater.*, vol. 318, p. 126024, Feb. 2022.

[18] W. Su, J. Darkwa, and G. Kokogiannakis, "Review of solid-liquid phase

change materials and their encapsulation technologies," *Renew. Sustain. Energy Rev.*, vol. 48, pp. 373–391, Aug. 2015.

[19] V. V. Tyagi and D. Buddhi, "PCM thermal storage in buildings: A state of art," *Renew. Sustain. Energy Rev.*, vol. 11, no. 6, pp. 1146–1166, Aug. 2007.

[20] K. Yang, N. Zhu, C. Chang, D. Wang, S. Yang, and S. Ma, "A methodological concept for phase change material selection based on multi-criteria decision making (MCDM): A case study," *Energy*, vol. 165, pp. 1085–1096, Dec. 2018.

[21] Y. Zhang, G. Zhou, K. Lin, Q. Zhang, and H. Di, "Application of latent heat thermal energy storage in buildings: State-of-the-art and outlook," *Build. Environ.*, vol. 42, no. 6, pp. 2197–2209, Jun. 2007.

[22] N. Soares, J. J. Costa, A. R. Gaspar, and P. Santos, "Review of passive PCM latent heat thermal energy storage systems towards buildings' energy efficiency," *Energy Build.*, vol. 59, pp. 82–103, Apr. 2013.

[23] R. K. Sharma, P. Ganesan, V. V. Tyagi, H. S. C. Metselaar, and S. C. Sandaran, "Developments in organic solid–liquid phase change materials and their applications in thermal energy storage," *Energy Convers. Manag.*, vol. 95, pp. 193–228, May 2015.

[24] K. Faraj, M. Khaled, J. Faraj, F. Hachem, and C. Castelain, "A review on phase change materials for thermal energy storage in buildings: Heating and hybrid applications," *J. Energy Storage*, vol. 33, p. 101913, Jan. 2021.

[25] J. Pereira da Cunha and P. Eames, "Thermal energy storage for low and medium temperature applications using phase change materials – A review," *Appl. Energy*, vol. 177, pp. 227–238, Sep. 2016.

[26] Q. Al-Yasiri and M. Szabó, "Case study on the optimal thickness of phase change material incorporated composite roof under hot climate conditions," *Case Stud. Constr. Mater.*, vol. 14, Jun. 2021.

[27] U. Berardi and A. A. Gallardo, "Properties of concretes enhanced with phase

change materials for building applications," *Energy Build.*, vol. 199, pp. 402–414, Sep. 2019.

[28] S. Cunha, P. Leite, and J. Aguiar, "Characterization of innovative mortars with direct incorporation of phase change materials," *J. Energy Storage*, vol. 30, p. 101439, Aug. 2020.

[29] P. K. S. Rathore and S. K. Shukla, "Potential of macroencapsulated PCM for thermal energy storage in buildings: A comprehensive review," *Constr. Build. Mater.*, vol. 225, pp. 723–744, Nov. 2019.

[30] E. Alehosseini and S. M. Jafari, "Nanoencapsulation of phase change materials (PCMs) and their applications in various fields for energy storage and management," *Adv. Colloid Interface Sci.*, vol. 283, p. 102226, Sep. 2020.

[31] Z. Liu *et al.*, "A review on macro-encapsulated phase change material for building envelope applications," *Build. Environ.*, vol. 144, pp. 281–294, Oct. 2018.

[32] D. Zhou, C. Y. Zhao, and Y. Tian, "Review on thermal energy storage with phase change materials (PCMs) in building applications," *Appl. Energy*, vol. 92, pp. 593–605, Apr. 2012.

[33] S. Yu, X. Wang, and D. Wu, "Microencapsulation of n-octadecane phase change material with calcium carbonate shell for enhancement of thermal conductivity and serving durability: Synthesis, microstructure, and performance evaluation," *Appl. Energy*, vol. 114, pp. 632–643, Feb. 2014.

[34] Z. Zhang, G. Shi, S. Wang, X. Fang, and X. Liu, "Thermal energy storage cement mortar containing n-octadecane/expanded graphite composite phase change material," *Renew. Energy*, vol. 50, pp. 670–675, Feb. 2013.

[35] S. S. Magendran *et al.*, "Synthesis of organic phase change materials (PCM) for energy storage applications: A review," *Nano-Structures and Nano-Objects*, vol. 20, p. 100399, 2019.

[36] S. Dhivya, S. I. Hussain, S. Jeya Sheela, and S. Kalaiselvam, "Experimental

study on microcapsules of Ag doped ZnO nanomaterials enhanced Oleic-Myristic acid eutectic PCM for thermal energy storage," *Thermochim. Acta*, vol. 671, pp. 70–82, Jan. 2019.

[37] Y. Zhu *et al.*, "Nanoencapsulated phase change materials with polymer-SiO2 hybrid shell materials: Compositions, morphologies, and properties," *Energy Convers. Manag.*, vol. 164, pp. 83–92, May 2018.

[38] Y. Shen *et al.*, "Experimental thermal study of a new PCM-concrete thermal storage block (PCM-CTSB)," *Constr. Build. Mater.*, vol. 293, p. 123540, Jul. 2021.

[39] Z. A. Qureshi, H. M. Ali, and S. Khushnood, "Recent advances on thermal conductivity enhancement of phase change materials for energy storage system: A review," *Int. J. Heat Mass Transf.*, vol. 127, pp. 838–856, Dec. 2018.

[40] M. Amin, N. Putra, E. A. Kosasih, E. Prawiro, R. A. Luanto, and T. M. I. Mahlia, "Thermal properties of beeswax/graphene phase change material as energy storage for building applications," *Appl. Therm. Eng.*, vol. 112, pp. 273–280, Feb. 2017.

[41] P. K. S. Rathore, S. K. Shukla, and N. K. Gupta, "Synthesis and characterization of the paraffin/expanded perlite loaded with graphene nanoparticles as a thermal energy storage material in buildings," *J. Sol. Energy Eng. Trans. ASME*, vol. 142, no. 4, Aug. 2020.

[42] M. Kazemi, A. Kianifar, and H. Niazmand, "A lab-scale study on thermal performance enhancement of phase change material containing multi-wall carbon nanotubes for buildings free-cooling," *Sustain. Energy Technol. Assessments*, vol. 50, Mar. 2022.

[43] J. Cheng *et al.*, "Preparation and characterization of carbon nanotube microcapsule phase change materials for improving thermal comfort level of buildings," *Constr. Build. Mater.*, vol. 244, May 2020.

[44] P. K. S. Rathore and S. kumar Shukla, “Improvement in thermal properties of PCM/Expanded vermiculite/expanded graphite shape stabilized composite PCM for building energy applications,” *Renew. Energy*, vol. 176, pp. 295–304, Oct. 2021.

[45] M. H. M. Isa, X. Zhao, and H. Yoshino, “Preliminary Study of Passive Cooling Strategy Using a Combination of PCM and Copper Foam to Increase Thermal Heat Storage in Building Facade,” *Sustain. 2010, Vol. 2, Pages 2365-2381*, vol. 2, no. 8, pp. 2365–2381, Jul. 2010.

[46] V. V. Rao, R. Parameshwaran, and V. V. Ram, “PCM-mortar based construction materials for energy efficient buildings: A review on research trends,” *Energy Build.*, vol. 158, pp. 95–122, Jan. 2018.

[47] M. Kheradmand, M. Azenha, J. L. B. de Aguiar, and J. Castro-Gomes, “Experimental and numerical studies of hybrid PCM embedded in plastering mortar for enhanced thermal behaviour of buildings,” *Energy*, vol. 94, pp. 250–261, Jan. 2016.

[48] S. S. Lucas, V. M. Ferreira, and J. L. B. De Aguiar, “Latent heat storage in PCM containing mortars—Study of microstructural modifications,” *Energy Build.*, vol. 66, pp. 724–731, Nov. 2013.

[49] Z. I. Djamai, A. S. Larbi, F. Salvatore, and G. Cai, “A new PCM-TRC composite: A mechanical and physicochemical investigation,” *Cem. Concr. Res.*, vol. 135, p. 106119, Sep. 2020.

[50] L. Olivieri, J. A. Tenorio, D. Revuelta, L. Navarro, and L. F. Cabeza, “Developing a PCM-enhanced mortar for thermally active precast walls,” *Constr. Build. Mater.*, vol. 181, pp. 638–649, Aug. 2018.

[51] J. H. Yeon, “Thermal behavior of cement mortar embedded with low-phase transition temperature PCM,” *Constr. Build. Mater.*, vol. 252, p. 119168, Aug. 2020.

[52] D. H. Yoo, I. K. Jeon, B. H. Woo, and H. G. Kim, “Performance of energy

storage system containing cement mortar and PCM/epoxy/SiC composite fine aggregate," *Appl. Therm. Eng.*, vol. 198, p. 117445, Nov. 2021.

[53] A. Yousefi, W. Tang, M. Khavarian, and C. Fang, "Development of novel form-stable phase change material (PCM) composite using recycled expanded glass for thermal energy storage in cementitious composite," *Renew. Energy*, vol. 175, pp. 14–28, Sep. 2021.

[54] Z. Wang, H. Su, S. Zhao, and N. Zhao, "Influence of phase change material on mechanical and thermal properties of clay geopolymer mortar," *Constr. Build. Mater.*, vol. 120, pp. 329–334, Sep. 2016.

[55] H. Cui, T. Feng, H. Yang, X. Bao, W. Tang, and J. Fu, "Experimental study of carbon fiber reinforced alkali-activated slag composites with micro-encapsulated PCM for energy storage," *Constr. Build. Mater.*, vol. 161, pp. 442–451, Feb. 2018.

[56] L. O. Afolabi, Z. M. Ariff, P. S. M. Megat-Yusoff, H. H. Al-Kayiem, A. I. Arogundade, and O. T. Afolabi-Owolabi, "Red-mud geopolymer composite encapsulated phase change material for thermal comfort in built-sector," *Sol. Energy*, vol. 181, pp. 464–474, Mar. 2019.

[57] M. Kheradmand, Z. Abdollahnejad, and F. Pacheco-Torgal, "European Journal of Environmental and Civil Engineering Alkali-activated cement-based binder mortars containing phase change materials (PCMs): mechanical properties and cost analysis Alkali-activated cement-based binder mortars containing phase change materials (PCMs): mechanical properties and cost analysis," *Eur. J. Environ. Civ. Eng.*, vol. 24, no. 8, pp. 1068–1090, 2018.

[58] S. Ramakrishnan, K. Pasupathy, and J. Sanjayan, "Synthesis and properties of thermally enhanced aerated geopolymer concrete using form-stable phase change composite," *J. Build. Eng.*, vol. 40, p. 102756, Aug. 2021.

[59] S. Pilehvar *et al.*, "Physical and mechanical properties of fly ash and slag geopolymer concrete containing different types of micro-encapsulated phase change materials," *Constr. Build. Mater.*, vol. 173, pp. 28–39, Jun. 2018.

[60] A. Hassan, A. H. I. Mourad, Y. Rashid, N. Ismail, and M. S. Laghari, “Thermal and structural performance of geopolymer concrete containing phase change material encapsulated in expanded clay,” *Energy Build.*, vol. 191, pp. 72–81, May 2019.

[61] C. Liu, R. Qian, Z. Liu, G. Liu, and Y. Zhang, “Multi-scale modelling of thermal conductivity of phase change material/recycled cement paste incorporated cement-based composite material,” *Mater. Des.*, vol. 191, p. 108646, Jun. 2020.

[62] A. Ricklefs, A. M. Thiele, G. Falzone, G. Sant, and L. Pilon, “Thermal conductivity of cementitious composites containing microencapsulated phase change materials,” *Int. J. Heat Mass Transf.*, vol. 104, pp. 71–82, Jan. 2017.

[63] B. Xu and Z. Li, “Paraffin/diatomite composite phase change material incorporated cement-based composite for thermal energy storage,” *Appl. Energy*, vol. 105, pp. 229–237, May 2013.

[64] G. Jing *et al.*, “Introducing reduced graphene oxide to enhance the thermal properties of cement composites,” *Cem. Concr. Compos.*, vol. 109, May 2020.

[65] C. Phrompet, C. Sriwong, and C. Ruttanapun, “Mechanical, dielectric, thermal and antibacterial properties of reduced graphene oxide (rGO)-nanosized C3AH6 cement nanocomposites for smart cement-based materials,” *Compos. Part B Eng.*, vol. 175, Oct. 2019.

[66] S. Zhai *et al.*, “Investigation on preparation and multifunctionality of reduced graphene oxide cement mortar,” *Constr. Build. Mater.*, vol. 275, Mar. 2021.

[67] S. Ghosh, S. Harish, M. Ohtaki, and B. B. Saha, “Enhanced figure of merit of cement composites with graphene and ZnO nanoinclusions for efficient energy harvesting in buildings,” *Energy*, vol. 198, May 2020.

[68] J. Wei, L. Zhao, Q. Zhang, Z. Nie, and L. Hao, “Enhanced thermoelectric properties of cement-based composites with expanded graphite for climate adaptation and large-scale energy harvesting,” *Energy Build.*, vol. 159, pp.

66–74, Jan. 2018.

[69] J. L. Provis, “Alkali-activated materials,” *Cem. Concr. Res.*, vol. 114, pp. 40–48, Dec. 2018.

[70] C. Shi, B. Qu, and J. L. Provis, “Recent progress in low-carbon binders,” *Cem. Concr. Res.*, vol. 122, no. May, pp. 227–250, 2019.

[71] M. Tokyay, *Cement and Concrete Mineral Admixtures*. .

[72] J. A. L. F. Pacheco-Torgal, A. P. and C. Leonelli, and P. Chindaprasirt, *Handbook of Alkaliactivated Cements, Mortars and Concretes*, vol. 53, no. 9. 2013.

[73] M. Zhang, N. A. Deskins, G. Zhang, R. T. Cygan, and M. Tao, “Modeling the Polymerization Process for Geopolymer Synthesis through Reactive Molecular Dynamics Simulations,” *J. Phys. Chem. C*, vol. 122, no. 12, pp. 6760–6773, 2018.

[74] B. Walkley, G. J. Rees, R. San Nicolas, J. S. J. Van Deventer, J. V. Hanna, and J. L. Provis, “New Structural Model of Hydrous Sodium Aluminosilicate Gels and the Role of Charge-Balancing Extra-Framework Al,” *J. Phys. Chem. C*, vol. 122, no. 10, pp. 5673–5685, 2018.

[75] J. Yang, D. Li, and Y. Fang, “Synthesis of nanoscale CaO-Al2O3-SiO2-H2O and Na2\O-Al2O3-SiO2-H2O using the hydrothermal method and their characterization,” *Materials (Basel).*, vol. 10, no. 7, 2017.

[76] Z. Luo, W. Li, P. Li, K. Wang, and S. P. Shah, “Investigation on effect of nanosilica dispersion on the properties and microstructures of fly ash-based geopolymer composite,” *Constr. Build. Mater.*, vol. 282, p. 122690, 2021.

[77] R. Samuvel Raj, G. Prince Arulraj, N. Anand, B. Kanagaraj, E. Lubloy, and M. Z. Naser, “Nanomaterials in geopolymer composites: A review,” *Dev. Built Environ.*, vol. 13, no. November 2022, p. 100114, 2023.

[78] D. Adak, M. Sarkar, and S. Mandal, “Effect of nano-silica on strength and durability of fly ash based geopolymer mortar,” *Constr. Build. Mater.*, vol.

70, pp. 453–459, 2014.

[79] K. Chen *et al.*, “Development of low-calcium fly ash-based geopolymer mortar using nanosilica and hybrid fibers,” *Ceram. Int.*, vol. 47, no. 15, pp. 21791–21806, 2021.

[80] P. S. Deb, P. K. Sarker, and S. Barbhuiya, “Sorptivity and acid resistance of ambient-cured geopolymer mortars containing nano-silica,” *Cem. Concr. Compos.*, vol. 72, pp. 235–245, 2016.

[81] H. K. Hamzah, Z. H. Joudah, D. P. Georgescu, N. H. A. Khalid, and G. F. Huseien, “Laboratory evaluation of alkali-activated mortars modified with nanosilica from glass bottle wastes,” *Mater. Today Proc.*, vol. 46, pp. 2098–2104, 2020.

[82] T. A. Hussein *et al.*, “Chemical resistance of alkali-activated mortar with nano silica and polypropylene fiber,” *Constr. Build. Mater.*, vol. 363, no. November 2022, p. 129847, 2023.

[83] K. Rathinam, S. Sakthivel, S. P. Vigneshwaran, M. Vinayagamoorthy, and N. K. U., “Properties of nano silica modified cement less geopolymer composite mortar using fly ash and GGBS,” *Mater. Today Proc.*, vol. 62, pp. 535–542, 2022.

[84] A. A. Ramezanianpour and M. A. Moeini, “Mechanical and durability properties of alkali activated slag coating mortars containing nanosilica and silica fume,” *Constr. Build. Mater.*, vol. 163, pp. 611–621, 2018.

[85] Z. Luo, W. Li, Y. Gan, X. He, A. Castel, and D. Sheng, “Nanoindentation on micromechanical properties and microstructure of geopolymer with nano-SiO2 and nano-TiO2,” *Cem. Concr. Compos.*, vol. 117, no. November 2020, 2021.

[86] I. M. El-Kattan, M. S. Saif, M. O. R. El-Hariri, A. H. Elgandy, L. Pérez-Villarejo, and D. Eliche-Quesada, “Assessing the individual impact of magnesia and titania nano- particles on the performance of alkali-activated

slag mortars," *Constr. Build. Mater.*, vol. 365, no. November 2022, 2023.

[87] M. Maiti, M. Sarkar, S. Maiti, M. A. Malik, and S. Xu, "Modification of geopolymer with size controlled TiO2 nanoparticle for enhanced durability and catalytic dye degradation under UV light," *J. Clean. Prod.*, vol. 255, p. 120183, 2020.

[88] E. Dişçi and R. Polat, "The influence of nano-CaO and nano-Al2O3 and curing conditions on perlite based geopolymer concrete produced by the one-part mixing method," *Constr. Build. Mater.*, vol. 346, no. June, 2022.

[89] H. Assaedi *et al.*, "Characterization and properties of geopolymer nanocomposites with different contents of nano-CaCO3," *Constr. Build. Mater.*, vol. 252, p. 119137, 2020.

[90] F. Matalkah, A. Ababneh, and R. Aqel, "Effects of nanomaterials on mechanical properties, durability characteristics and microstructural features of alkali-activated binders: A comprehensive review," *Constr. Build. Mater.*, vol. 336, no. April, p. 127545, 2022.

[91] A. Caggiano, C. Mankel, and E. Koenders, "Reviewing theoretical and numerical models for PCM-embedded cementitious composites," *Buildings*, vol. 9, no. 1, 2018.

[92] K. M. Kodjo, J. Yvonnet, M. Karkri, and K. Sab, "Multiscale modeling of the thermomechanical behavior in heterogeneous media embedding Phase Change Materials particles," *J. Comput. Phys.*, vol. 378, pp. 303–323, Feb. 2019.

[93] P. K. Singh Rathore, S. K. Shukla, and N. K. Gupta, "Potential of microencapsulated PCM for energy savings in buildings: A critical review," *Sustain. Cities Soc.*, vol. 53, no. August 2019, p. 101884, 2020.

[94] L. Derradji, F. B. Errebai, and M. Amara, "Effect of PCM in Improving the Thermal Comfort in Buildings," *Energy Procedia*, vol. 107, no. September 2016, pp. 157–161, 2017.

[95] M. Saffari, A. De Gracia, S. Ushak, and L. F. Cabeza, “Economic impact of integrating PCM as passive system in buildings using Fanger comfort model,” *Energy Build.*, vol. 112, pp. 159–172, 2016.

[96] G. P. Panayiotou, S. A. Kalogirou, and S. A. Tassou, “Evaluation of the application of Phase Change Materials (PCM) on the envelope of a typical dwelling in the Mediterranean region,” *Renew. Energy*, vol. 97, pp. 24–32, 2016.

[97] J. F. Belmonte, P. Eguía, A. E. Molina, and J. A. Almendros-Ibáñez, “Thermal simulation and system optimization of a chilled ceiling coupled with a floor containing a phase change material (PCM),” *Sustain. Cities Soc.*, vol. 14, no. 1, pp. 154–170, 2015.

[98] N. Soares *et al.*, “Validation of different numerical models with benchmark experiments for modelling microencapsulated-PCM-based applications for buildings,” *Int. J. Therm. Sci.*, vol. 159, no. June 2020, 2021.

[99] A. H. N. Al-mudhafar, M. T. Hamzah, and A. L. Tarish, “Potential of integrating PCMs in residential building envelope to reduce cooling energy consumption,” *Case Stud. Therm. Eng.*, vol. 27, no. July, p. 101360, 2021.

[100] S. Ručevskis, P. Akishin, and A. Korjakins, “Parametric analysis and design optimisation of PCM thermal energy storage system for space cooling of buildings,” *Energy Build.*, vol. 224, 2020.

[101] N. P. Sharifi, G. E. Freeman, and A. R. Sakulich, “Using COMSOL modeling to investigate the efficiency of PCMs at modifying temperature changes in cementitious materials – Case study,” *Constr. Build. Mater.*, vol. 101, pp. 965–974, Dec. 2015.

[102] C. Shi, Q. Zhao, P. Wang, and L. Yang, “Preparation, performance study and application simulation of gypsum-paraffin/EG composite phase change building wallboard,” *J. Build. Eng.*, vol. 65, no. December 2022, p. 105813, 2023.

[103] A. H. Korayem, N. Tourani, M. Zakertabrizi, A. M. Sabziparvar, and W. H. Duan, “A review of dispersion of nanoparticles in cementitious matrices: Nanoparticle geometry perspective,” *Constr. Build. Mater.*, vol. 153, pp. 346–357, 2017.

[104] S. C. Paul, A. S. van Rooyen, G. P. A. G. van Zijl, and L. F. Petrik, “Properties of cement-based composites using nanoparticles: A comprehensive review,” *Constr. Build. Mater.*, vol. 189, pp. 1019–1034, 2018.

[105] Astm, “Standard Test Method for Flow of Hydraulic Cement Mortar: C1437-01,” *Standard*, pp. 7–8, 2001.

[106] S. Park, M. C. Kang, Y. Oinam, A. Amoozegar, and S. Pyo, “Measurement of skeletal density and porosity of construction materials using a new proposed vacuum pycnometer,” *Measurement*, vol. 196, p. 111209, Jun. 2022.

[107] Y. Huang, L. Gong, L. Shi, W. Cao, Y. Pan, and X. Cheng, “Experimental investigation on the influencing factors of preparing porous fly ash-based geopolymer for insulation material,” *Energy Build.*, vol. 168, pp. 9–18, Jun. 2018.

[108] D. V. Ribeiro and M. R. Morelli, “Influence of the addition of grinding dust to a magnesium phosphate cement matrix,” *Constr. Build. Mater.*, vol. 23, no. 9, pp. 3094–3102, 2009.

[109] J. Temuujin and A. van Riessen, “Effect of fly ash preliminary calcination on the properties of geopolymer,” *J. Hazard. Mater.*, vol. 164, no. 2–3, pp. 634–639, May 2009.

[110] ASTM C 348 – 14, “Standard Test Method for Flexural Strength of Hydraulic-Cement Mortars,” *Norma ASTM Int.*, 2018.

[111] ASTM C349, “Standard test method for compressive strength of hydraulic-cement mortars (Using portions of prisms broken in flexure),” *ASTM Int.*, pp. 1–6, 2002.

[112] A. Jayalath *et al.*, “Properties of cementitious mortar and concrete containing

micro-encapsulated phase change materials," *Constr. Build. Mater.*, vol. 120, pp. 408–417, 2016.

[113] M. Kooshafar and H. Madani, "An investigation on the influence of nano silica morphology on the characteristics of cement composites," *J. Build. Eng.*, vol. 30, no. February, p. 101293, 2020.

[114] C. A. Casagrande, W. L. Repette, and D. Hotza, "Effect of environmental conditions on degradation of NOx gases by photocatalytic nanotitania-based cement mortars after long-term hydration," *J. Clean. Prod.*, vol. 274, no. x, 2020.

[115] A. Kozbial, F. Zhou, Z. Li, H. Liu, and L. Li, "Are Graphitic Surfaces Hydrophobic?," *Acc. Chem. Res.*, vol. 49, no. 12, pp. 2765–2773, Dec. 2016.

[116] M. M. Barbero-Barrera, N. Flores Medina, and C. Guardia-Martín, "Influence of the addition of waste graphite powder on the physical and microstructural performance of hydraulic lime pastes," *Constr. Build. Mater.*, vol. 149, pp. 599–611, Sep. 2017.

[117] D. Frattini, G. Accardo, C. Ferone, and R. Cioffi, "Fabrication and characterization of graphite-cement composites for microbial fuel cells applications," *Mater. Res. Bull.*, vol. 88, pp. 188–199, Apr. 2017.

[118] T. H. A. Al-Saadi, E. G. Daway, S. H. Mohammad, and M. K. Mejbel, "Effect of graphite additions on the intumescent behaviour of alkali-activated materials based on glass waste," *J. Mater. Res. Technol.*, vol. 9, no. 6, pp. 14338–14349, Nov. 2020.

[119] X. Bao *et al.*, "Development of high performance PCM cement composites for passive solar buildings," *Energy Build.*, vol. 194, pp. 33–45, Jul. 2019.

[120] P. S. Deb, P. K. Sarker, and S. Barbhuiya, "Effects of nano-silica on the strength development of geopolymer cured at room temperature," *Constr. Build. Mater.*, vol. 101, pp. 675–683, 2015.

[121] P. Jędrzejczak *et al.*, "The influence of various forms of titanium dioxide on

the performance of resultant cement composites with photocatalytic and antibacterial functions," *Mater. Res. Bull.*, vol. 160, p. 112139, Apr. 2023.

[122] D. Shafaei, S. Yang, L. Berlouis, and J. Minto, "Multiscale pore structure analysis of nano titanium dioxide cement mortar composite," *Mater. Today Commun.*, vol. 22, p. 100779, Mar. 2020.

[123] N. Essid, A. Eddhahak-Ouni, and J. Neji, "Experimental and Numerical Thermal Properties Investigation of Cement-Based Materials Modified with PCM for Building Construction Use," *J. Archit. Eng.*, vol. 26, no. 3, p. 04020018, Sep. 2020.

[124] S. G. Jeong, J. Jeon, J. Cha, J. Kim, and S. Kim, "Preparation and evaluation of thermal enhanced silica fume by incorporating organic PCM, for application to concrete," *Energy Build.*, vol. 62, pp. 190–195, 2013.

[125] M. Pomianowski, P. Heiselberg, and Y. Zhang, "Review of thermal energy storage technologies based on PCM application in buildings," *Energy Build.*, vol. 67, pp. 56–69, Dec. 2013.

[126] Q. Zeng, T. Mao, H. Li, and Y. Peng, "Energy & Buildings Thermally insulating lightweight cement-based composites incorporating glass beads and nano-silica aerogels for sustainably energy-saving buildings," *Energy Build.*, vol. 174, pp. 97–110, 2018.